UNIVERSIDADE FEDERAL DE MINAS GERAIS

Escola de Engenharia

Programa de Pós-Graduação em Engenharia Elétrica

Caio César Souza Mariano Fraga

APPLICATION OF ACTIVE IMPEDANCE DEVICES IN MICROGRIDS, IMPROVING HARMONIC ROUTING AND MANAGING DISTORTIONS

Belo Horizonte

2022

Caio César Souza Mariano Fraga

APPLICATION OF ACTIVE IMPEDANCE DEVICES IN MICROGRIDS, IMPROVING HARMONIC ROUTING AND MANAGING DISTORTIONS

Versão final

Dissertação apresentada ao Programa de Pós-Graduação em Engenharia Elétrica da Universidade Federal de Minas Gerais, como requisito parcial à obtenção do título de Mestre em Engenharia Elétrica.

Orientador: Prof. Dr. Sidelmo Magalhães Silva

Coorientador: Prof. Dr. Hélio Marcos André Antunes

Belo Horizonte

2022

Fraga, Caio César Souza Mariano.
F811a Application of active impedance devices in microgrids, improving harmonic routing and managing distortions [recurso eletrônico] / Caio César Souza Mariano Fraga. - 2022.
1 recurso online (112 f. : il., color.) : pdf.

Orientador: Sidelmo Magalhães Silva.
Coorientador: Hélio Marcos André Antunes.

Dissertação (mestrado) - Universidade Federal de Minas Gerais, Escola de Engenharia.

Apêndices: f. 101-112.

Inclui bibliografia.
Exigências do sistema: Adobe Acrobat Reader.

1. Engenharia elétrica - Teses. 2. Redes elétricas - Teses. 3. Impedância (Eletricidade) - Teses. 4. Harmônicos (Ondas elétricas) - Teses. 5. Energia elétrica - Qualidade - Teses. I. Silva, Sidelmo Magalhães. II. Antunes, Hélio Marcos André. III. Universidade Federal de Minas Gerais. Escola de Engenharia. IV. Título.

CDU: 621.3(043)

Ficha catalográfica elaborada pela Bibliotecária Roseli Alves de Oliveira CRB/6 2121
Biblioteca Prof. Mário Werneck, Escola de Engenharia da UFMG

UNIVERSIDADE FEDERAL DE MINAS GERAIS
ESCOLA DE ENGENHARIA
PROGRAMA DE PÓS-GRADUAÇÃO EM ENGENHARIA ELÉTRICA

FOLHA DE APROVAÇÃO

"APPLICATION OF ACTIVE IMPEDANCE DEVICES IN MICROGRIDS IMPROVING HARMONIC ROUTING AND MANAGING DISTORTIONS"

CAIO CÉSAR SOUZA MARIANO FRAGA

Dissertação de Mestrado submetida à Banca Examinadora designada pelo Colegiado do Programa de Pós-Graduação em Engenharia Elétrica da Escola de Engenharia da Universidade Federal de Minas Gerais, como requisito para obtenção do grau de Mestre em Engenharia Elétrica. Aprovada em 22 de julho de 2022. Por:

Prof. Dr. Sidelmo Magalhães Silva
DEE (UFMG) - Orientador

Prof. Dr. Hélio Marcos André Antunes (co-orientador)
Engenharia Elétrica (UFES)

Prof. Dr. Igor Amariz Pires
(UFMG)

Prof. Dr. Thiago Morais Parreiras
ICT (UNIFEI)

Documento assinado eletronicamente por **Sidelmo Magalhaes Silva**, **Professor do Magistério Superior**, em 22/07/2022, às 16:29, conforme horário oficial de Brasília, com fundamento no art. 5º do Decreto nº 10.543, de 13 de novembro de 2020.

A autenticidade deste documento pode ser conferida no site https://sei.ufmg.br/sei/controlador_externo.php?acao=documento_conferir&id_orgao_acesso_externo=0, informando o código verificador **1622366** e o código CRC **52CD547F**.

I dedicate this work mainly to my family
for all the support and affection today and always.

Acknowledgements

This wasn't an easy journey, to tell the truth, it was one of the hardest I've ever had. A real challenge and for many, many times, I thought I couldn't. Giving up was a common and overwhelming thought. There were very difficult times, ups and downs, and a pandemic, which we are still experiencing and who knows for how long. It all starts with my graduation on August 2018, when I stipulated a period of one year for myself to look for a job opportunity, before choosing to start a master's in order to qualify myself more and not be idle. After this one year, I was here starting my project. This project was expected to last two years, but it took me two and a half years to complete it.

Right at the beginning of the master's, with about six months, I found the long-awaited job opportunity. That's when everything started to get even more difficult, combining a job, master's and home can be very stressful and I don't put myself in this situation as someone special, because I know it's the most common thing we have among students throughout Brazil. For someone who was so anxious about entering the job market, frustration soon knocked. As much as I learned and acquired knowledge in this process, the company policies was a huge demotivator, so I was unable to complete even a year there.

It was just a few months into the job that the pandemic began. It was and is scary. There were countless moments of depression and anxiety. I am enormously indebted to my advisor Sidelmo for his conversations, support and teachings on the most difficult topics during the project. I thank the co-advisor Hélio who accompanied us in the final stretch of the project, but who was crucial to the progress and conclusion with his suggestions, patience and wisdom. I thank my family, Rose, Luiz and Igor for accompanying me daily with concern and affection, nothing would ever be possible or would make sense without you. I thank my friends at *Galera Relâmpago*, it's been years of friendship and partnership, shared joys and difficulties that have helped us to always move forward and increasingly united. I thank my friends from *Garage* for all the songs, laughs and stories we experienced. Thanks to my friends at *Tesla Laboratory* in my first few months as a scholarship holder.

This work was developed within the scope of the Research and Technological Development Program of the Electric Sector regulated by ANEEL under the title "Technical and commercial arrangements for the insertion of energy storage systems in the Brazilian electric sector", project id ANEEL PD-00553- 0046 / 2016, with Petrobras as the project proponent. The authors also acknowledge the financial support from CAPES, FAPEMIG (APQ-02518-16 grant) and CNPq (420850/2016-3 grant), in addition to the Postgraduate Program in Electrical Engineering (PPGEE-UFMG) for supporting this research.

"It's the questions we can't answer that teach us the most.
They teach us how to think. If you give a man an answer, all he gains is a little fact.
But give him a question and he'll look for his own answers."
(Patrick Rothfuss, from The Wise Man's Fear)

Abstract

This work aimed to contribute with a new option for an already known technology, which can be widely used in several applications, but was mainly thought and detailed here in the context of microgrids. It is the so-called *Active Impedance*, which is, basically, a series active filter. Every day, new connections are added to the electrical network and more distributed generation is available. Certainly, new challenges arise from advances like these.

In this way, more and more harmonic distortions are inserted in the system and the Power Quality decreases, due to these harmonics and resonances found in low voltage systems. Thus, the use of technologies as the one proposed here seeks to solve the main problems and challenges encountered in microgrids and distributed generation, the most prominent being the harmonic treatment. This technology of active impedance is modeled from an electronic power converter and aims to emulate inductances at specific frequencies. By doing this, it is possible to define the paths through which we want certain harmonics to flow in the system.

A microgrid example was used, in which the main focus in this work was to perform the harmonic routing of the distortions present in this system. The microgrid, three-phase four-wire centralized AC, operated connected to the power grid. It consisted of a linear load, a non-linear load, a passive filter and a distributed generation. The total power of the loads is 56 kVA. In the studied scenario, the simulation was divided into three cases: the first being the operation of the system disregarding the distributed generation and the active impedance. In the second case, the distributed generation is inserted. At last, the active impedance of 1.27 kVA is inserted in order to prevent harmonics from flowing towards the power grid and intensifying their presence in the passive filter.

Results were obtained regarding THD and, mainly, TDD, making a comparison between them and understanding why the second one is more interesting, since its definition and calculation are immune to load variations. A considerable reduction in the harmonic distortions of the power grid was verified, being even smaller than in the initial case. Another highlight was that the power of the active impedance was considerably lower than the power of the loads, corresponding to 2.26%. Such satisfactory result and the modular ability to use this technology of active impedances allow its application in several topics in a promising way and with many more still to be explored.

Keywords: Microgrids, Distributed generation, Active impedance, Series active filter, Harmonic routing, Harmonic distortions, Power Quality.

Resumo

Este trabalho tem o intuito de contribuir com uma nova opção para uma tecnologia já conhecida, a qual pode ser largamente utilizada em diversas aplicações, mas foi principalmente pensada e detalhada aqui no que tange o assunto de microrredes. Esta tecnologia é a *Impedância Ativa*, a qual, basicamente, se trata de um filtro ativo série. A cada dia, novas conexões são inseridas à rede elétrica e mais geração distribuída está disponível ao nosso redor. Certamente, novos desafios surgem de avanços como estes.

Desta forma, cada vez mais distorções harmônicas são inseridas no sistema e a Qualidade da Energia Elétrica decai, devido a tais harmônicos e ressonâncias encontradas nos sistemas de baixa tensão. Assim, o uso de tecnologias como a proposta aqui procura solucionar os principais problemas e desafios encontrados em microrredes e geração distribuída, sendo o de maior destaque o tratamento harmônico. Esta tecnologia da impedância ativa é modelada a partir de um conversor estático de potência e tem o objetivo de emular indutâncias em frequências específicas. Ao fazer isto, é possível definir os caminhos pelos quais almejamos que determinados harmônicos percorram no sistema.

Usou-se uma microrrede de exemplo, na qual o principal foco neste trabalho foi fazer o roteamento harmônico das distorções presentes nesse sistema. A microrrede, trifásica a quatro fios centralizada e em corrente alternada, operava conectada à rede elétrica. Ela consistia de uma carga linear, uma não linear, um filtro passivo e uma geração distribuída. As cargas totalizam 56 kVA. No cenário aqui estudado, dividiu-se a simulação em três casos: o primeiro sendo o funcionamento do sistema desconsiderando a geração distribuída e a impedância ativa. No segundo caso, insere-se a geração distribuída. Por último, insere-se a impedância ativa com potência igual a 1.27 kVA visando impedir os harmônicos de fluírem em direção à rede elétrica e intensificando a presença desses no filtro passivo.

Foram obtidos resultados quanto ao THD e, principalmente, o TDD, fazendo-se uma comparação entre eles e entendendo porque este é mais interessante, uma vez que sua definição e cálculo são imunes às variações de carga. Foi verificada uma queda considerável nas distorções harmônicas da rede elétrica, sendo ainda menores do que no caso inicial. Outro ponto de destaque foi o da potência da impedância ativa ser consideravelmente inferior a potência das cargas, correspondendo a 2.26%. Tal resultado satisfatório e a capacidade modular de se utilizar esta tecnologia de impedâncias ativas permite sua aplicação em diversos tópicos de maneira promissora e com muito ainda a ser explorado.

Palavras-chave: Microrredes, Geração distribuída, Impedância ativa, Filtro ativo série, Roteamento harmônico, Distorções harmônicas, Qualidade da Energia Elétrica.

List of Figures

List of Tables

List of abbreviations and acronyms

ABNT	Associação Brasileira de Normas Técnicas
AC	Alternating Current
AEP	American Electric Power
AMI	Advanced Measurement Instruments
BES	Battery Energy Storage
DC	Direct Current
DER	Distributed Energy Resource
DFT	Discrete Fourier Series
DOE	Department of Energy
Celpe	Companhia Energética de Pernambuco
CHP	Combined Heat and Power
CMG	Coupled Microgrids
CO_2	Carbon Dioxide
ECI	European Copper Institute
EEUFMG	Escola de Engenharia da Universidade Federal de Minas Gerais
EMI	Electromagnetic Interference
EU	Eurepean Union
FACTS	Flexible Alternating Current Transmission System
FFT	Fast Fourier Transform
Fundep	Fundação de Desenvolvimento da Pesquisa
IEC	International Eletrotechnical Comission
IEEE	Institute of Electrical and Electronics Engineers
IGBT	Insulated-gate bipolar transistor

LPF	Low-pass Filter
MG	Microgrid
MPPT	Maximum Power Point Tracking
NaS	Sodium-sulfur
NBR	Norma Brasileira
NEDO	New Energy and Industrial Technology Development Organization
NIC	Negative Impedance Circuit
NTUA	National Technical University of Athens
PCC	Point of common coupling
PLL	Phase-locked Loop
PnP	Plug and Play
PPGEE	Programa de Pós-Graduação em Engenharia Elétrica
PQ	Power Quality
PV	Photovoltaic
PWM	Pulse-width modulation
R&D	Research and Development
RMS	Root mean-square
SIN	Sistema Interligado Nacional
SHS	Solar Home Systems
TDD	Total Demand Distortion
TGEN	Tecogen
THD	Total Harmonic Distortion
UFMG	Universidade Federal de Minas Gerais
UK	United Kingdom
UNESCO	United Nations Educational, Scientific and Cultural Organization
USA	United States of America
VSI	Voltage Source Inverter

List of symbols

v_s	Voltage source
ω	Angular frequency
R_s	Voltage source resistance
L_s	Voltage source inductance
R_L	Load resistance
$m(t)$	Generic function
a_0	Average value of $m(t)$
A_h	Effective value of the order component h
α_h	Phase angle
a_h	Fourier series coefficient
b_h	Fourier series coefficient
$R_{D(on)}$	Diode resistance when conducting
v_D	Diode voltage
R_{th}	Thévenin resistance
V_{th}	Thévenin voltage
V_{thh1}	Fundamental frequency of the Thévenin voltage
V_{thh}	Thévenin voltage of higher frequencies
L_h	Inductance emulated for the h^{th} harmonic
I_h	Current magnitude for the h^{th} harmonic
v_h	Voltage magnitude for the h^{th} harmonic
Z_L	Inductive impedance
Z_C	Capacitive impedance
v_L	Voltage over inductance

v_C	Voltage over capacitance
$V_{1,rms}$	RMS voltage on the primary of the transformer
$V_{2,rms}$	RMS voltage on the secundary of the transformer
V_h	RMS voltage of the h^{th} harmonic
N_1	Numbers of turns on the primary of the transformer
N_2	Numbers of turns on the secondary of the transformer
$I_{1,rms}$	RMS current on the primary of the transformer
$I_{2,rms}$	RMS current on the secundary of the transformer
V_{DC}	DC link voltage of the active filter
I_{AF}	Peak current of the active filter
S_{AF}	Apparent power of the active filter
L_f	Inductor of the active filter
R_f	Resistor of the active filter
C_f	Capacitor of the active filter
S_{pc}	Pre-charge switch of the active filter
R_{pc}	Pre-charge resistor of the active filter
L_{max}	Maximum inductance
S_n	Three-phase converter power
V_f	Converter phase voltage
f	Fundamental electrical frequency
T	Period of fundamental electrical frequency
T_sw	Sample period of converter control
T_{st}	Phase advance to correct the low pass filter effect
ϕ_c	Phase correction
k	Percentage of LC filter reactives
k_{iv}	Integral gain of the voltage loop

k_{pv}	Proportional gain of the voltage loop
k_{pi}	Proportional gain of the current loop
k_{inv}	Converter gain
c_k	Harmonic component on a resonant controller
k_r	Proportional gain for the repetitive controller
ω_{sw}	Switching frequency
ω_i	Pole frequency of the current loop
$\omega_{v(1)}$	First pole frequency of the voltage loop
$\omega_{v(2)}$	Second pole frequency of the voltage loop
V_{max}	Maximum DC link voltage
k_{DC}	Proportional gain of the DC link loop
S_{sc}	Short-circuit power
p.f.	Power factor
C_{NL}	Capacitor of the nonlinear load
R_{NL}	Resistor of the nonlinear load
L_{NL}	Inductor of the nonlinear load
Q_5	Quality factor of the 5^{th} order passive filter
R_5	Resistor of the 5^{th} order passive filter
L_5	Inductor of the 5^{th} order passive filter
C_5	Capacitor of the 5^{th} order passive filter
Q_7	Quality factor of the 7^{th} order passive filter
R_7	Resistor of the 7^{th} order passive filter
L_7	Inductor of the 7^{th} order passive filter
C_7	Capacitor of the 7^{th} order passive filter
Q_{11}	Quality factor of the 11^{th} order passive filter
R_{11}	Resistor of the 11^{th} order passive filter

L_{11}	Inductor of the 11^{th} order passive filter
C_{11}	Capacitor of the 11^{th} order passive filter
I_{DER}	Current of the DER
L_{DER}	Inductor of the DER
C_{DER}	Capacitor of the DER
S_{ϕ}	Single-phase converter power
THD_v	Total Harmonic Distortion of the Voltage
THD_i	Total Harmonic Distortion of the Current
TDD	Total Demand Distortion
	TH – RMS value of the harmonics above the fundamental
I_n	RMS value of the harmonic n
I_F	RMS value of the fundamental current

Contents

1 Introduction

In this chapter, a brief description of the thesis is presented. It starts with a general context and then the objectives are listed, the motivations that aroused interest in this work and, finally, a brief structuring of how the text is organized.

1.1 Context and Relevance

The demand for energy worldwide is growing. In addition, electronic equipments have been increasingly used (AMARAL et al., 2015). These devices commonly use Power Electronics to interface with the power grid. In this way, more and more harmonic distortions are inserted in the system and the Power Quality has been decreasing, due to these harmonics inserted and resonances in the low voltage electrical system (AMARAL et al., 2015). A poor Power Quality implies losses such as:

- More need for maintenance;
- Reduced equipment life;
- Inaccuracy in energy measurements for future invoices;
- Improper operation of protective devices.

In addition, the need for uninterrupted power supply has become a major focus in recent studies. Thus, microgrid systems and distributed generation have been studied and implemented all over the world as a solution, in addition to the possibility of taking energy to places without power supply through the utility grid (FALCÃO, 2009).

In this scenario, the use of solutions that are easy to insert into the system in order to mitigate these harmonic distortions, for example, through an intelligent routing of these harmonics is a promising solution. They are attractive, providing reliability and versatility compared to classic solutions. In addition, there is also the possibility of improving the power factor, depending on how such a solution is inserted into the system and, ultimately, improving the stability of the system as a whole. Therefore, one of the keys to the success of microgrids comes from distributed solutions. However, there is still a long way to go for its consolidation and this depends on the development of technology with nominal power levels suitable for allocation in commercial and industrial low voltage electrical installations and whose cost is competitive compared to existing solutions in the market.

1.2 Objectives

1.2.1 General Objective

As a general objective, this work aims to deepen the study of a series compensator acting as an *Active Impedance* in a microgrid.

1.2.2 Specific Objectives

As specific objectives, this work seeks the implementation of an Active Impedance Device, or simply *Active Impedance*, as a distributed solution for part of the problems and challenges found in microgrids and distributed generation. Among these challenges, the main focus is harmonic treatment, that is, harmonic distortions that negatively affect the Power Quality. Briefly, these active impedances aim to synthesize a quadrature reactance with the harmonic component in question. In this way, it is possible to determine the preferred paths within the circuit to be followed by each harmonic. These active impedances are modeled after a static power converter, which is magnetically coupled to the system, therefore, there is no need to interrupt the circuit to use them.

1.3 Contributions

The idea of using active impedances in a system is not new and it was initially proposed to be applied in the control of power flow in high voltage transmission lines, as seen in (ROGERS; OVERBYE, 2009). From then on, other applications for this technology have been proposed, among them, a solution for Power Quality in low voltage electrical networks by mitigating harmonic distortions in commercial and industrial electrical systems (FRANÇA, G. J.; CARDOSO, 2012) and (PIRES; FRANÇA; CARDOSO, 2014).

Finally, this work intends to contribute to fill this gap of further studies of applications of this technology, by making a survey on the topic of microgrids and a study on the advantages and disadvantages encountered when using this technology. Here the main objective was to prove the benefits of applying these active impedances in the system, using a compensator emulating this impedance.

1.4 Methodology

This thesis begins by making a historical commentary on the electrical system as it is known today. Then, the microgrid theme itself is introduced, citing this technological framework and motivations for studies in this area. After this introduction, the international scene is pointed out, mentioning some of the countries that stood out the most

over the years, and the national scene. In the national scenario, the *Laboratório Tesla* of UFMG stands out with several projects being developed in the area of microgrids and distributed generation. Then, the topic of microgrids itself is addressed. The components of the microgrids are elucidated, in addition to their greatest challenges, such as protection aspects, energy storage, stability problems, control strategies and so on.

Then, the main focus of the present thesis begins, which intends to deepen the use of compensators, in order to emulate active impedances. By making such emulation, the harmonic routing through paths that are preferable provides changes in the harmonic distortion. This entire study is done using the software MATLAB/Simulink®.

1.5 Work Structure

The text was structured and divided into six chapters with this introductory chapter as the first. Chapter 2 brings the literature review on the topic, containing all the theoretical foundation and motivation necessary for the later chapters. It addresses an overview, the international and national scenario, the constituent components of a microgrid, differences in centralized and decentralized control, in addition to listing the various existing challenges. By the end of this chapter, the primary intention of this thesis is formally presented with details on the proposed theme, in addition to the different possible uses of these active impedances in the electrical system.

In Chapter 3, the static power converter is modeled emulating an active impedance based on control techniques such as proportional and integrative controllers and repetitive control, which takes into account requirements such as frequency response curves and, mainly, its dynamic stiffness.

In Chapter 4, the results obtained with the converter and the control strategies in question are exposed through computer simulations that can prove their effectiveness in working through harmonic distortions.

Finally, in Chapter 5, the conclusions obtained with this dissertation are presented, in addition to proposals for continuity in future works and related publications.

2 Microgrids: Context and Characteristics

This chapter aims to address the state of the art of this topic. Here, initially, an introduction to the electrical system as we know it today is presented, in addition to general information about microgrids. Then, it has an international and national comparison of how this subject has been developed. Subsequently, it enters the microgrids themselves, by making a survey on their components, in addition to the various challenges encountered for their operation. Secondly, harmonic distortion is addressed, such as its history, characteristics and regulations. This section ends with a discussion about active impedance itself and its applicatoins.

2.1 Microgrid Overview

The electrical power system as it is known is just over a hundred and thirty years old. Namely, a historic milestone in electric power is due to the famous *War of the Currents* starring ideologically by Thomas Edison and Nikola Tesla at the end of the 19^{th} century. Due to the grandeur of such events, it will not be treated here how it all happened – despite strongly recommending that the reader, if unfamiliar, search enthusiastically for the subject, as in (HUGHES, 1983).

The fact is that on one side there was Edison defending the use of direct current (DC), while Tesla the use of alternating current (AC). While the first option aimed at servicing through generators close to the consumption points, the second aimed at making the generating plants located close to the primary sources and transmitting them over long distances. As we well know, Tesla emerged victorious. All subsequent developments were technologically complementary to that proposed by Tesla. However, despite many years being widely used worldwide, direct current has reappeared as an option for long distances due to the considerable development of Power Electronics.

We are currently experiencing a new milestone with the themes *Microgrid* and *Distributed Generation*, which are widely studied due to their proven importance in obtaining reliable, robust and efficient system. Microgrids are considered a basic feature of future active distribution networks (HATZIARGYRIOUA et al., 2007). Among the factors that made this rise possible, there is the economic viability of small energy sources, advances in data communication, improving in measuring, sensing and control instruments (FALCÃO, 2009). What before seemed somewhat surreal, compared to remote times like those of Edison and Tesla, has become a reality: the possibility for the consumer to have the autonomy to generate their own energy and still be able to supply it to other consumers, the so-called *prosumer*.

There are several points to be cited as motivation for this theme. In a first example, with the use of this new system, there is an increase in the continuity of energy supply. This is due to the consumer being able to use, in addition to the utility's energy, energy produced by himself, be it solar, wind, or other. Another example is the environmental aspect. Hydroelectric, thermoelectric, or nuclear power plants face increasing difficulties in their construction due to how much they affect the place where they will be installed, both from the point of view of the population, and of the local fauna and flora.

These changes from the well known electrical system to microgrids itself and from consumer to prosumer were partly driven by technological advances in the implementation of smart meters and Advanced Measurement Instruments (AMI). The distributed generation systems and microgrids not only reduce the energy needed from the utility, but also start to supply energy to it. The internet mediates this demand and assists in the power flow. In addition, the energy market becomes more interesting, from the point of view of having a real-time response regarding pricing and demand variation.

2.2 International vs. National Scenario

The environmental factor is perhaps one of the most concerned about the use of microgrids. This encourages the widespread use of renewable energy sources by the consumer, along with reducing the need to build large plants, such as hydroelectric plants. Therefore, it is good practice to constantly decrease usage of the large-scale generation of electric energy by steam power plants. However, it is thought that the race for new technologies also has another bias, the political one. Usually, those who have knowledge have power. A study published by UNESCO in 2015 and with projections for 2030 shows that Brazil both public and private R&D have progressed significantly and its strength is on agriculture and life science, among EU countries, public R&D increased only in Germany while it declined in France and the UK (UNESCO, 2015).

The truth is that with the consolidation of microgrids, this revolutionary change causes many problems, usually complex, which are unknown to most of power engineers (CURRIE et al., 2004). There are many technical problems encountered on this topic. The way the power system was conceived does not support the leveraged use of distributed generation, as this system was designed for passive consumers. Therefore, much still needs to be studied and adapted. Namely, decentralized or radial power generation presents difficulties in protection circuits, Power Quality, in addition to reliability and stability (USTUN; OZANSOY; ZAYEGH, 2011). Thus, the expertise acquired in transmission and distribution systems is vast and consolidated, but these concepts of distributed generation and widespread use of renewable sources are becoming increasingly popular, stimulating changes in the approach of electrical engineers and, consequently, more investment policies

are needed. And, in this scenario, the microgrids enter as the key to coordinate and manage this transformation of distributed generation from passive to active networks and having their potential taken full advantage (HATZIARGYRIOU, 2008). Worldwide, different technologies and topologies have been studied. The advantage of this theme being so versatile is that it allows several approaches, from something purely theoretical, like island implementations, as it happens in Fernando de Noronha, archipelago in the State of Pernambuco. The current scenario around the world will be briefly discussed on the following regions in Figure 1.

Figure 1 – Insight of microgrids in European Union, United States, Japan and Brazil.

2.2.1 European Union

Perhaps what allows the European Union to stand out the most on this issue is the awareness of climate problems and the need to migrate to a more renewable energy matrix, in addition to the reduction in carbon dioxide emissions (CO_2). There are several guidelines that stipulate certain quantities to be achieved in these two items (AHRENS, 2007). In this way, the EU provides several incentives in R&D projects on this subject, which started in 1998. It is estimated that by 2030, the investment required by the EU will be 500 billion euros with regard to topics such as microgrids and smart grid if investment in transmission and distribution is taken into account (CENTRE, 2011).

The first project funded by the EU was the *Microgrids Project* led by the National Technical University of Athens (NTUA), whose main objective was to investigate the dynamics of distributed generation when applied to microgrids. Strategies were developed with a series of issues, such as control algorithms, protection, intelligence requirements, among others (KATIRAEI et al., 2008). This project had as pilot installation the island of

Kythnos, in Greece. Meanwhile, a study on microgrid control methods was performed in Germany. A continuation of this project, entitled *More Microgrids Project*, was again led by NTUA with the purpose of studying alternative methods, together with the concepts of universalization and *plug-and-play* (PnP). In (ERGE, 2007) is shown the description of the Kyhthnos system, in addition to Stutensee and Mannhelm-Wallstadt, in Germany. Denmark deserves to be highlighted within the EU for its promising advances and bold goals. A series of projects was developed by the University of Aalborg in conjunction with the Polytechnic University of Catalunya, in Spain. These researches aimed at advances in relation to DC/AC systems in paralallel, advanced converter control, anti-islanding algorithms, among others. This partnership results in a 350 kW (GUERRERO, 2011) microgrid implemented in Spain. Still in Denmark, it is possible to see an extensive report at (CLUSTER, 2011) about its competencies regarding R&D, in addition to tests and demonstrations. Its development in recent decades is unique in relation to the integration of renewable energy sources and deserves attention.

2.2.2 Japan

Japan is a country that continues its technological advances. As it is a small and isolated country, it has many renewable energy systems, mainly wind turbines and photovoltaic systems. In (KOYAMA, 2020), it is possible to understand a little of its current energy scenario and the challenges encountered. Japan is a country well known for their Power Quality, but, inevitably, distributed generation due to its intermittency and interface through Power Electronics affects this quality.

A notable project was the one presented in 2005 at the World Exhibition in Aichi. The system used fuel cells, photovoltaic panels and its energy storage was based on Sodium Sulfur (NaS). This system underwent two tests, one in 2005, the other in 2007. The first showed errors in the control of voltage and frequency, while the second was more successful (MOROZUMI, 2003). Many of the subsequent projects were carried out by the private sector. A great example is Shimizu Corporation, which has been developing *Shimizu Microgrid* in cooperation with the University of Tokyo. This project aims to develop an optimal operation and control system. Tokyo Gas, on the other hand, also in partnership with the University of Tokyo, developed an integrated control system for distributed generation through simulations and experiments in Yokohama (KROPOSKI et al., 2008).

A more recent one is the *Sendai Microgrid*. This is a well-known microgrid project functioning in Tohuku Fukushi University. The project is funded by New Energy and Industrial Technology Development Organization (NEDO). The microgrid achieved stardom, as it performed for 2 days during the blackout to power the teaching hospital in 2011 earthquakes and tsunami. The power sources of the energy center are two 350 kW gensets

fired by natural gas, a 50 kW solar power plant, and a DC storage device (CHANDAK; ROUT, 2021).

2.2.3 United States

The United States has many audacious and fruitful projects. CERTS (Consortium for Solutions in Electrical Reliability Technology) is the most known in the USA in microgrids. This involves the collaboration of a number of entities: AEP (American Electric Power), TGEN (Tecogen), Northern Power Systems, S&C Electric Co, Sandia National Laboratories and the University of Wisconsin (BARNES et al., 2007). This project consists of microgrid and distributed generation to allow the isolation of the utility grid. As a major breakthrough in the sector, three advanced concepts were obtained: a method to guarantee the automatic and continuous transition between the network-connected and islanded modes, a protection method within the microgrids that does not depend on high fault currents and a control scheme of microgrid to stabilize the system frequency and voltage without using high speed communication (BERKELEY et al., 2009).

The DOE (Department of Energy) *Smart Grid* Research and Development Program considers microgrids to be an essential element. In this way, it established this theme as the main focus area. The number of R&D challenges is constantly increasing. In (TON, D.; SMITH, 2012) there is a summary of ongoing projects. Meanwhile, (BOWER et al., 2014) aims to go deeper into the studies and experiments on microgrids. This report addresses this issue in a more advanced way from the point of view of integration and interoperability. It is possible to have understanding about advanced architecture systems, technical challenges and, most interestingly, a detailed list with the areas of impact from these advanced studies in microgrids. Finally, as another example, (HARRIS, 2017) proposes microgrid architecture topologies, including photovoltaic, biomass gasifier, and wind turbine generators as well as generator hybridization topologies. As an example, a microgrid topology and business model is constructed for a model village case study using the methodology and architectures described.

Another project is the *Microgrid at the New York University*. The microgrid setup in New York University is one of the largest microgrid setup in the university campus since 1960. The microgrid has adopted the evolution of power sources from the conventional to the non-conventional power source, by observing the capabilities, reliability, and cost-effectiveness. The 13.4 MW combined heat and power (CHP) microgrid comprises of 5.5 MW of two gas turbines and a 2.4 MW steam turbine. The microgrid sources electrify 22 buildings and heat up 37 buildings in the campus. The control operation of microgrid executes seamless transition between the grid-connected and islanded mode of operation, and it has been successfully tested during the hurricane Sandy (CHANDAK; ROUT, 2021).

2.2.4 Brazil

Brazil has developed several theses on this topic, precisely because it is a very broad, important and current topic. The *Laboratório Tesla Engenharia de Potência*, at UFMG, develops a series of projects in this area, such as, for example, the implantation of a microgrid at the *Escola de Engenharia da UFMG* (EEUFMG). This project is developed in partnership with Petrobras and UFMG. In summary, this is a practical study regarding the use of different energy storage technologies, in addition to the control of different loads present in the electrical engineering building, including integration with the Solar Plant – installed on the roof of Building I of the EEUFMG – as an example of distributed generation. The present theme of this thesis has as its final objective on a future project to apply in practice, in the microgrid above-mentioned, the concept studied here. Bringing other examples of projects developed and implemented nationally related to the topic of microgrids in the academic area and with applications on campus, we have (BELLIDO, 2018) and (CARNEIRO, 2017).

In Brazil, the vast majority of projects developed related to microgrids focus on isolated locations. After all, it is estimated that about two million Brazilians are not yet connected to the *Sistema Interligado Nacional* (SIN) (RIBEIRO et al., 2011). This makes research in this area even more attractive and important for the country's development.

Among other developed projects, a well-known microgrid is that of Fernando de Noronha, located in the State of Pernambuco. This microgrid serves approximately 2500 people. The island's energy matrix is currently composed of generation through thermo-electric and solar energy, and the first, in 2019, represented 90% of the electric energy generated and solar energy approximately 10% (WWF-BRASIL, 2020).

With an installed capacity of 400 kWp, *Usina Solar Noronha I* was inaugurated in 2014, while Noronha II was inaugurated in 2018 with an installed capacity of 550 kWp. Celpe (*Companhia Energética de Pernambuco*) intends to deploy the first Smart Grids in the State on the island, with an investment of approximately 17.6 million reais in areas such as measurement, telecommunications and automation (RODRIGUES, 2017).

In 2019, the first battery complex connected to a generation system in Brazil was installed in the archipelago. These batteries are connected to the *Usina Solar Tubarão*. The idea is that these batteries play an important role, since during the day they will accumulate surplus energy, supporting the system in the event of instability, in addition to the benefits at night when it comes to the time of greatest consumption. In (CELPE, 2019), it is possible to see in detail the energy data of the generation and distribution systems of the so-called "Innovation Island".

2.3 Components of a Microgrid

A microgrid is a group of interconnected loads and distributed energy resources within clearly defined electrical boundaries that acts as a single controllable entity with respect to the grid as seen on IEEE 2030.7 (DANLEY, 2019), but this could be further divided in a didactic way into options such as nanogrid and picogrid, for example. Figure 2 provides a simple comparison between these three options.

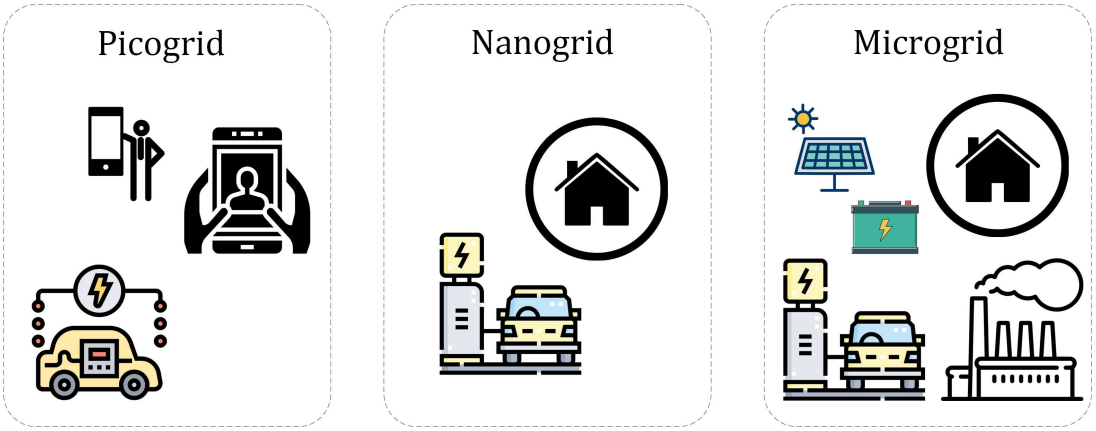

Figure 2 – Functional classification of a microgrid.

First, for a picogrid think of a cluster of homes connected to a single solar panel, or these battery-charging energy kiosks. The picogrid provides enough power to keep the lights on and charge cell phones. Picogrids fill in where people do not have access to a mini-grid or cannot afford connection fees. Nanogrids are single domains of power with a single physical layer of power distribution. Though still supplying energy with limited capacity, the scale of the applications are more important than those of a picogrid. For example nanogrid applies for Solar Home Systems (SHS) where each home is powered by an autonomous photovoltaic system. Most common SHS are composed of a single solar panel, a battery with a prepaid meter and electrical plug offering enough energy to supply a house with basic electricity needs (ADB, 2020).

In short, microgrids can be defined as a small-scale power system with a *cluster* of loads and distributed generators operating in conjunction with power management, control, protection and associated software devices. These devices include flexible control for the AC transmission system (FACTS) (PENG; LI; TOLBERT, 2009). FACTS devices incorporate Power Electronics and controllers to enhance controllability and increase transfer capability (EDRIS et al., 1997). A person using a cell phone to listen to music, chat, among other possibilities on the same device, can be considered illustratively as a picogrid, as well as, for example, an electric vehicle alone. By joining an electric vehicle and a home to exchange energy bi-directionally with one another, one can already consider a nanogrid. In the case of energy exchange between several DERs and loads, an microgrid is considered. A microgrid can be represented with different micro sources and

loads. However, the remote microgrids do not have the utility connections. The utility microgrids span geographically a larger area compared to the facility microgrids. The micro sources, loads, network parameters, control topologies vary in different microgrids (SHREYAS et al., 2019).

It is interesting to note that microgrids can be DC (XIALING; XIAOMING, 2007), AC, or even AC at high frequencies (CHAKRABORTY; WEISS; SIMÕES, 2007). The innovative feature they have is their ability to operate *autonomously* in the event of a power outage from the main grid. That is, its operation in what is called *islanded mode* is possible. In this way, the consumer does not have his energy supply interrupted. However, for example, photovoltaic systems operation in island mode are currently prohibited for safety reasons as found in ABNT NBR IEC 62116. If it worked, technical teams that performed maintenance on the main system could be exposed to the electricity generated by these secondary systems. Therefore, there are methods provided by this standard, which must be followed by the inverters used for this purpose. Evaluation of these anti-islanding methods can be found at (REIS et al., 2015). In addition to the problem of interrupting the supply of energy from the primary system, the microgrid can be easily disconnected in events such as a voltage drop, frequency variation, or other problems in the main network. Thus, microgrids assist not only in providing an uninterrupted service, but also in maintaining the quality of the system.

In summary, the main issue today not for microgrids, but for DERs is *overvoltage*. When inverters start injecting elevated current/power, this tends to increase the voltage (PICCINI et al., 2021). So, overvoltage is the main villain here. In urban areas, the *overload* of conductors/feeders is the second villain (LEGRAND, 2009). In rural areas, the *voltage imbalance* is the main big villain (CIONTEA; IOV, 2021). The microgrid is a way to solve these problems. The concept of DERs changes from country to country. The global concern in the scope of DER is the lack of inertia to maintain the power balance (MILANO et al., 2018). For example, electromechanical converters as in wind have inertia, electronic converters as in solar do not. Systems based on electromechanical elements can have very high overloads, reaching up to 10x the rated capacity of the motor and remaining in this state for seconds, without burning out. In the case of power converters, they can have an overload of 1.5x or 2x and can remain on it for milliseconds, so it is a great challenge, how to transition from a high overload rate to a low overload rate system (SEP, 2020). Besides the DER causing an increase in voltage, the bidirectional power flow causes difficulty in the protection system (HUSSAIN et al., 2010). Techniques as volt-var and volt-watt functions tends to increase the *hosting capacity* of the system (PICCINI et al., 2021). The impact of DER on Power Quality depends to a large extend on the criteria that are considered in the design of the unit. When the design is optimized for energy production only, massive DER penetration will probably adversely impact quality, reliability and security. Several types of interfaces are however capable of improving the

Power Quality. In a deregulated system this will require economic incentives, for example in the form of a wellfunctioning ancillary services market (BOLLEN; HAGER, 2005).

In order to make the features outlined above available, the microgrids cover a range of equipments, interfaces, controls, supervision and protection devices, among others. These can be classified into three groups (SOSHINSKAYA et al., 2014): generation, storage system and loads; physical network for distribution and advanced controls. Figure 3 exemplifies a microgrid consisting of energy storage, grid connection possibility, generation by solar and wind energy, in addition to consumers at the center – control aspects not represented. These three mentioned groups are part of the challenges to be faced during the advances in microgrids studies. Finally, in order to make it even clear, Figure 4 brings a comparison between a conventional grid and a modern grid.

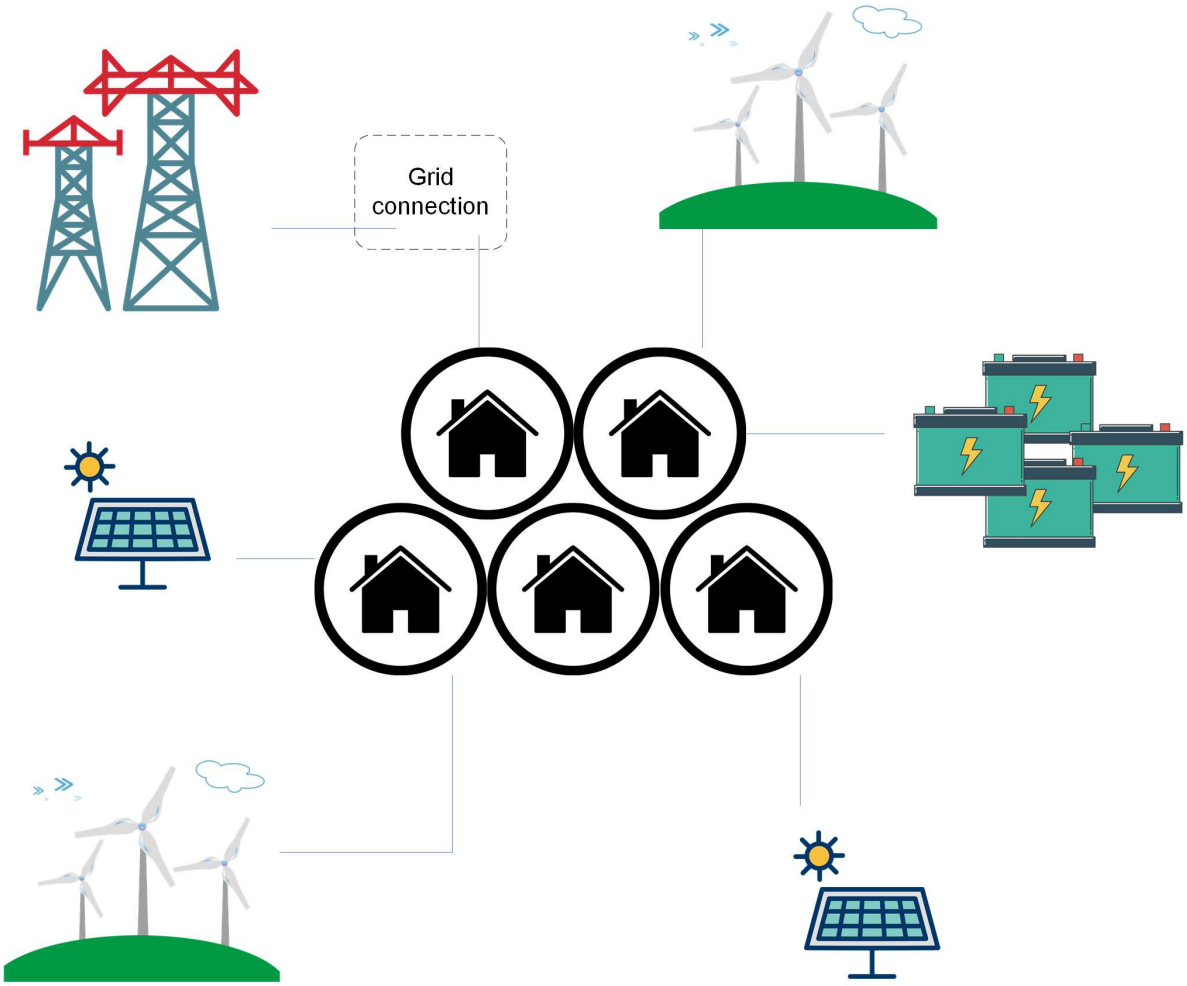

Figure 3 – Microgrid concept.

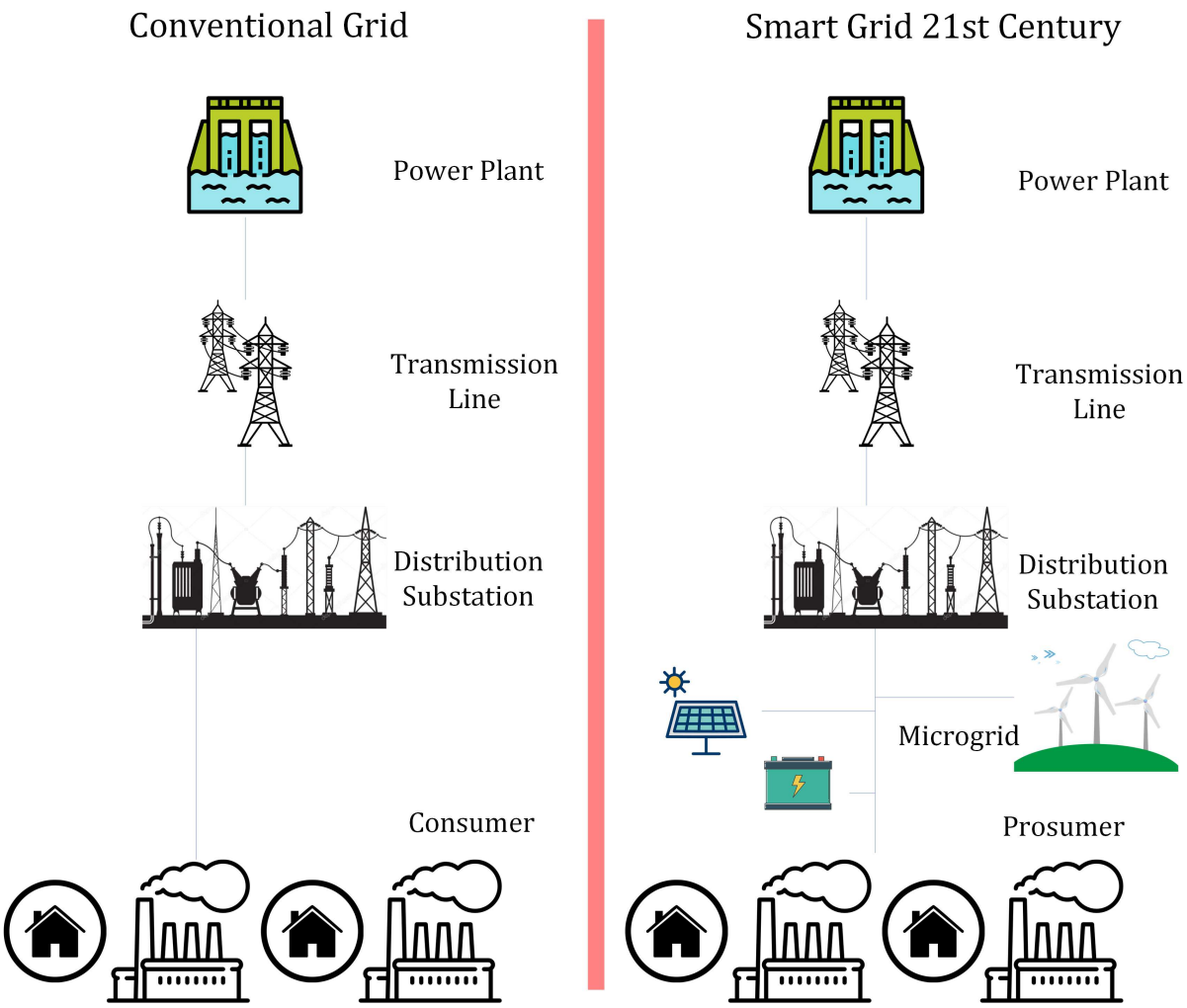

Figure 4 – Comparison between conventional grid and Smart Grid.

2.3.1 Energy Storage

Storage systems are indispensable for the proper functioning of the microgrids, as one of its purposes is to store the surplus energy generated throughout the day. In this way, it becomes possible for these storage units to supply this energy in the event of a fault, or to prevent the system voltage drop. As an example, a microgrid is assumed in which its distributed generation basically consists of solar energy. Thus, during the night, in the event of a power outage at the utility, the system starts operating in island mode. However, there is no more solar energy to supply the needs. Thus, energy storage facilities could supply the loads of this system with what was stored throughout the day, either through solar generation or through energy from the utility. This brings more reliability to the system, since it improves the power supply attribute without interruptions. The greater the efficiency of these storage units, in addition to features such as fast loading and slow unloading, the better it will be for the overall operation of the system. This will not be the focus of this work, but more about this topic can be found at (DIVYA; ØSTERGAARD, 2009).

One of the most promising technologies is that of NaS battery system (Sodium-Sulfur). It has several advantages such as higher energy density, high efficiency and no self-discharge. In contrast, it requires high operation at high temperatures. With this in mind, several companies in the United States and Japan have developed in this area. Another interesting option has been batteries based on high-purity graphite blocks. In short, these batteries heat up due to energy from either solar or wind generation, as examples. This heat can be used in the production of steam and through heat exchangers generate electricity again with generators (USTUN; OZANSOY; ZAYEGH, 2011).

2.3.2 Protection

Protection is a very important aspect to be taken into account. As previously stated, it is intended that, even if the utility ceases to supply energy, the microgrid is able to continue operating. This mode of operation is the island mode, when one or more sources of distributed generation continue to provide energy (LOPES; ZHANG, 2008). It is important to differentiate these two terms, *cease to supply* is related to system stability, while *island mode* is related to galvanic disconnection and safety. Currently, the islanded mode is not allowed as a rule and that is why several references such as (BRITO et al., 2018) look for strategies and algorithms – which are divided among passive, active and hybrid techniques – to avoid this scenario. One of the main objectives of microgrids is precisely the uninterrupted energy supply. Consequently, we may encounter problems regarding security during the maintenance of the utility grid; it is possible that loss of control over the frequency and voltage of the system occurs – quantities of extreme importance for the power flow; damage to equipment if the utility's reclosure occurs out of phase; among others.

It is a fact that current protection projects are not suitable for the scenario that awaits. The increasing integration of distributed generation and the development of microgrids means that current protection is difficult at different levels and directions. There are several loads and several generators that can connect or disconnect from the system at any time. Some of the most imminent problems in this matter are short circuit energy, level and direction of the fault current, erroneous trips, among others (OUDALOV; FIDIGATTI, 2009), (WANG; SUN; DONG, 2011). It is interesting to note that, in a short circuit, power usually flows from the highest voltage to the lowest voltage. In addition, the short-circuit current decreases with increasing distance from the source. However, this changes drastically in the microgrids scenario, since there are several generation points connected to the system and can even supply energy to the utility, this joint current of all generations can be high (BARAN; EL-MARKABY, 2005). Figure 5 exemplifies this case in which the total current can be increased by adding all the contributions from each distributed generation.

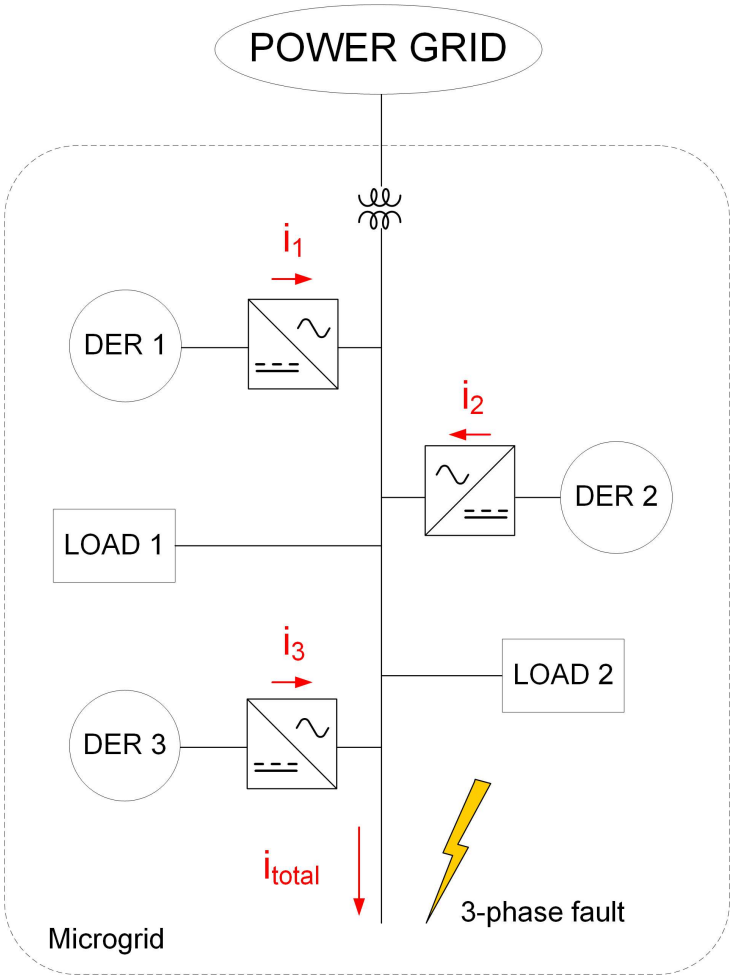

Figure 5 – Fault current during island mode.

It is difficult to estimate this current, especially when Power Electronics is needed at the interface of these distributed generations, as the short-circuit currents in this case are not high enough to trigger protection devices (MARNAY; RUBIO; SIDDIQUI, 2001). It is at this moment that the problem of undesirable tripping becomes so difficult to be mitigated, as it is susceptible to system transients. In addition, it is possible that the meter is measuring only part of the fault current, since several possible paths exist (HUSSAIN et al., 2010). Other characteristics researched at this point are overvoltages (CHEN; YU, 2010), voltage sags (LEI; AI; CUI, 2010) and communication issues. Regarding communication, there are quite innovative systems, which consist of determining the needed parameters for its operation and make the necessary calculations (OUDALOV; FIDIGATTI, 2009), (LAAKSONEN, 2010). However, a major drawback of communication can be the distance in the transmission of information, in addition to making it more expensive and perhaps even unfeasible to implement (POGAKU; PRODANOVIĆ; GREEN, 2007). Therefore, it is important that the protection system is adaptive and uses, for example, techniques such as machine learning, artificial intelligence and fuzzy logic in an attempt to predict these microgrid states.

2.4 Microgrid Architecture

The control aspect of a microgrid is one of the most crucial for its consolidation. This aspect is completely dependent on the quantity, depth of the distributed generation in question and the characteristics of the system loads, in addition to the Power Quality restrictions, since for a microgrid this must vary significantly in relation to the conventional grid (SANCHEZ, 2008).

The microgrid (MG) control has three different architectures: centralized control, decentralized control and distributed control, as seen in the Figure 6 (MARIAM; BASU; CONLON, 2016). Table 1 provides a small comparative summary among these possibilities with their discriminated advantages and disadvantages.

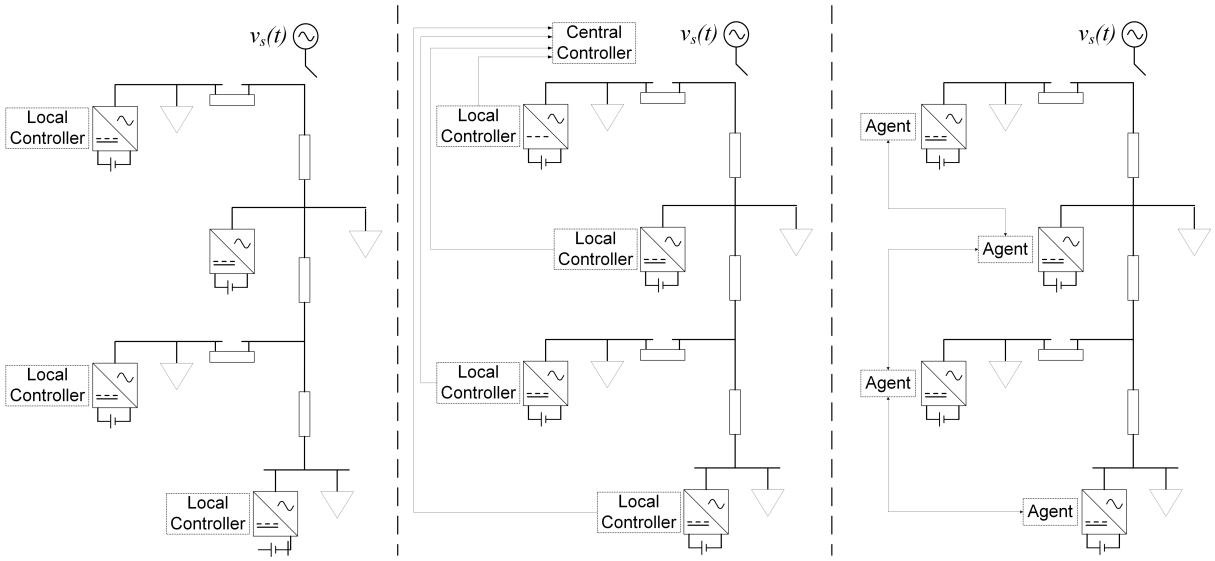

Figure 6 – Decentralized on the left; centralized on the middle; distributed on the right.

Table 1 – Microgrid architecture, adapted from (MARIAM; BASU; CONLON, 2016)

Decentralized	Centralized	Distributed Multi-Agent
Autonomous converter	Adjust the load sharing	Autonomous agents/converters
Based on local information	The scalability is of concern	Use local information and neighbour-to-neighbour communication
Without communication link	Communication may be impractical for MG with many small distributed units	Achieve cooperative objectives
Reliable	Data centralizes introduces privacy and security concerns	Improved performance over decentralized
PnP capability		Has advantages in terms of robusteness, scalability and flexibility over centralized
Limited information		
It is unable to fully utilize the combined power and energy capacities of ESS		

In addition, DERs can be classified within a MG as *grid-feeding*, *grid-forming* and *grid-supporting* (JADEJA et al., 2020). It depends on the responsibilities of which each DER and, consequently, on the constructive aspect of the converter that it uses. Hence, the DER usually operates as a grid-feeding, but it can also operate as a grid-forming when associated with a battery system. This classification can be described simply as follows and illustratively in the Figure 7.

- Grid-forming – voltage forming device defining the voltage for the islanded microgrid;
- Grid-feeding – inject active power reducing energy bill;
- Grid-supporting – current-controlled or voltage-controlled that may provide ancillary services solving power quality problems.

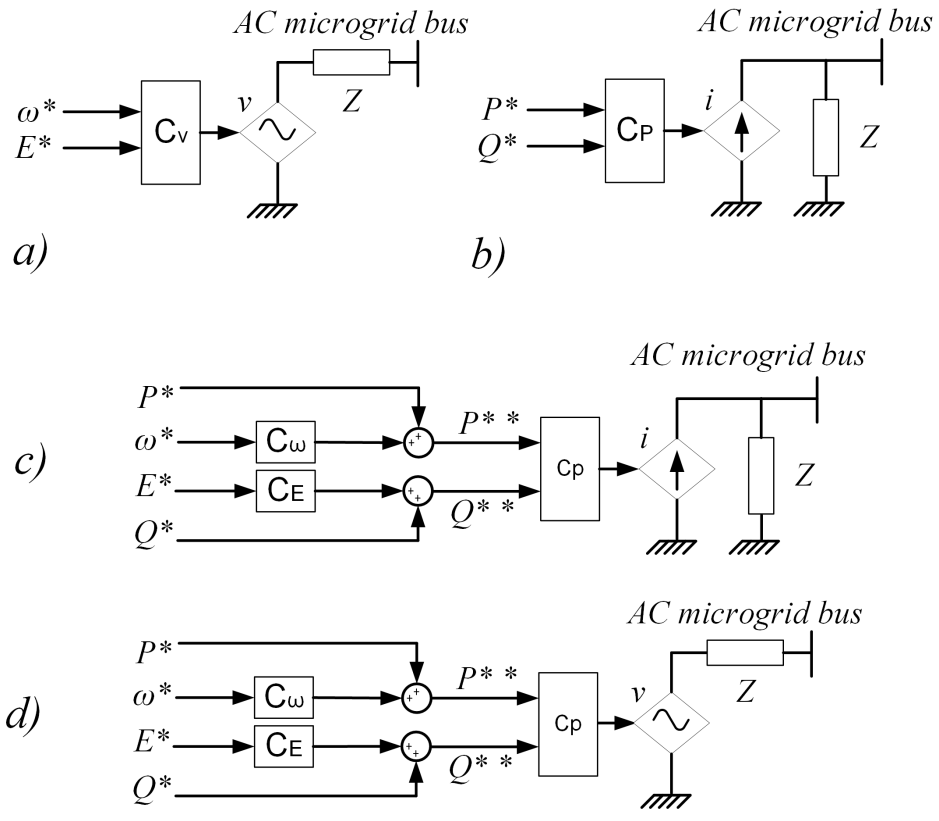

Figure 7 – DERs classifications within a MG: a) grid-forming; b) grid-feeding; c) current-source-based grid-supporting and d) voltage-source-based grid-supporting.

2.5 Harmonic Distortion Overview

Historically, our electrical system was designed with well-defined voltage and frequency values for its operation. However, with the advent of Power Electronics, these values can vary over a wide range of values. More and more equipments use this electronics as an interface in relation to the electrical system and this imposes that each equipment can have its own voltage and frequency values for its operation (DAS, 2015). A common aspect in the vast majority of these equipments is the need to rectify the voltage, for example with a diode rectifier, as we can see in the Figure 8, to then convert the original signal to the desired operating values of voltage and frequency.

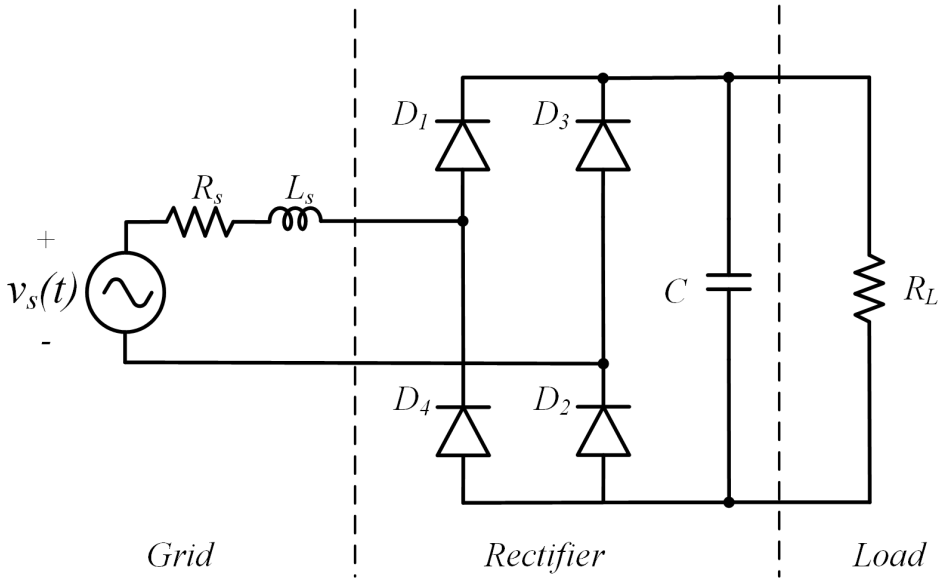

Figure 8 – Single-phase example of application of a rectifier diode bridge, adapted from (MOHAN; UNDELAND; ROBBINS, 2003).

A current that is deformed, which means it does not have a waveform only defined by its fundamental value of the *Fourier Series*, has harmonics. In fact, it is through this same analysis by Fourier series that it is possible to discover the exactly magnitude of each of these harmonics when it is a continuous and periodical signal (BOYCE, 2006). This harmonic equation can be seen in 2.1, which brings a generic function $m(t)$. In this equation, a_0 is the average value; A_h is the effective value of the harmonic component h; α_h is the phase angle of the component h and ω is the angular frequency.

$$m(t) = a_0 + \sum_{h=1}^{\infty} \sqrt{2} A_h \cdot sin(h\omega t + \alpha_h) \tag{2.1}$$

$$A_h = \sqrt{\frac{{a_h}^2 + {b_h}^2}{2}} \tag{2.2}$$

$$\alpha_h = tan^{-1}\left(\frac{a_h}{b_h}\right) \tag{2.3}$$

$$a_0 = \frac{1}{2\pi}\int_{-\pi}^{\pi} m(\omega t)\cdot d(\omega t) \tag{2.4}$$

Where:

$$a_h = \frac{1}{2\pi}\int_{-\pi}^{\pi} m(\omega t)\cdot cos(h\omega t)\cdot d(\omega t) \tag{2.5}$$

$$b_h = \frac{1}{2\pi}\int_{-\pi}^{\pi} m(\omega t)\cdot sin(h\omega t)\cdot d(\omega t) \tag{2.6}$$

Generally, representation by Fourier approximations is required for voltages and currents from measurements made in practice or from computer simulations, which are discrete over time, i.e. discontinuous. In these cases, the *Discrete Fourier Transform* (DFT) is used in the decomposition into frequency components.

In (AMARAL, 2016), a detailed study is made based on the example circuit of the Figure 8. An analysis is initially made about the possible modes of operation of the rectifier, which are:

- State 1: when D_1 and D_2 start driving, as in the Figure 9;
- State 2: when D_3 and D_4 start driving, as in the Figure 10;
- State 3: when all diodes are blocked, as in the Figure 11.

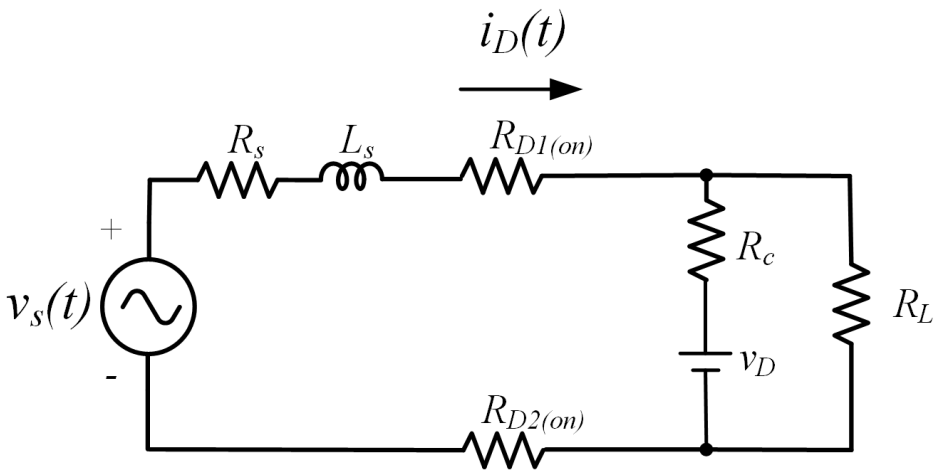

Figure 9 – State 1, adapted from (AMARAL, 2016).

With these modes of operation, the equations that govern each state are developed using the Thévenin equivalent circuit. Then, using the DFT it is possible to identify the

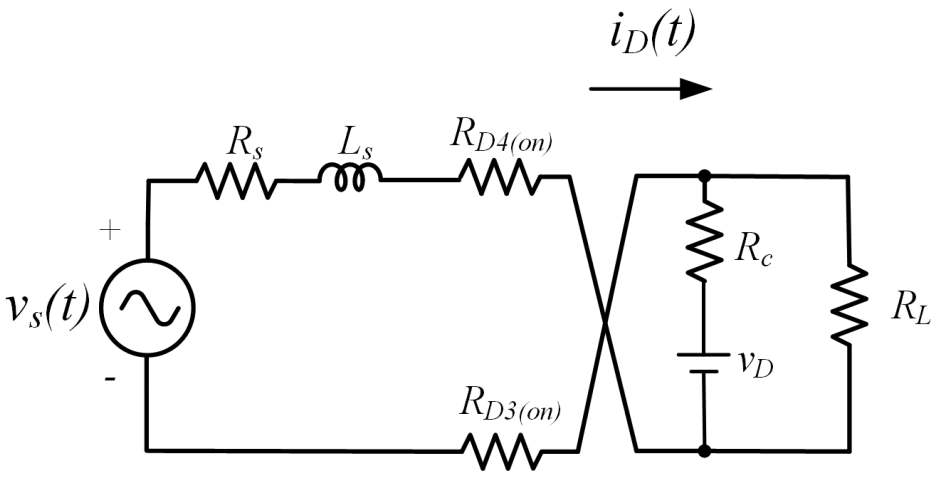

Figure 10 – State 2, adapted from (AMARAL, 2016).

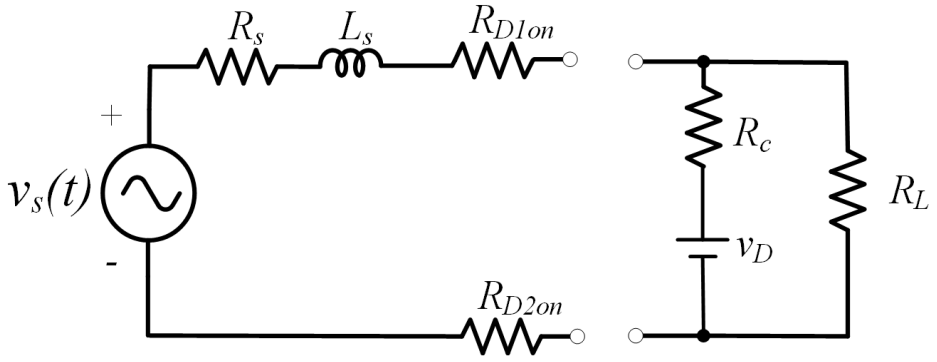

Figure 11 – State 3, adapted from (AMARAL, 2016).

coefficients of each spectral component, which in the following example it means up to the 13^{th} order. From the Superposition Theorem, a circuit is made with the fundamental voltage and the voltage of each of the 13 harmonics. Then, this analysis reaches and interesting conclusion. The power flow when at the fundamental frequency occurs from the grid to the rectifier. At higher frequencies, power flows from the rectifier to the grid. Therefore, part of the energy absorbed by the rectifier at the fundamental frequency is converted into grid losses at higher frequencies. This can be seen in the Figures 12 and 13, respectively. Finally, even if the grid voltage is as pure as possible, this losses will occur and it brings the importance of mitigating the harmonic distortion, because it will improve the Power Quality, subject of the next subsection.

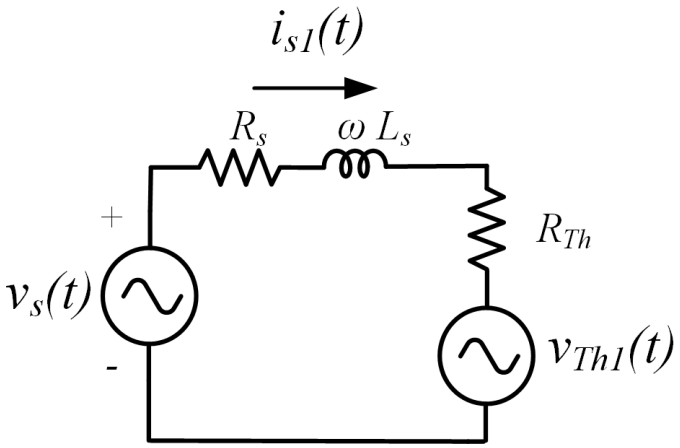

Figure 12 – Power flow from the grid to the rectifier at fundamental frequency, adapted from (AMARAL, 2016).

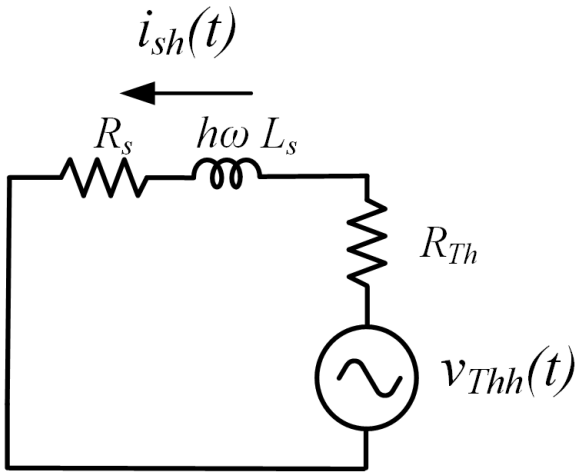

Figure 13 – Grid losses at higher frequencies, adapted from (AMARAL, 2016).

2.5.1 Power Quality

All agents involved in the generation, transmission, distribution or consumption of energy are interested in this matter. This is because the sensitivity of electrical equipment is increasingly pronounced from disturbances on the grid voltage (ANDREI et al., 2017). In addition, these same equipment can cause disturbances in the electrical grid through harmonics and electromagnetic interference, for example. Such disturbances contribute to poor Power Quality, as these affect the voltage supplied to consumers and, consequently, the operation of the equipment in the installation.

Power Quality is a subject that has been increasingly studied. In Brazil, as we have regulations for Power Factor like the ones found in (ANEEL, 2012), we have the Prodist module 8 for Power Quality (MARIANO, 2020). The consolidation of norms is extremely important in order to be possible to define the responsibilities for everyone involved in the electricity sector, from consumers, utility companies to electrical and electronic equipment manufacturers, in addition to applying penalties to those who fail to comply with these standards. On one hand, for example, IEC defined Power Quality on the IEC 61000-4-30 standard as "the characteristics of the electricity at a given point on an electrical system, evaluated against a set of reference technical parameters" (FAU; UFU, 2014). On the other hand, IEEE has defined it on the IEEE 100 (IEEE, 1996) as "a wide variety of electromagnetic phenomena that characterize the voltage and current at a given time and at a given location on the power system". However, this is best expressed lately as "voltage, current, or frequency deviations and subsequent failure, misoperation or premature aging of customer's equipment" (BANTRAS et al., 2012).

One might want to see in detail why this harmonic compensation of non-linear loads is important. The truth is that the distortion caused by the load is best seen in the current. However, as voltage and current are coupled electrical quantities, this distortion can also be seen indirectly in the voltage. An electrical system with high short-circuit capacity, means a rigid system, a strong grid. It means that the series impedance seen by the electrical source is very small, then voltage drops in the line impedances are small. It means that the *the current will have little impact on the voltage*. The following is an example illustrating this idea.

In Figure 14, the non-linear load drains a current with a very distorted waveform. As much as the grid voltage is sinusoidal, this current when passing through the line impedance causes a distortion in the voltage at the node in question. Thus, even though a second load in another branch is purely resistive, its current will also be distorted. This distortion will be greater or less depending on the magnitude of the current drained by the non-linear load and depending on the absolute value of the line impedance. If this impedance is high, the voltage drop in it will be greater and therefore more distortion. Briefly, the impact of a non-linear load on the degradation of Power Quality is direct on

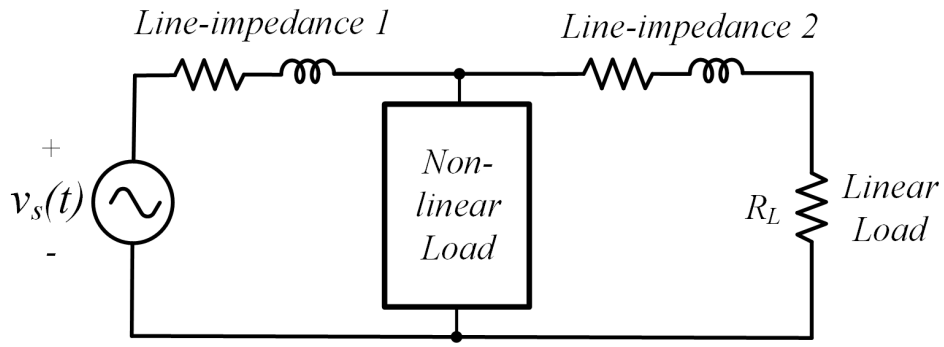

Figure 14 – Disturbance propagation caused by non-linear loads.

the current and indirect on the voltage. The spread of such disturbances occurs through voltage, since the harmonic currents can flow into any part of an AC system to which it is connected, as determined by the impedances of the various branches of the system at the harmonic frequency.

The harmonic distortion has been increasing, as well as the interest in it, due to financial aspects, which consists of losses for both consumers and distributors (AMARAL et al., 2015). There are several economic studies carried out in order to quantify this loss. The European Copper Institute (ECI) conducted a series of interviews and surveys over a period of two years in eight European countries, across different sectors of activity (BELEIU, 2011). It found out that costs due to unsatisfactory Power Quality in the analyzed countries represent over 25 billion of Euros in the EU economy for the year of study. Over 90% of these losses were in the industry sector. In (BELEIU et al., 2018), there is a recent study from 2018, which describes the economic effects on industry in three categories:

- Partial or total loss of one or more processes (e.g., loss of control due to a voltage sag);
- Poor long-term productivity or low product quality (e.g., because of employee fatigue due to flicker)
- Increased costs due to reduced equipment life, leading to premature failure (e.g., overheating of transformers due to harmonics).

The economic consequences of the Power Quality disturbances is summarized as in Figure 15, while Figure 16 brings the classification costs due to Power Quality disturbances.

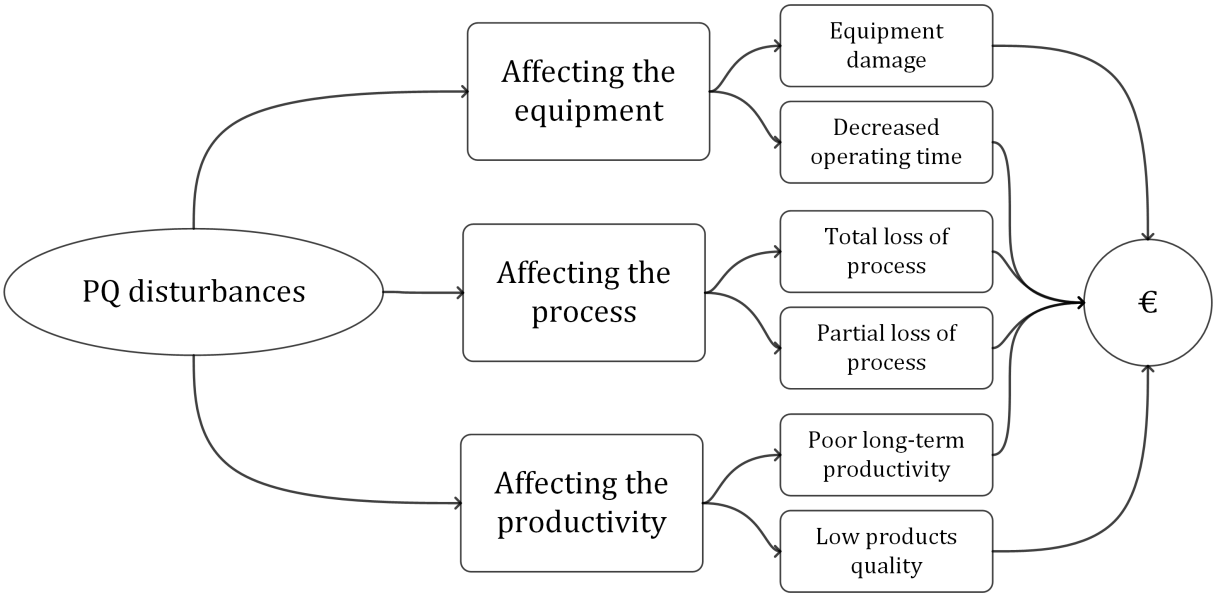

Figure 15 – Economic consequences of Power Quality disturbances, adapted from (BELEIU et al., 2018).

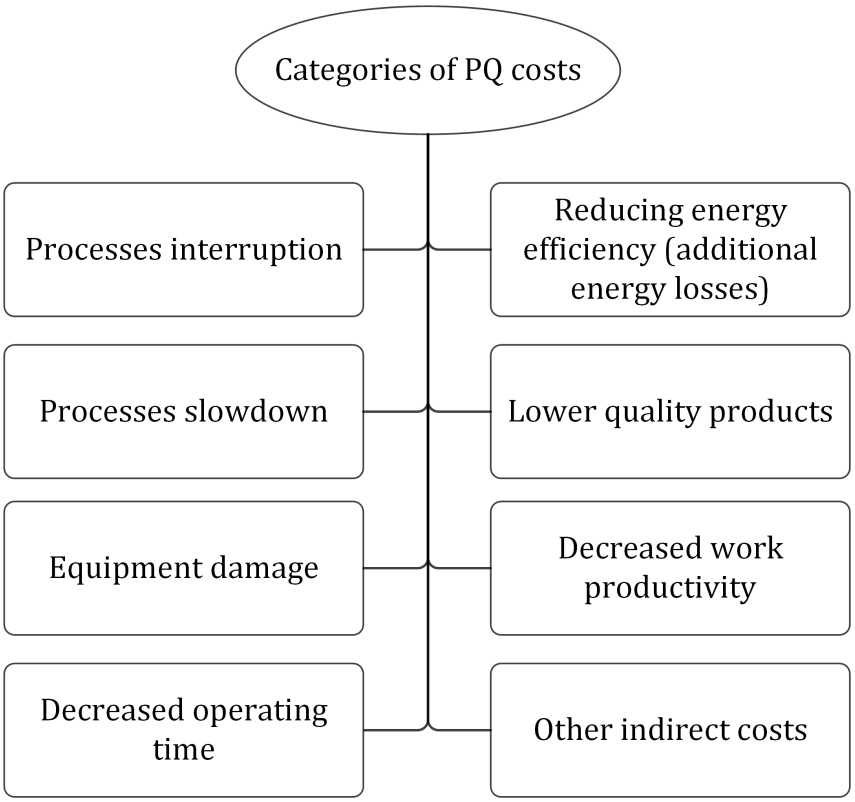

Figure 16 – Classification costs due to Power Quality disturbances, adapted from (BELEIU et al., 2018).

2.5.2 Conventional Solutions for Harmonic Distortions

First, before dealing with the active impedances technology, it is interesting to review more conventional solutions, which are consolidated and disseminated throughout the systems.

A three-phase 4-wire system provides a ground path for homopolar harmonics (3^{rd} and multiple), since they are zero-sequence. In the case of a delta connection, they circulate within the delta. All of this and the fact that there are resistive loads in the system help to make the waveform more sinusoidal. Successively, the power systems dilute the harmonics based on the presence of neutral conductors and transformers for the same previous reason. In short, the further upstream, the more sinusoidal. The more at the ends of the grid, the more distorted.

The most common solution for minimizing the inconveniences caused by the circulation of harmonic currents in a system is the installation of tuned passive filters. The intention is to create an alternative path for the circulation of these currents, avoiding their circulation upstream the system and consequent harmonic voltage distortions, additional losses in transformers and cables and possible resonances. In general, passive filters are formed by capacitors, inductors and resistors sized in a way that the resulting impedance is minimal at the frequency of the harmonic to be mitigated. Figure 17 brings an example illustrating the allocation of passive filters in a typical system, with one for the 5^{th} order, another for the 7^{th} and finally one for the higher order.

Another solution would be to use an electronic converter, i.e. active filter, in order to improve the Power Quality on the grid side. In this way, this would prevent the disturbances from spreading to other nodes. The concept of an active filter is to inject a waveform that is contrary to the disturbance of the load, so that they will cancel each other out as seen in Figure 18. Parallel devices improve current quality, while serial devices improve voltage quality. Usually, series filters have high current capacity, but reduced voltage capacity. In the parallel filter, the opposite occurs, with low current capacity and high voltage capacity. DERs are parallel elements and therefore act directly on the current and can indirectly affect the voltage. Figure 18a and figure 18b bring some simple examples.

2.6 Active Impedance

Active impedance is a distributed mitigation of harmonic distortions, which has been reported in several works. In (CHENG; LEE, 2015) is proposed the application of distributed parallel active filters controlled as harmonic conductances. In (KUO et al., 2007) is used this same technique in order to suppress resonances in industrial systems with power factor correction capacitors.

Active impedances technology consists of the synthesis of controlled voltage harmonic components, for instance, in quadrature with the current harmonic components present in the installation, inserting, in this case, reactances at the frequencies of interest. For this, a compensator based on a static power converter is used, whose coupling with the electrical system is made magnetically. In this way, there is the great benefit of the

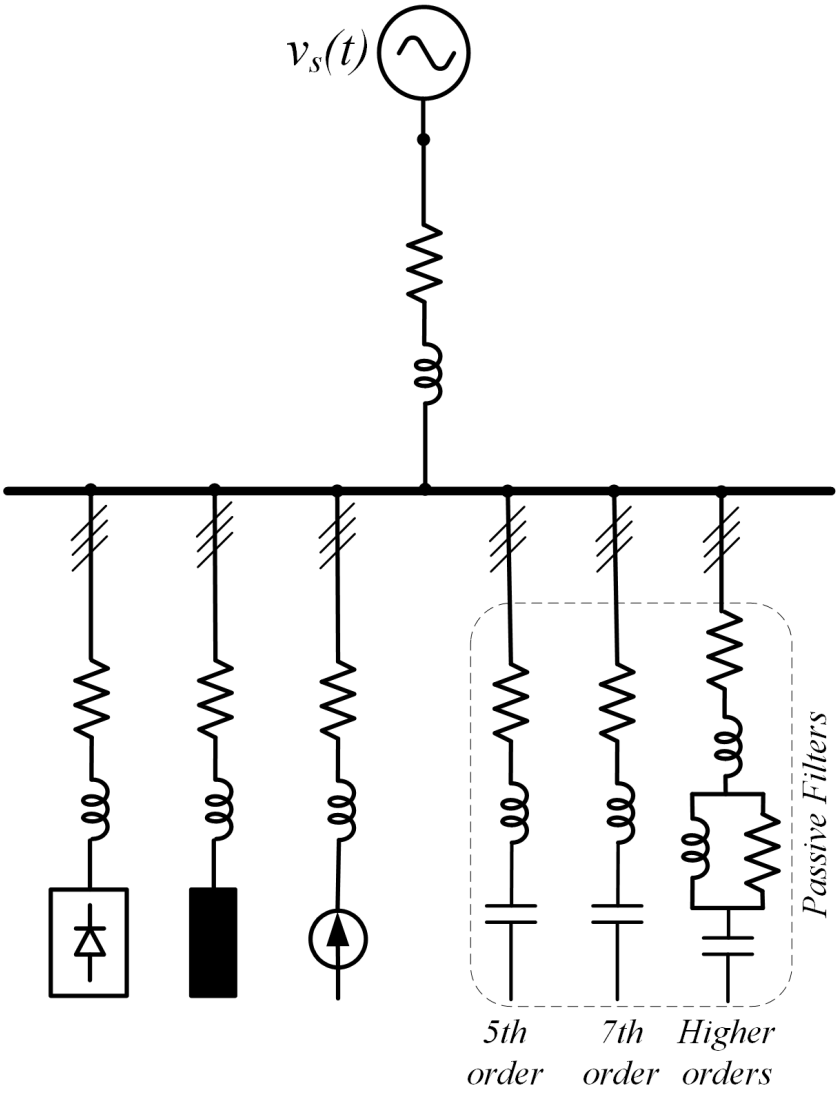

Figure 17 – Application of passive filters in a typical installation.

practicality of inserting this compensator wherever it is necessary in the system so that it has the desired performance, as it becomes modular. It is interesting to point out that this technique has a lot of versatility and can, therefore, emulate either a resistance, or an inductive or capacitive reactance. It will basically depend on the angle difference between voltage and current in the converter winding (AMARAL, 2016). In the case of a resistance, the filter must also be able to drain active power.

This technology can provide a multitude of applications. In the present study, the benefit verified was the improvement of THD and TDD of the network through harmonic routing management. It is interesting to determine a strategy for dynamically defining the reference values of harmonic inductances, based on the load current spectrum. Obviously, the set of inductances must be synthesized in such a way that the power corresponding is within the compensation limit of the static converter (AMARAL et al., 2015). Initially, the objective is to develop the Fourier analysis (FFT) of a microgrid system, in order to

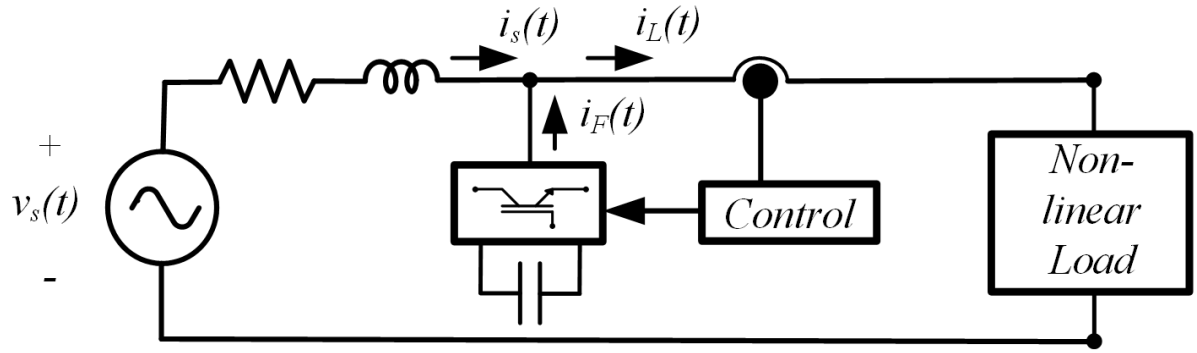

(a) Parallel active filter example.

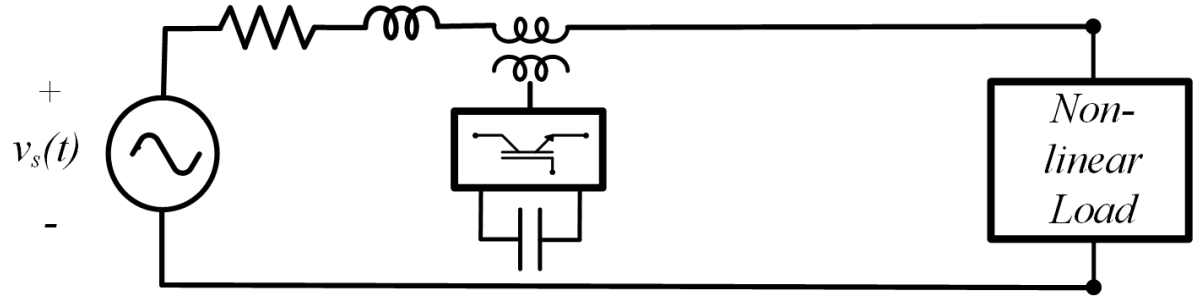

(b) Series active filter example.

Figure 18 – Active filter examples.

know its harmonics magnitudes. From there, inductances are emulated at these specific frequencies in order to reduce the current of these harmonics in the network. The mathematical formulation and algorithm for this are explained below for one of the phases:

- The current from the point of inserction and compensation on the power grid is measured;
- Harmonic analysis is performed using FFT to verify which harmonics need to be compensated, as well as which ones you want to compensate;
- Obtain the waveform of these harmonics of interest, as well as their amplitudes ($\mathrm{I}_h(t)$);
- The derivative signal for each of these harmonics is generated;
- The sum of all the inductances to be emulated correspond to the maximum inductance (L_{max}). For example, in order to emulate inductances for the 3^{rd}, 5^{th} and 7^{th} order harmonics it would be:

$$L_{max} = L_3 + L_5 + L_7 \tag{2.7}$$

- A weighted average from the maximum inductance that the converter in question is capable of emulating is performed between the amplitude of the harmonics to

be compensated. The greater each ones amplitude, the greater the corresponding inductance to be emulated. Using the same example as before, for each current (I_h) is obtained its inductance (L_h):

$$L_h = \frac{I_h(t)}{I_3(t) + I_5(t) + I_7(t)} \cdot L_{max} \tag{2.8}$$

- The voltage (v_h) corresponding to each of them is determined through the following equation:

$$v_h(t) = L_h \frac{di_h(t)}{dt} \tag{2.9}$$

2.6.1 Harmonic Routing

The harmonic current components of a non-linear load flow through the system impedances. In an installation like the one in Figure 19, this impedance is composed of cables, transformers and capacitor banks, and there may be more than one path for the circulation of harmonic currents of a non-linear load, with the one that offers the lowest total impedance being preferred. In the case of the rectifiers, one of the possible paths is towards the distribution network. In this case, the circulation of harmonic currents results in additional heat dissipation in the cable and transformer resistances and consequent unwanted overheating. Furthermore, harmonic voltages are produced in the busbars due to the circulation of harmonic currents through the impedances of these elements.

An interesting and important application would be to give a preferential path to unwanted harmonics, that is basically the *harmonic routing*. Since we have already defined obstacles for harmonics to flow towards the power grid, a preferential path can also be defined. Therefore, it uses the concept of hybrid filters. As a first step, active impedance is used in series with the power grid and a passive filter, for example, tuned to the frequency of unwanted harmonics in order to direct them to ground as seen in Figure 20. In this subject, (FRANÇA, 2013) brings a study concerning the development of series compensator for distributed harmonic mitigation and dynamic correction of power factor.

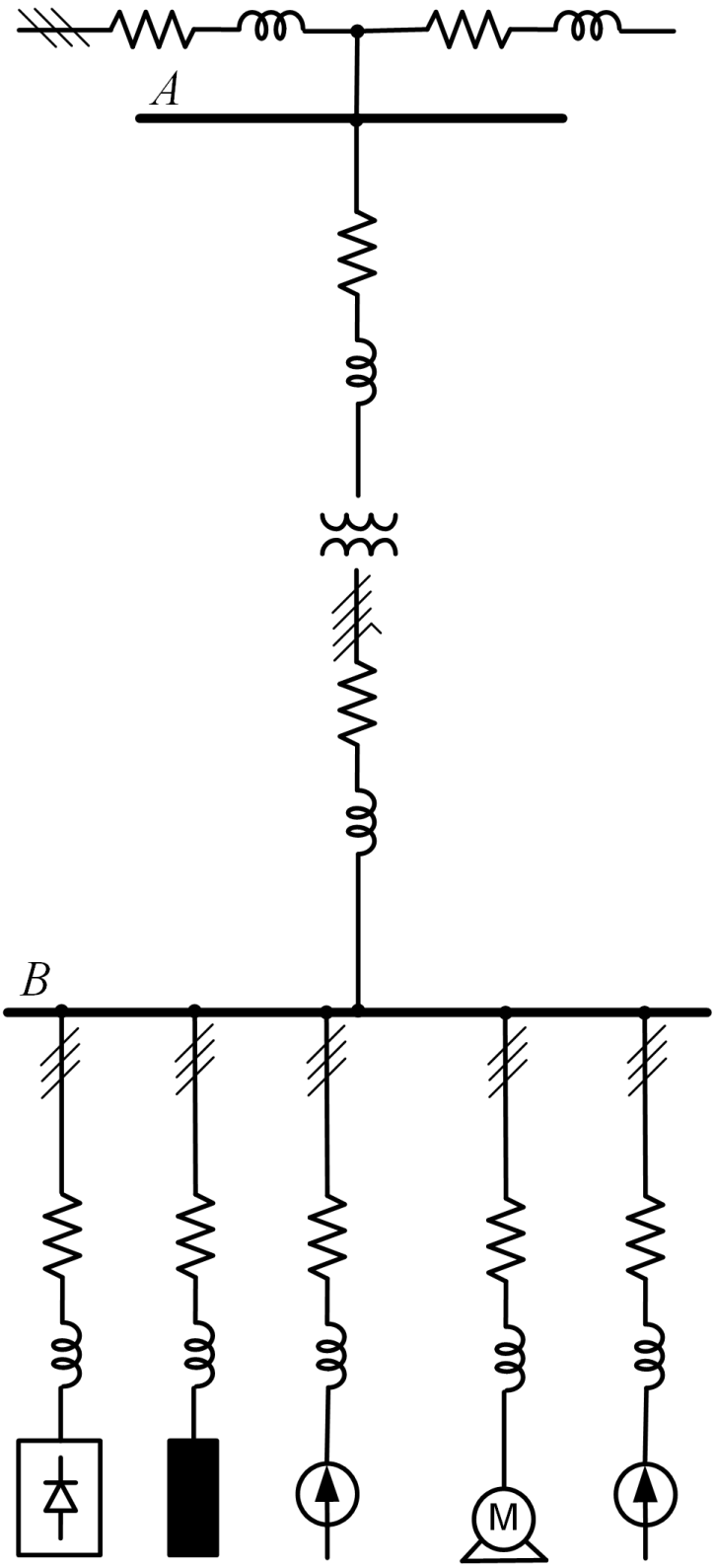

Figure 19 – Simplified diagram of a typical installation.

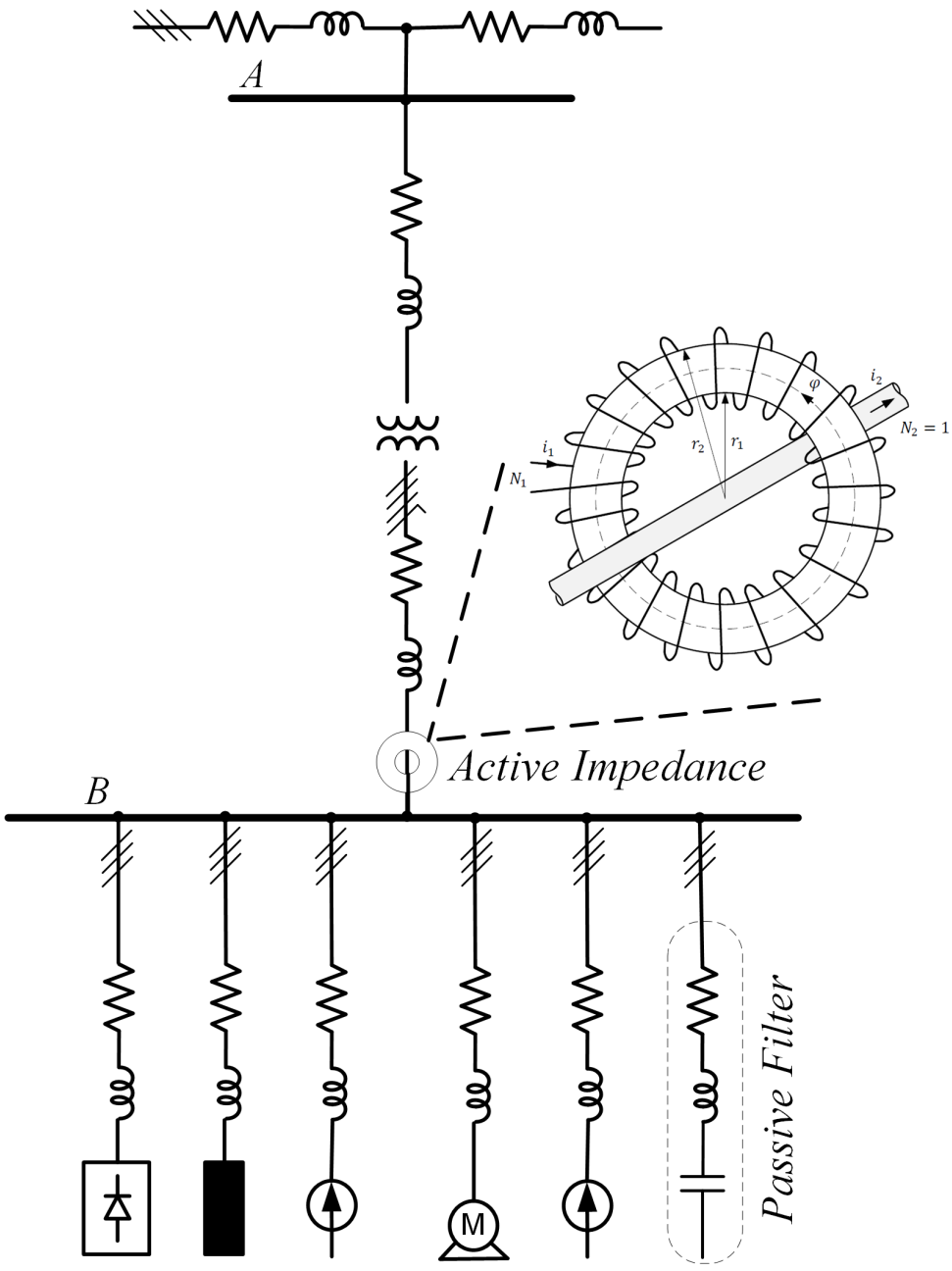

Figure 20 – Harmonic routing from the combination of active impedance and a passive filter resulting in a hybrid filter, adapted from (AMARAL, 2016).

2.7 Conclusion

In this chapter, a general summary of microgrids was initially addressed, where a preliminary idea of where their advances are standing, whether around the world or in Brazil, with several projects as examples. Then, the different classifications of microgrids are defined, in addition to their aspects such as energy storage, protection and architectures. Well-established conventional networks are compared with smart grids and the challenges and benefits that the latter imposes on us. An overview is made on harmonic distortions and then the concept of active impedance is introduced, in addition to its applicability.

3 Active Impedance Design and Control

This chapter presents a study on the turns of the transformer in its primary and secondary based on the converter power and the RMS voltage values of the harmonics to be compensated. Then, the design of the main components of the converter and the LC filter is discussed, in addition to the particularities that must be taken into account. Afterwards, a study is made on the control loops on the AC side of the converter using PI and repetitive controllers, how they work complementary. Finally, the control on the DC side of the converter is studied. In every control study, the important aspect of the dynamic stiffness takes place for its validation.

3.1 Coupling Transformer

The need to establish low-voltage values allows the use of a secondary winding with only one turn, this turn being the cable or busbar of the electrical system where harmonic suppression is desired (PIRES; FRANÇA; CARDOSO, 2014). In addition, the use of a toroidal core adds modularity and great ease of installation and maintenance of the compensator, eliminating any type of sectioning for connection. Detailed study regarding the losses of this transformer, whether in its core or windings, in addition to the determination of all its parameters can be seen thoroughly in (AMARAL, 2016).

Briefly, the transformer primary windings is considered to be the voltage generated by the converter, while the secondary is the voltage actually applied to the circuit ($V_{2,rms}$). This RMS voltage is obtained considering the voltage of each harmonic to be compensated (V_h). To determine the maximum voltage that the converter is capable of emulating, we have Equation 3.1.

$$V_{2,rms} = \sqrt{\sum_{h=1}^{\infty} {V_h}^2} \tag{3.1}$$

The RMS voltage at the transformer primary, $V_{1,rms}$, can be chosen by the designer and makes it possible to determine the number of turns of the primary (N_1), as seen in Equation 3.2. The determination of the RMS primary voltage must be made based on the nominal currents and voltages of the switches used in the inverter and the bypass switch (AMARAL, 2016).

$$N_1 = \frac{V_{1,rms}}{V_{2,rms}} \tag{3.2}$$

Meanwhile, the rated current of the transformer primary, $I_{1,rms}$, is given by Equation 3.3.

$$I_{1,rms} = I_{2,rms} \cdot \frac{1}{N_1} \tag{3.3}$$

The transformer design and other elements of the compensator will be based on a case study. It is important to remember that, in addition to the harmonic voltage components offset by 90^o from the respective currents, it is necessary to synthesize the fundamental component in series with the fundamental current, in order to provide active power to supply the losses in the compensator elements. A detailed discussion of this aspect will be made later. Considering, therefore, that the components of the 3^{rd}, 5^{th}, 7^{th}, 9^{th}, 11^{th} and 13^{th} harmonics will be emulated, the compensator must synthesize as in Equation 3.4:

$$V_{2,rms} = \sqrt{{V_1}^2 + {V_3}^2 + {V_5}^2 + {V_7}^2 + {V_9}^2 + {V_{11}}^2 + {V_{13}}^2} \tag{3.4}$$

3.2 Converter Design

The rated power required for the active filter is defined by (AKAGI, 2005) as in Equation 3.5:

$$|S_{AF}| = \sqrt{3} \cdot \frac{V_{DC}}{\sqrt{2}} \cdot \frac{I_{AF}}{\sqrt{2}} \tag{3.5}$$

Where:

- V_{DC} – DC link Voltage of the active filter;
- I_{AF} – Transformer primary peak current of the active filter;
- S_{AF} – Apparent power of the active filter.

To determine the maximum inductance that the converter is capable of emulating, the previous rated power is used and an inductance emulated at the fundamental frequency (f) is estimated. As part of the converter's power is destined to supply losses in both its components and its switching, it is arbitrated that about 90% of its power would be available for the purpose of interest, as follows in Equation 3.6:

$$L_{max} = 0.9 \cdot \frac{{V_f}^2}{2\pi f \cdot S_{AF}} \tag{3.6}$$

3.3 LC Filter Design

Figure 21 shows the inverter and the output filter in a simplified way. Such circuit has the following equations 3.7, 3.8 and 3.9:

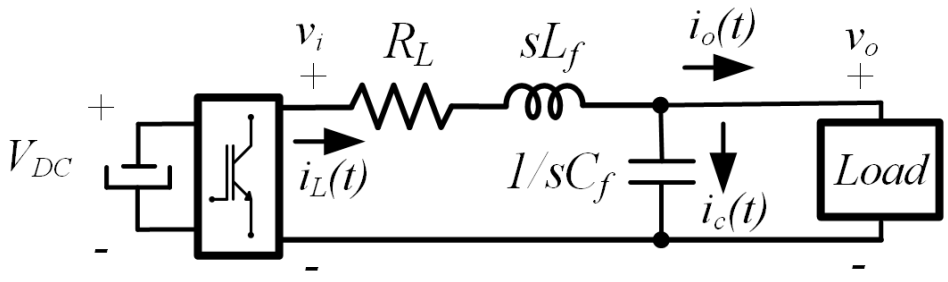

Figure 21 – Basic inverter model with output filter.

$$i_L(t) = i_o(t) + i_c(t) \tag{3.7}$$

$$i_L(t) = \frac{v_i(t) - v_o(t)}{R_L + L_f \frac{di_L(t)}{dt}} \tag{3.8}$$

$$i_c(t) = C_f \frac{dv_o(t)}{dt} \tag{3.9}$$

The application of the Laplace Transform and the rearrangement of the terms allows the representation in a block diagram as shown in Figure 22.

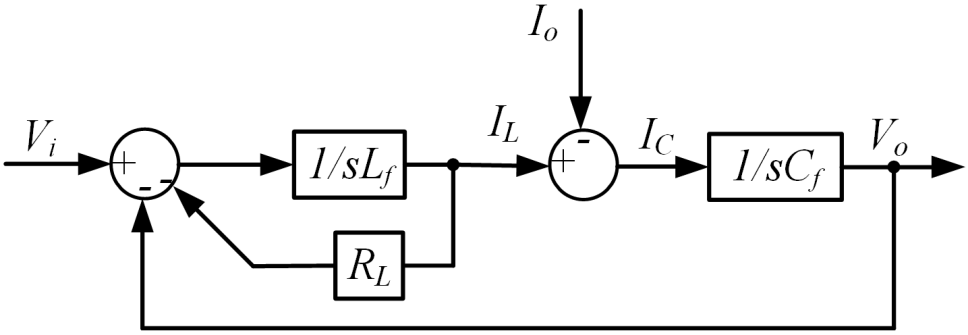

Figure 22 – Block diagram representation of inverter and filter.

For the output voltage to be sinusoidal, it is necessary to use at least one LC filter, in order to eliminate the switching ripple. The LC is a second order filter, with an attenuation equal to 40 $dB/decade$, so that a separation of a decade between the cutoff frequency and the switching frequency reduces the impact at the output from the

switching ripple (SILVA, 1999). The relationship between the filter's cutoff frequency and its parameters is shown in Equation 3.10:

$$f_c = \frac{1}{2\pi\sqrt{L_f C_f}} \tag{3.10}$$

Once the cutoff frequency of the LC filter is defined, there is an infinite variety of inductance and capacitance values that can satisfy the previous equation. It is important to note that the higher the capacitance, the better the voltage filtering, but there will be an increase in the power demanded from the electronic converter. A commonly adopted design criterion is to limit the LC filter capacitive branch current to between 10 to 15% of the converter rated current (SILVA, S. M.; FILHO, 2002). The following Equation 3.11 defines the filter capacitor.

$$C = \frac{kS_n}{6\pi f V_{ph}^2} \tag{3.11}$$

Where:

- S_n – Three-phase converter power;
- V_{ph} – Converter phase voltage;
- f – Fundamental electrical frequency;
- k – Percentage of LC filter reactives.

3.4 Converter Control

Considering the system in question, Figure 23 illustrates a typical control diagram that can be applied to inverters that operate as an series active filter. The diagram can be applied to single-phase and three-phase topologies. The converter operates in closed loop, and the voltage loop has a PI controller, k_{pv} and k_{iv}, which generates a reference for the faster and more internal current loop, which uses only a proportional controller, k_{pi}.

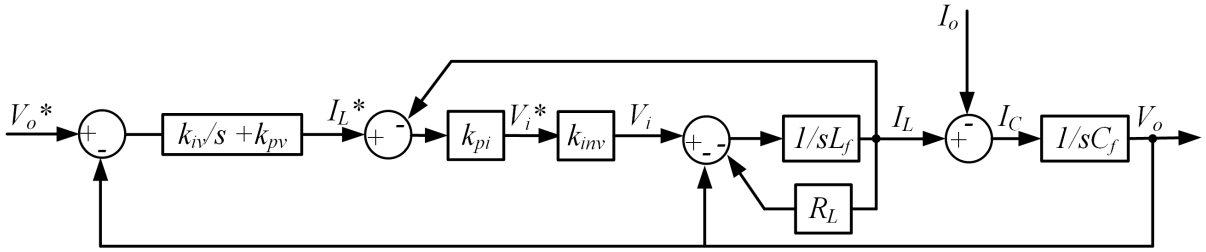

Figure 23 – Cascade control of inverter output voltage.

The conventional diagram would have limitations due to characteristics of the plant itself, which implies a misuse of the controllers. Since the current, I_L, and the voltage, V_o, are measured quantities for the implementation of the control system, a significant improvement in this system would be obtained through the use of such values for the compensation of the internal feedbacks (SILVA, 1999). In the case of I_L, the parasite resistance of the inductor is estimated ($\hat{R}_L$) and its loss compensated. Furthermore, sudden variations in the load current, I_o, are corrected by the current control loop only from the moment they cause variations in the output voltage, V_o, so that the system dynamics is restricted to the operation of the voltage loop. In this sense, a significant improvement in the performance of this control loop can be obtained from the use of I_o measurement to compensate its disturbance previously. These topics can be seen Figure 24. Operating the inverter with a sufficiently high switching frequency (much higher than the frequency of I_o and V_o, which means about ten times) allows considering $k_{inv} = 1$.

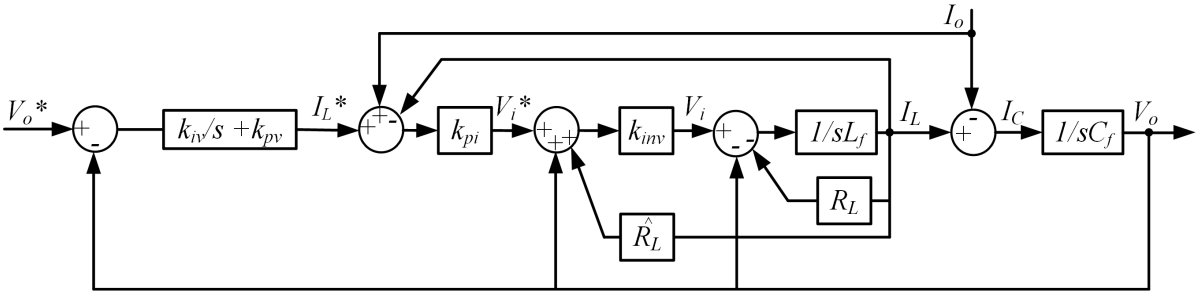

Figure 24 – Simplified system representation with internal feedback and disturbance compensations.

In order to improve the reference voltage tracking, it is implemented a repetitive controller. The repetitive controller emerged from the need to elimination of load disturbances and the tracking of periodic references in control systems (OLIVEIRA et al., 2013). This mainly improves the severe limitation of the conventional control of having frequency-dependent angular lag response. This controller is based on the principle of the internal model (BRITAIN, 2015), which establishes that for a system to have zero error in steady state in the presence of any reference or load disturbance, the input signal models must be present in the stable closed-loop control system. As an example, for a system with step inputs (1/s) to have zero error in steady state, an integrator must be present in the stable closed loop of the system. This concept can be extended to systems that have periodic inputs. In this case, the harmonic components of the input signal are presented in Equation 3.12:

$$c_k = \frac{k\omega_0}{s^2 + (k\omega_0)^2} \tag{3.12}$$

Where k = 1, 2, 3, ... ∞ and ω_0 is the fundamental frequency (rad/s), must be positioned in the stable closed loop of the system, in a structure similar to Figure 25. In

this figure, there are poles at $\omega_0 k$ for k = 1, 2, 3... ∞. The resonant filter bank structure works like an integrator for each of the frequencies, which allows to eliminate steady-state error at these frequencies.

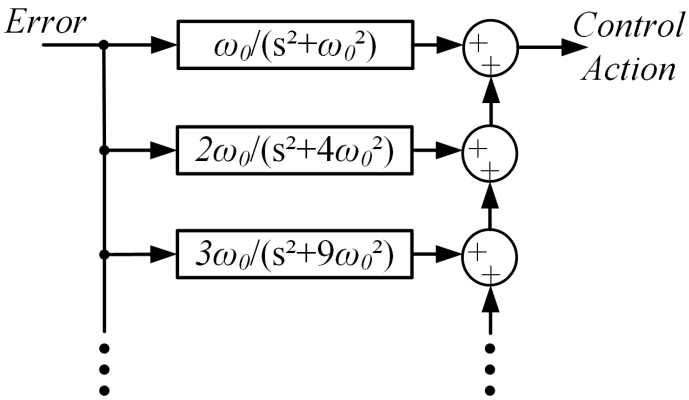

Figure 25 – Controller based on the principle of the internal model applied to systems with periodic inputs and filter association resonant, adapted from (OLIVEIRA et al., 2013).

The implementation of this structure may become impracticable since the number of harmonic components in the signals input becomes excessively large. That is where repetitive control takes place as an alternative. The repetitive controller enables the implementation of the internal model principle for systems with periodic inputs by delaying a fundamental period of the input signal (T_0) positioned in a negative feedback loop, as illustrated in Figure 26.

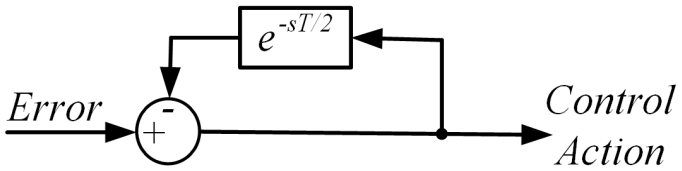

Figure 26 – Repetitive controller block diagram for odd harmonics, adapted from (OLIVEIRA et al., 2013).

The repetitive controller is positioned parallel to the voltage loop as seen in Figure 27. To guarantee a stable operation of the repetitive controller, a low-pass filter (LPF) is used, in order to adapt the bandwidth that the converter can operate (CHEN et al., 2008). The chosen LPF is of second order and with a cutoff frequency equal to that of the voltage loop, since it is necessary for the filter to have a cutoff frequency lower than the one of the current loop. Furthermore, it is necessary to define the gain k_r, in order to provide, together with the proportional action of the voltage loop controller PI, fast response in transient conditions. However, high values of this gain can make the control loop unstable. Thus, its value should be as high as possible as long as it does not cause instability in the control loop or saturation of the PWM inverter. Another point that

should be highlighted is that the filter must have a null phase characteristic, to avoid poles displacement of the repetitive controller. For this, a phase advance was performed using the *Padé Approximation* (ANTUNES, 2018).

In the present study, for the time delay (e^{-s}), the use of its first-order function as seen in the Equation 3.16 was sufficient for satisfactory results, in order to carry out this correction. In case of an even more rigorous study, i.e. a better approximation, the second or third order equations could be used, as seen respectively in Equation 3.17 and Equation 3.18. Both the k_r gain and the phase advance were obtained through simulation considering what was discussed in the previous paragraph. To adjust the phase correction, it was calculated a certain amount of delay samples on the repetitive controller. It was implemented as follow in Equation 3.13:

$$\phi_c = z^{(-n+N_a)} \tag{3.13}$$

Where:

$$n = \frac{T}{2 * T_{sw}} \tag{3.14}$$

$$N_a = T_s t / T_{sw} \tag{3.15}$$

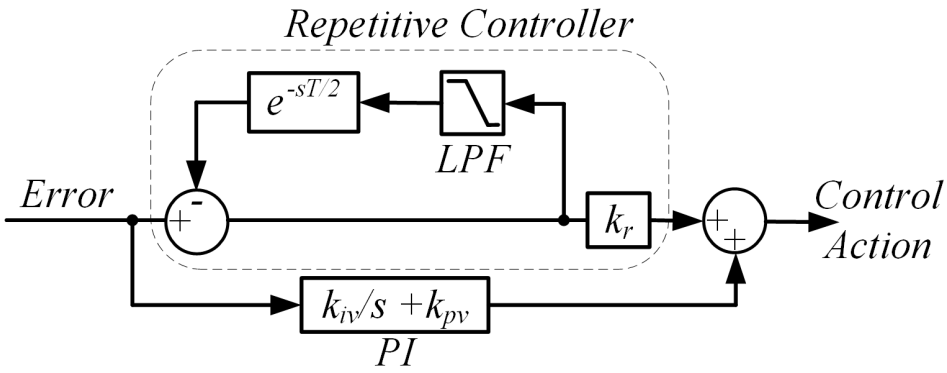

Figure 27 – Controller composed of repetitive controller for odd harmonics and PI controller, adapted from (OLIVEIRA et al., 2013).

$$R_1(s) = \frac{-s+2}{s+2} \tag{3.16}$$

$$R_2(s) = \frac{s^2 - 6s + 12}{s^2 + 6s + 12} \tag{3.17}$$

$$R_3(s) = \frac{-s^3 + 12s^2 - 60s + 120}{s^3 + 12s^2 + 60s + 120} \tag{3.18}$$

Finally, the complete control loop is found in Figure 28, the voltage loop with PI is in parallel with the repetitive controller branch, LPF and n quantity of delay samples for phase correction. Internally, there is the current loop with a proportional controller.

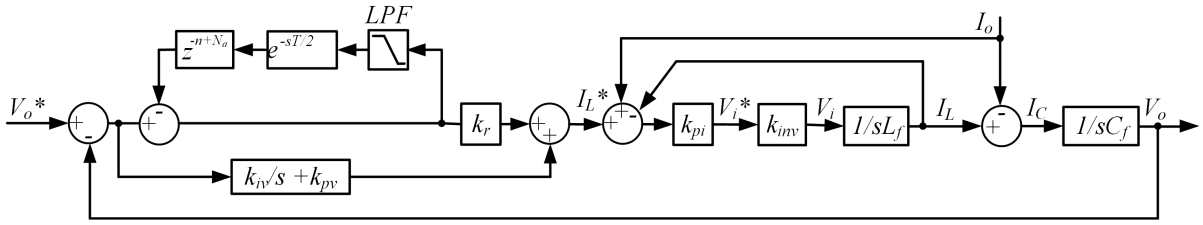

Figure 28 – Complete control loop.

Many control techniques aim solely for the controlled variable to follow a reference value. However, it is extremely important to analyze the system's ability to reject external disturbances. This characteristic can be evaluated from its dynamic stiffness, given by the relationship between the load current I_o and the output voltage V_o when the voltage reference is zero ($V_o^* = 0$). The transfer function is shown in Equation 3.19:

$$\frac{I_o}{V_o}\bigg|_{V_o^*=0} = -\frac{s^2 L_f C_f + C_i(s) C_f + C_i(s)[R(s) + C_v(s)]}{sL_f} \tag{3.19}$$

Where:

$$C_v(s) = k_{pv} + \frac{k_{iv}}{s} \tag{3.20}$$

$$C_i(s) = k_{pi} \tag{3.21}$$

$$R(s) = \frac{k_r}{1 + e^{-\frac{sT}{2}}} \tag{3.22}$$

Therefore, ω_i, $\omega_{v(1)}$ and $\omega_{v(2)}$ (with $\omega_i > \omega_{v(2)} > \omega_{v(1)}$) constitute the frequencies of the zeros of the dynamic stiffness function $|I_o/V_o|$. So that there is no degradation of the dynamics of controllers designed for lower switching frequencies, the pole frequency ω_i is assigned a value 5 times smaller than the switching frequency ω_{sw}. The ratio between adjacent poles is also set at 5, so that the dynamic stiffness at frequencies around 60 Hz was higher (COTA, 2016). This allocation criterion is summarized in Table 2.

To calculate these gains, the equations 3.23, 3.24 and 3.25, seen in (ANTUNES, 2018), were used. The expected result for the dynamic stiffness disregarding repetitive control is found in Figure 29.

$$k_{pi} = \omega_i L_f \tag{3.23}$$

Table 2 – Summarizing the methodology of the allocation of poles.

Variable	Premise
Switching frequency	ω_{sw}
Pole frequency of the current loop (ω_i)	$\omega_{sw}/5$
Second pole frequency of the voltage loop ($\omega_{v(2)}$)	$\omega_i/5$
First pole frequency of the voltage loop ($\omega_{v(1)}$)	$\omega_{v(2)}/5$
LC filter cutoff frequency (ω_c)	$\omega_{sw}/5$

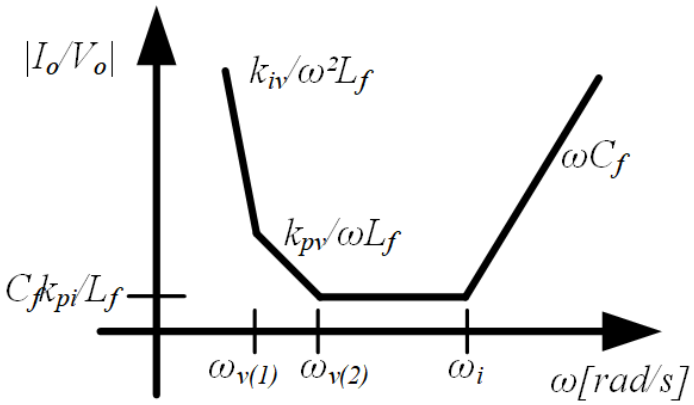

Figure 29 – Asymptotes in dynamic stiffness, adapted from (COTA, 2016).

$$k_{pv} = (\omega_{v(1)} + \omega_{v(2)})C_f \tag{3.24}$$

$$k_{iv} = \omega_{v(1)}\omega_{v(2)}C_f \tag{3.25}$$

3.5 DC Link Design

The simplified DC link is shown in Figure 30 and the DC side currents will be discussed next. The initial criterion for its minimum capacitance is based on the maximum allowable voltage variation in relation to the established nominal voltage, which is considerated here as 5% (AMARAL, 2016), then in Equation 3.26:

$$\Delta V_{DC} = 0.05 \cdot V_{DC} \tag{3.26}$$

It is up to the applicability and the designer which harmonics will be compensated by the converter. Regardless of the composition of harmonic voltage, the DC link must be continuously regulated, as discharge occurs due to the energy used to supply losses in the converter. In this work, the proposal is that the energy necessary for its operation is absorbed from the power grid itself by the synthesis of fundamental voltage in phase with the fundamental current, emulating a resistance at this frequency. The greater the

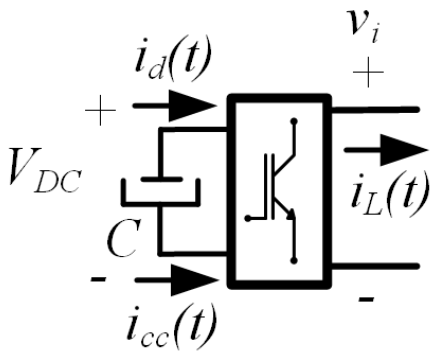

Figure 30 – Currents on the DC link, adapted from (AMARAL, 2016).

voltage amplitude, the greater the resistance value and, consequently, the active power drained.

The gain k_{DC} is obtained considering that the current in the DC link is composed of two parcels. The portion i_{cc} is responsible for the charge on the capacitor, and is directly related to the voltage synthesized by the compensator at the fundamental frequency. On the other hand, the portion i_d is related to the active power drained from the bus to supply the losses in the compensator elements. The voltage on the DC link must be set to a predetermined nominal value, V^*_{DC}. Comparing this value with the measured voltage, V_{DC}, and using a proportional controller, k_{DC}, which provides the amplitude of the fundamental voltage to be synthesized. Currents seen in Figure 30 are related to the voltage V_{DC} as shown in the block diagram in Figure 31.

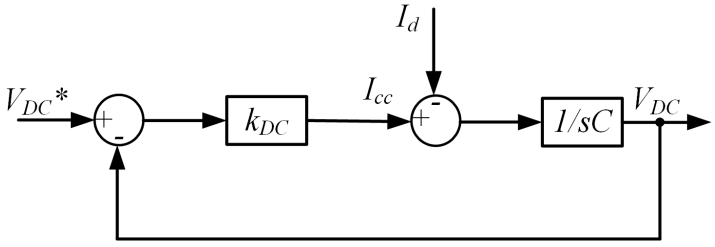

Figure 31 – Block diagram for the voltage control on the DC link, adapted from (AMARAL, 2016).

The closed loop transfer function and the dynamic stiffness of this loop are given by Equations 3.27 and 3.28 respectively.

$$\left.\frac{V_{DC}}{V^*_{DC}}\right|_{I_d=0} = \frac{k_{DC}}{sC + k_{DC}} \tag{3.27}$$

$$\left.\frac{I_d}{V_{DC}}\right|_{V^*_{DC}=0} = -(sC + k_{DC}) \tag{3.28}$$

Therefore, Figure 32 shows, in block diagram form, the obtention of v_{h1}. The determination of the fundamental frequency angle is done by a simple *PLL algorithm* (AMARAL, 2016).

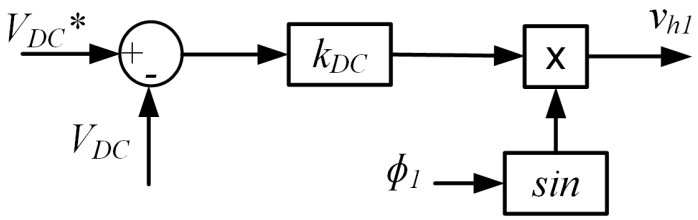

Figure 32 – Block diagram model for generating the reference voltage at the fundamental frequency, adapted from (AMARAL, 2016).

3.6 Voltage Reference

The voltage to be synthesized by the compensator can include multiple harmonic components, depending on the dynamics of the system where it is installed. The generation of voltage references at harmonic frequencies must be done so that the emulated impedance is purely inductive, according to Equations 3.29 and 3.30. Here, h is the harmonic order; L_h represents the inductance to be synthesized; v_h and i_h voltage and current of the corresponding harmonic; ϕ_h is the phase angle. Figure 33 shows the implementation of the voltage reference in block diagram form, considering the fundamental frequency and the other ones of interest.

$$v_h = L_h \cdot \frac{di_h}{dt} = L_h\sqrt{2}I_h h\omega \cdot sin\Big(h\omega t + \phi_h + \frac{\pi}{2}\Big) = L_h\sqrt{2}I_h h\omega \cdot cos(\Phi_h) \tag{3.29}$$

$$\Phi_h = \omega t + \phi_h \tag{3.30}$$

Electrical systems are basically made up of sine or cosine waves. This brings a range of very important benefits for us mathematically speaking. One of these points is precisely the derivative of these functions. The derivative of a sine function is basically its displacement in time of 90^o in addition to having its magnitude multiplied by its angular velocity. Details on obtaining the derivative of the signal are shown on Appendix A.

3.7 Harmonic Distortion Study

In the next chapter of *results*, several studies will be carried out. Among them, simulations in relation to the THD of a given case study. It is calculated as shown in

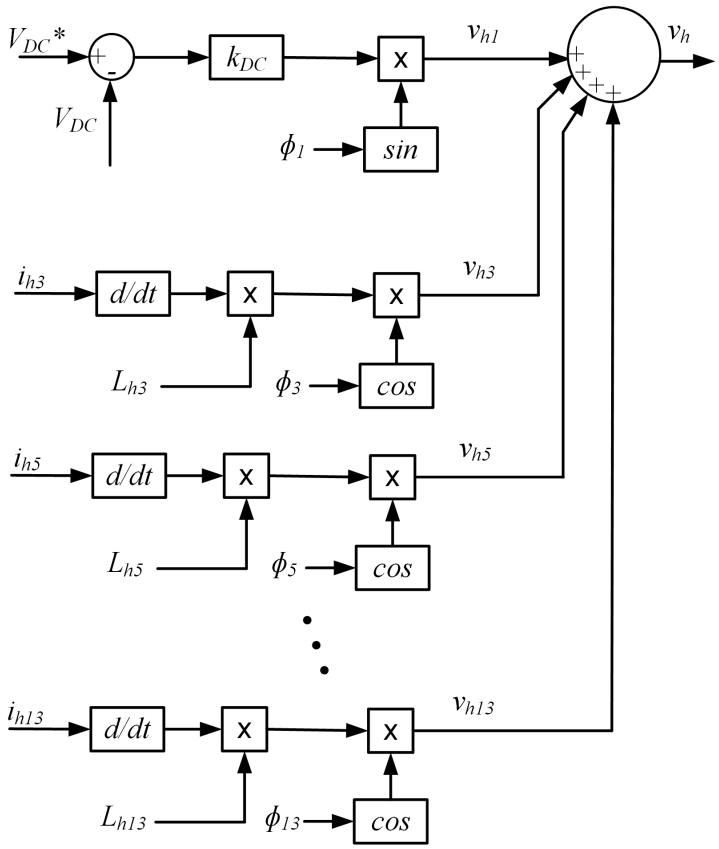

Figure 33 – Block diagram model showing voltage reference generation containing fundamental, 3^{rd}, 5^{th} and further harmonics, adapted from (AMARAL, 2016).

Equation 3.31.

$$THD = \frac{I_H}{I_F} = \frac{\sqrt{{I_2}^2 + {I_3}^2 + ... + {I_n}^2}}{I_F} \tag{3.31}$$

Where:

- TH – RMS value of the harmonics above the fundamental;
- I_n – RMS value of the harmonic n;
- I_F – RMS value of the fundamental current.

Another important measure for distortion value is the Total Demand Distortion (TDD). Unlike THD, TDD is the harmonic current distortion given in % of maximum load demand (I_L) and for this current is considered the fundamental frequency component at PCC. It condenses harmonic information in a current waveform without depending on the time function of the waveform. It is the calculated harmonic current distortion in an

electrical system against the full load demand. It can be mathematically expressed as in Equation 3.32. Both concepts can be seen in detail in (IEEE, 2014).

$$TDD = \frac{I_H}{I_L} = \frac{\sqrt{{I_2}^2 + {I_3}^2 + ... + {I_n}^2}}{I_L} = THD \cdot \frac{I_1}{I_L} \tag{3.32}$$

When it comes to current harmonics, it can not completely rely on the current THD index, as the fundamental current changes with load variations. Current in the circuit or system can be full load current for a duration of time or can get reduced according to the load. Considering the load variations in the circuit or system, it is not advisable to follow the current THD, which is the ratio of summation of current harmonics to the fundamental current. Current distortions are instead measured using TDD.

A high THD value with low TDD indicates any harmonic effects on the system are insignificant. At full load, THD and TDD values are equal and this is a matter of serious Power Quality concern. TDD can describe the current distortion as a percentage of full load demand current and it is the best Power Quality index to explain current harmonics at the consumer end. The TDD value provides information regarding the linearity of the load connected to an electrical system. Current distortion is less when the loads are linear, therefore, the TDD value is low in those cases. When the load introduces non-linearity to the system, the TDD value increases. If the percentage of non-linear loads is small compared to the full system load demand, TDD is less.

3.8 Conclusion

In this chapter, it was explained how to determine the transformer turns from the value of the RMS voltage seen by the secondary of the transformer, which are a consequence of the value of the RMS voltage of each one of the harmonics to be compensated. The converter power is projected from the voltage on the DC link and the peak current of the active filter. For the LC filter, the capacitance value is determined primarily and then the inductance value, which is a consequence of the value chosen for the cutoff frequency of the filter. It is shown in detail all the loop control, its equations and curves. The starting point was the classic cascade control and its limitations. Next step, was to improve the control system by compensating its internal feedbacks. This strategy is simple, yet of great value. Then it is shown the resonant control, its benefits and limitations. Finally, it is implemented the repetitive controller. The DC Link is studied therefore completing the control loop. The voltage reference for each harmonic stands out, as well as their respective inductance and how it is obtained. At the end, a comparison between THD and TDD is made, as well as its possible interpretations.

4 Simulation Results

This chapter brings the results arising from the topics that were discussed throughout this work. All results described here were obtained through simulation using the software MATLAB/Simulink®. The first step here was to establish a case study with a microgrid. Through it, it is possible to draw different conclusions about the application of active impedance technology. The design and definition of each part of the system is done based on the step by step found in the methodology.

4.1 Case Study

The case study is based on a microgrid that was presented in (ANTUNES et al., 2018). This power electrical system is an example of a three-phase four-wire centralized AC microgrid, which has its electrical parameters in Table 3 and can be seen in Figure 34.

The analyzed system operates in grid-connected mode and it is composed of linear and non-linear loads, a passive filter and a grid-feeding converter, which is the DER. The performance and control of a hybrid filtering system, in relation to compensation of current and voltage harmonic distortion at PCC is evaluated.

Table 3 – Electrical parameters of the studied microgrid.

System	Characteristics
Power grid	220 V; 60 Hz; $S_{sc} = 750\ kVA$; $X/R = 0.5$
Linear load	220 V; 35 kVA; $p.f. = 0.73$ lagging
Non-linear load	220 V; 30 kW; 6 $kVAr$; $L_{NL} = 0.1\ mH$; $C_{NL} = 18.8\ mF$; $R_{NL} = 2.5\ \Omega$
Active filter	$f_c = 4.8\ kHz$; $C_f = 20.88\ \mu F$; $L_f = 52.64\ mH$; $R_f = 49\ m\Omega$; $C_{DC} = 12\ mF$
Passive filter	220 V; $5^{th}: Q_5 = 42$; $L_5 = 2.7\ mH$; $C_5 = 105\ \mu F$ $7^{th}: Q_7 = 42$; $L_7 = 1.3\ mH$; $C_7 = 107\ \mu F$ $11^{th}: Q_{11} = 2.2$; $L_{11} = 0.5\ mH$; $C_{11} = 109\ \mu F$
DER	18 kVA; $p.f. = 1$, more details on Appendix B

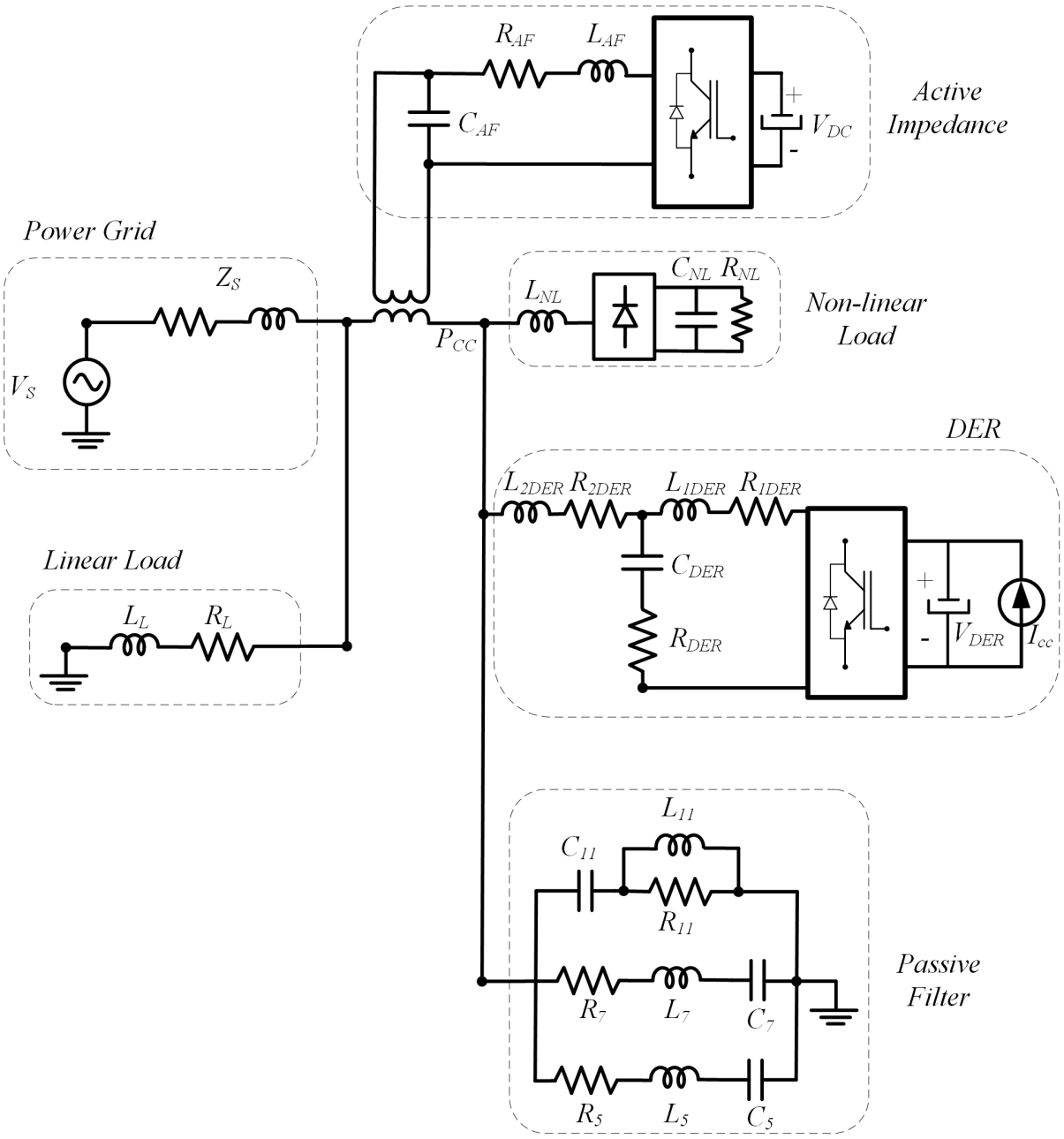

Figure 34 – Three-phase balanced centralized microgrid with four wires, adapted from (ANTUNES et al., 2018).

4.2 Transformer Turns

After defining the series active filter power and simulating the microgrid in question, the following RMS values for the harmonic components were obtained and summarized in Table 4. Each voltage value is determined by the respective emulated inductance at each frequency of interest. This inductance, in turn, is obtained from the weighted average of the currents of each harmonic as seen in the previous chapter.

Table 4 – RMS voltage of the harmonic components.

Harmonic	RMS Value
Fundamental	11.47 V
3^{rd}	≈ 0 V
5^{th}	1.73 V
7^{th}	0.81 V
9^{th}	≈ 0 V
11^{th}	3.70 V
13^{th}	2.31 V

In view of the previous result, the voltage to be emulated by the converter corresponds using the Equation 3.4 is equal to 12.42 V on its secondary.

$$V_{2,rms} = \sqrt{11.47^2 + 0^2 + 1.73^2 + 0.81^2 + 0^2 + 3.70^2 + 2.31^2} = 12.42\ V \tag{4.1}$$

Considering a nominal voltage of 220 V in the primary and the RMS value on the secondary of 12.42 V, it is obtained the transformer turns using the Equation 4.2:

$$N_1 = \frac{220}{12.42} \approx 18 \tag{4.2}$$

The crest factor is the ratio of the peak value and the true RMS value as shown in Equation 4.3:

$$k = \frac{V_{2,pk}}{V_{2,true-rms}} = \frac{25.03}{12.69} = 1.97 \tag{4.3}$$

For the value of its current in the primary, we have the Equation 4.4.

$$I_{1,rms} = I_{2,rms} \cdot \frac{1}{N_1} = 74.97 \cdot \frac{1}{18} \approx 4.17\ A \tag{4.4}$$

4.3 Converter Values

As seen on Equation 3.5, we have the values for the case study:

- $V_{DC} = 400\ V$ – Voltage in DC link of the active filter;
- $I_{AF} = 3.67\ A$ – Peak current of the active filter;
- $S_{AF} = 1.27\ kVA$ – Apparent power of the active filter.

4.4 LC Filter Values

As seen on Equation 3.10, we have the values for the LC filter:

- $S_{3\phi} = 1.27\ kVA$ – Apparent converter power;
- $V_f = 127\ V$ – Converter phase voltage;
- $f = 60\ Hz$ – Fundamental electrical frequency;
- $k = 10\%$ – Percentage of LC filter reactives.

Using Equation 3.11, it is obtained a capacitor of value 20.88 μF. Then, using the Equation 3.10 and defining the cutoff frequency of 4.8 kHz it is obtained an inductance of 52.64 μH.

4.5 Converter Control Values

A summary with the allocation of poles and the controllers' gains can be seen in Tables 5 and 6, respectively. The result for the dynamic stiffness disregading the repetitive controller can be seen in Figure 35, while the one considering the repetitive controller with the first-order Padé approximlation is found in Figure 36. A comparison between using only the PI controller, or combining it with the repetitive controller can be seen respectively in Figures 37a and 37b and how the voltage across the active impedance output capacitor manages to follow the reference voltage produced by the control loop. In all these studies and figures, it is evident that using PI combined with repetitive control considerably improves the obtained results.

Table 5 – Allocation of poles and frequencies of interest.

Variable	Value
Switching frequency (ω_{sw})	24 kHz
Pole frequency of the current loop (ω_i)	4.8 kHz
Second pole frequency of the voltage loop ($\omega_{v(2)}$)	960 Hz
First pole frequency of the voltage loop ($\omega_{v(1)}$)	192 Hz
LC filter cutoff frequency (ω_c)	4.8 kHz

Table 6 – Controllers' gains.

Gain	Value
k_{pi}	3.18 Ω
k_{pv}	0.15 Ω^{-1}
k_{iv}	152 $\Omega^{-1} \cdot s^{-1}$
k_r	1

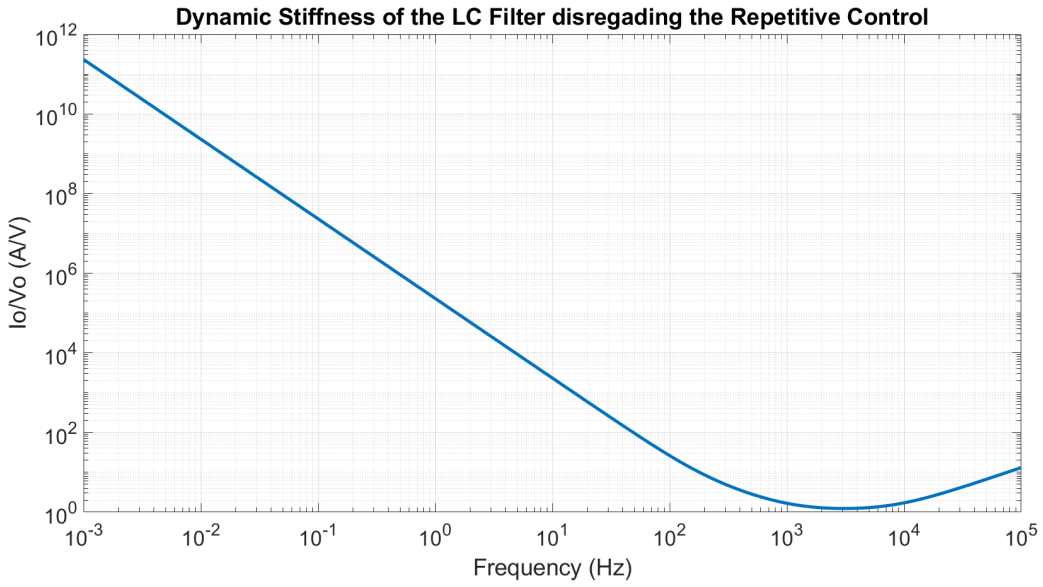

Figure 35 – Dynamic stiffness disregading the repetitive control.

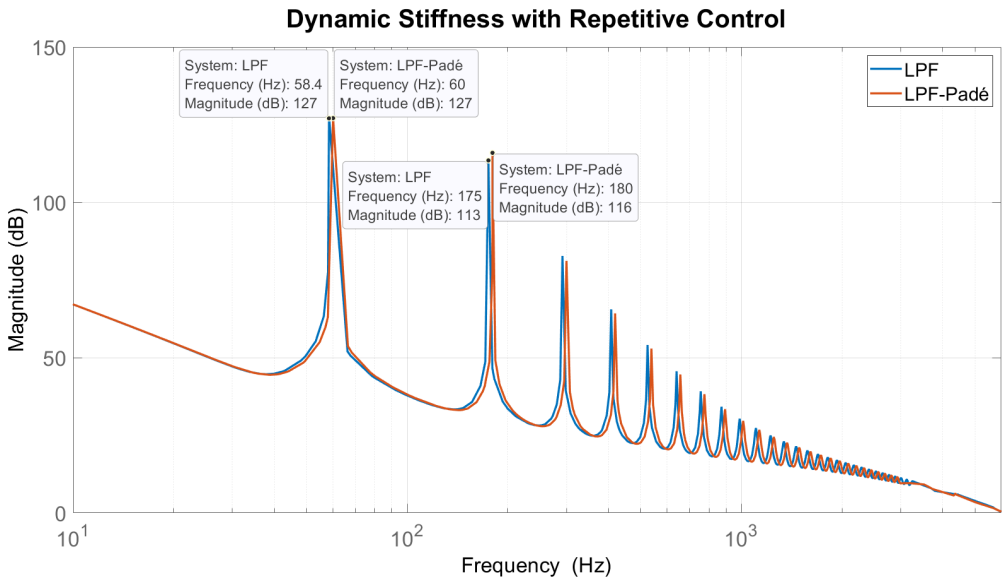

Figure 36 – Dynamic stiffness comparison with (LPF curve) and without (LPF-Padé curve) phase correction.

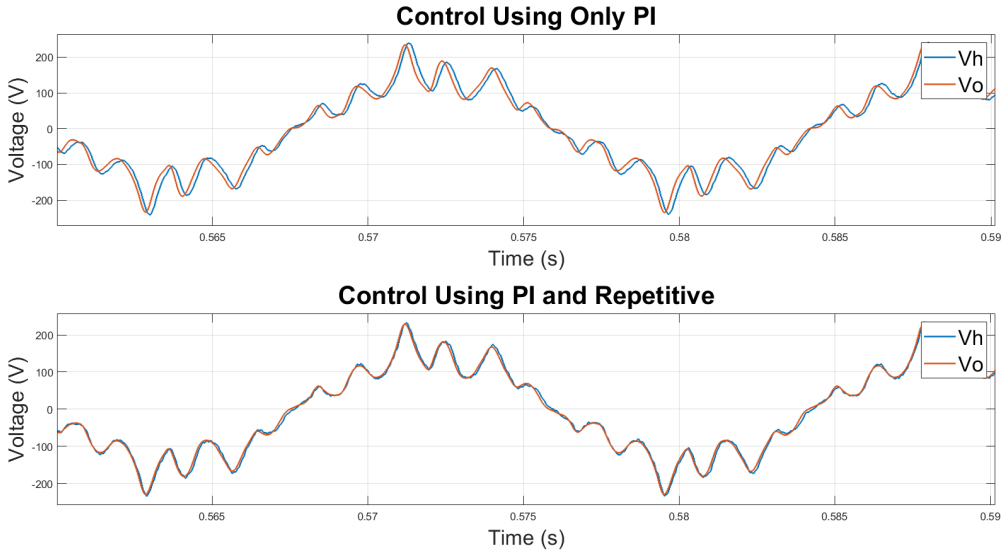

(a) Control strategies comparison.

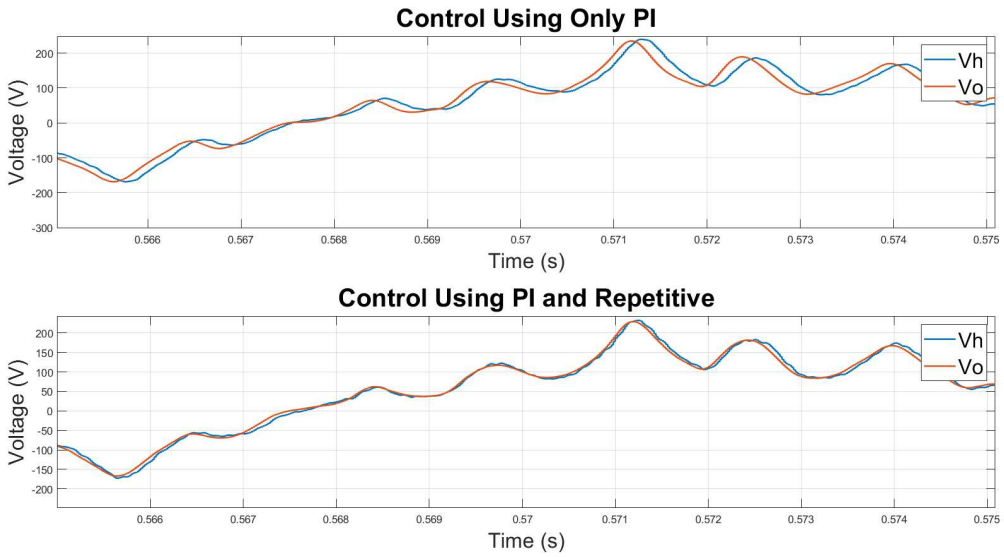

(b) Control strategies comparison in detail.

Figure 37 – Qualitatively analyzed control strategies.

4.6 DC Link Values

The DC link capacitance was chosen through simulations as 12 mF. Figure 38 shows the dynamic stiffness as a function of the capacitance and values of k_{DC}. It can be seen from the figures that the greater the value of k_{DC}, the greater the bandwidth and the better the dynamic stiffness of the voltage control. On the other hand, the increase in bandwidth makes the dynamic response faster, which can lead to a faster voltage reference calculation than the inverter can synthesize (AMARAL, 2016). In this sense, the k_{DC} chosen was 20.

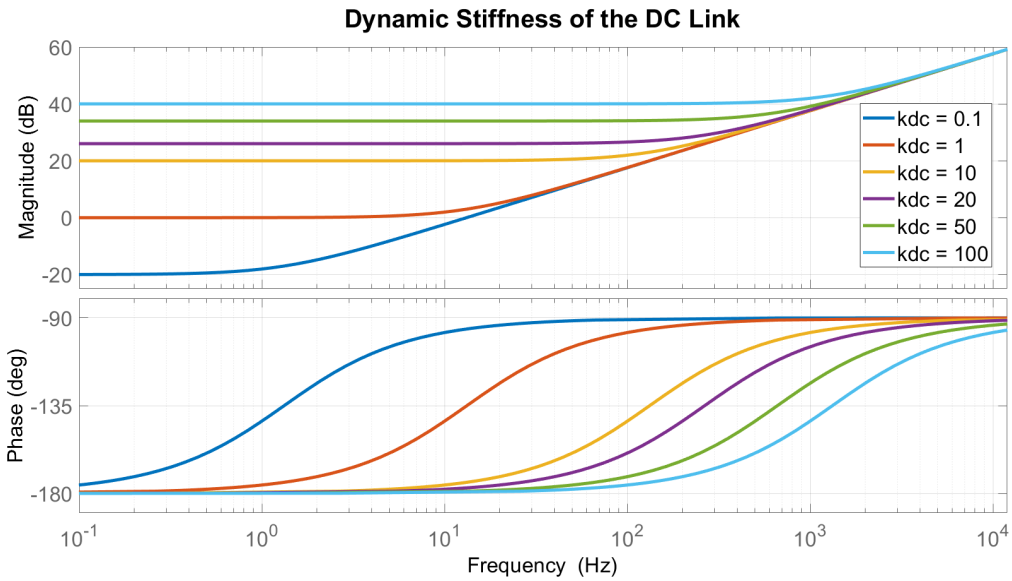

Figure 38 – Dynamic stiffness of the DC Link.

4.7 Pre-charge of the DC Link

The study of the pre-charge phase is divided into two steps. During the first second of simulation, the microgrid works normally without the action of the active impedance. Then, the compensation performed by the active impedance starts to act. This can be summarized in Figure 39, as well as the obtained result.

What is most interesting in Figure 39 is the fact that the DC link can be charged by the power grid without the need for a pre-charge circuit, as it is usually done thinking in terms of safety and limitations of electronic components. In the next paragraphs, more details about an example of a pre-charge circuit, in addition to the situation studied here, to understand why it is possible to dispense this circuit.

A way to start up the converter can be described below and was based on (AMARAL, 2016) as in Figure 40. In this step, the IGBTs of the DC/AC will remain off, as

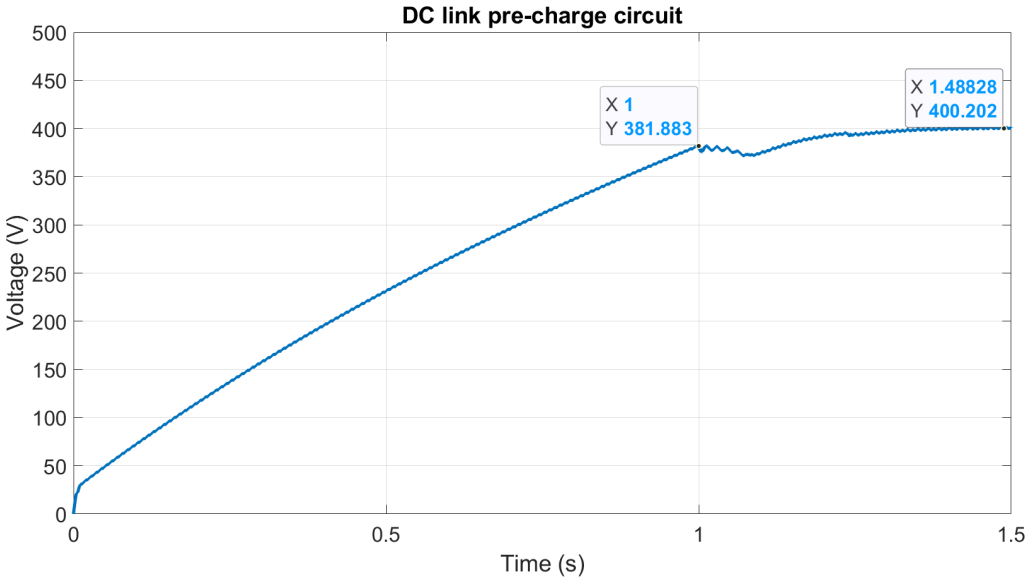

Figure 39 – DC link pre-charge circuit result.

well as switch S_{pc}. For the purpose of demonstrating the procedure, the electrical system and the coupling transformer will be replaced by a current source.

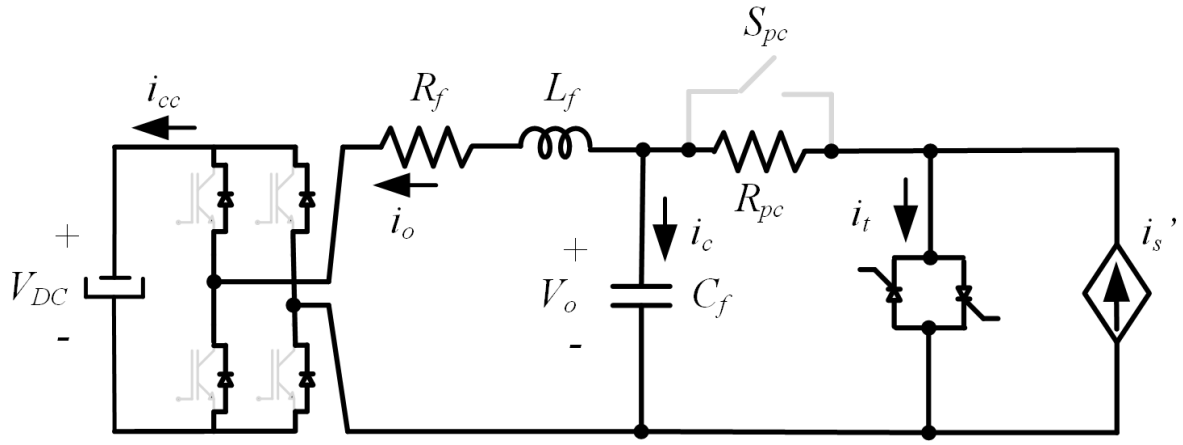

Figure 40 – DC link precharge circuit, adapted from (AMARAL, 2016).

Initially, the converter is in the bypass mode and current i'_s flows through the thyristor switch. When this switch is opened, current flows through the pre-charge resistor, R_{pc}, and then the filter capacitor, establishing alternating voltage V_o in this element. With this, the free-wheeling diodes of the DC/AC operate as rectifiers, and the current i_o flows through the DC link as long as $|V_o| > V_{DC}$. Once the DC link is charged, the S_{pc} switch is activated and the pre-load resistor is short-circuited. Therefore, the IGBTs control start to act emulating the active impedance. In addition to simplicity and speed, this pre-charge technique has the advantage of minimal impact on the electrical system.

Now let us look at the simulation developed in this project as seen in Figure 41. First, it is noticed that the charging occurs naturally through the diodes present in the

IGBTs of the converter. At first, one can imagine this would lead to an overcurrent in the converter. However, it is noticeable that up to 1 second the voltage rises in a well-behaved way and this occurs for two reasons that will be discussed below.

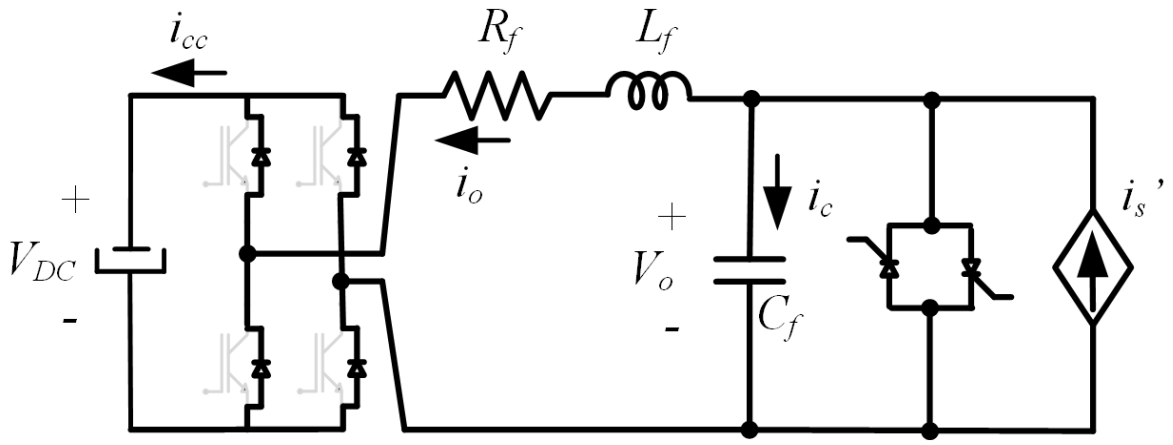

Figure 41 – DC link precharge circuit as developed on simulation.

The first and most important reason is that the transformer turns ratio between primary and secondary is quite high, which makes the system to be seen and to behave as a current source. The higher this ratio, more pronounced this behavior. Secondly, the C_f works as a path for part of this current, reducing even more the current that will charge the DC link.

Therefore, in this study the need for a pre-charge circuit composed of S_{pc} and R_{pc} was disregarded. The bypass switch continues in the circuit, since it has the function of protecting the compensator in the event of a short-circuit in the electrical system. The current i_s is very high in this situation, and therefore i'_s , making it necessary to provide an alternative circulation path during the fault. Under normal circumstances, the bypass switch is kept open.

4.8 Harmonic Distortion Study

For this simulation, initially there is only the power grid supplying the power required by the loads and passive filter. Then, the DER enters supplying part of the active power of the system. Finally, the active impedance starts to act. The simulation time is divided like this: only the power grid supplies the load until 0.3 seconds, when the DER comes in and in 0.5 seconds the active impedance enters. First, the improvement in THD will be studied. Then, an analysis is made from the TDD point of view, as well as the justification for such choice.

4.8.1 THD Improvement

The simulation results for the distortion study can be summarized in FIgure 42. Figure 42a brings the results obtained regarding the grid side, while Figure 42b regards the passive filter. The comparison of the results appears in the Table 7 and the Table 8. Here, L_{max} corresponds to 6.7 mH and was obtained having as an initial basis the Equation 3.6.

Table 7 – THD on the grid side for three different cases.

Case	THD_v	THD_i
Case 1	3.24%	8.23%
Case 2	3.29%	20.83%
Case 3	2.09%	8.08%

Table 8 – THD on the passive filter for three different cases.

Case	THD_v	THD_i
Case 1	3.27%	99.14%
Case 2	3.30%	98.96%
Case 3	4.24%	114.80%

All the values for each odd harmonic in each case is found in Figure 43. Regarding the grid side in Figure 43a and Figure 43b regarding the passive filter. It brings an important observation. The converter in Case 3 was able to reduce the more pronounced harmonics on the grid side, that is, 5^{th}, 7^{th}, 11^{th} and 13^{th} order, which became even lower than in Case 1. On the other hand such harmonics increase in the passive filter which acts as a sink to these harmonics. However, harmonics 5^{th} and 7^{th} were better compensated than 11^{th} and 13^{th} order. The explanation for this is due to the inductance weighted average. When performing it, the algorithm present in the control loop focuses on the harmonics that stand out the most.

For Case 3, it is possible to see, in Figure 44, the voltage through the coupling transformer on its secondary. This voltage is equivalent to the sum of the voltages of each

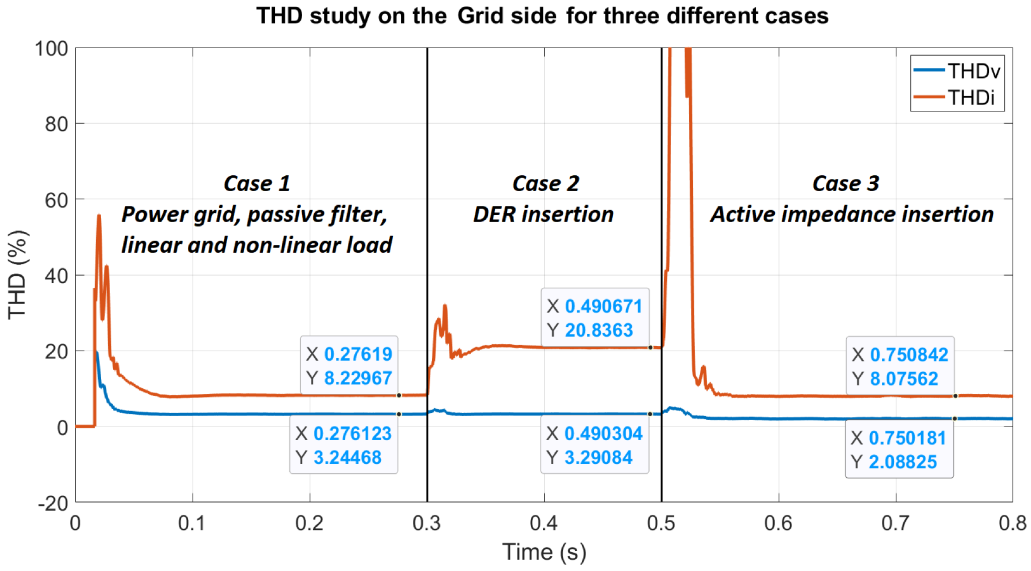

(a) THD study on the grid side for three different cases.

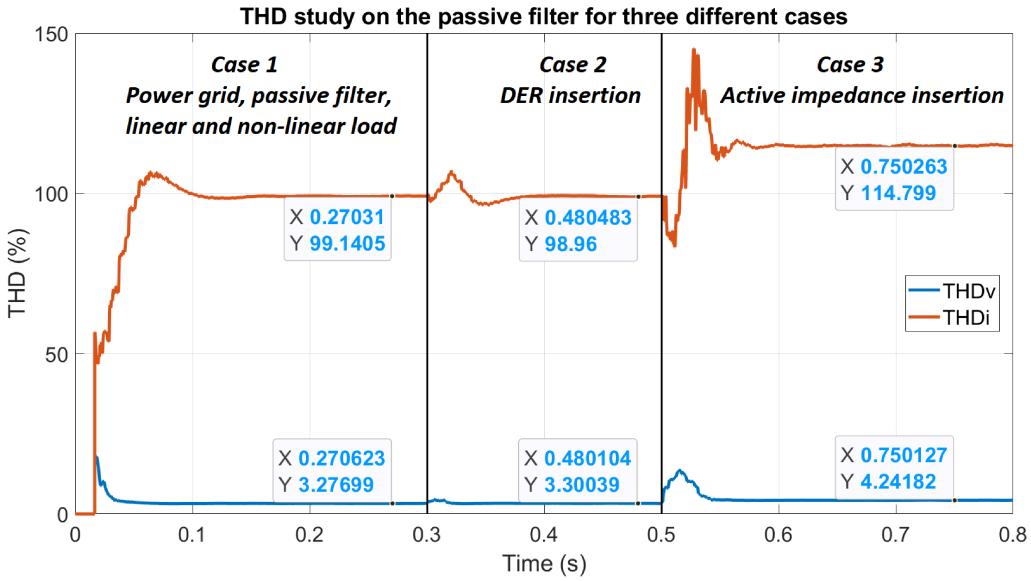

(b) THD study on the passive filter for three different cases.

Figure 42 – THD study on three different cases.

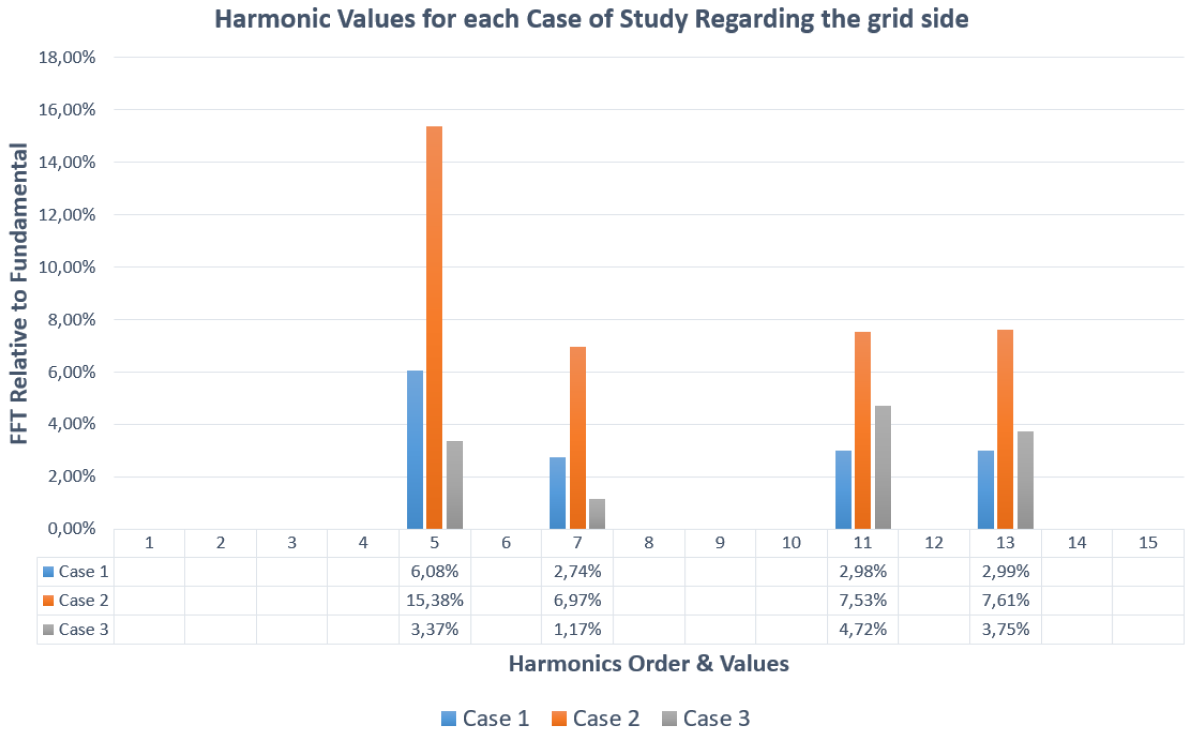

(a) FFT for three different cases regarding the current through the power grid.

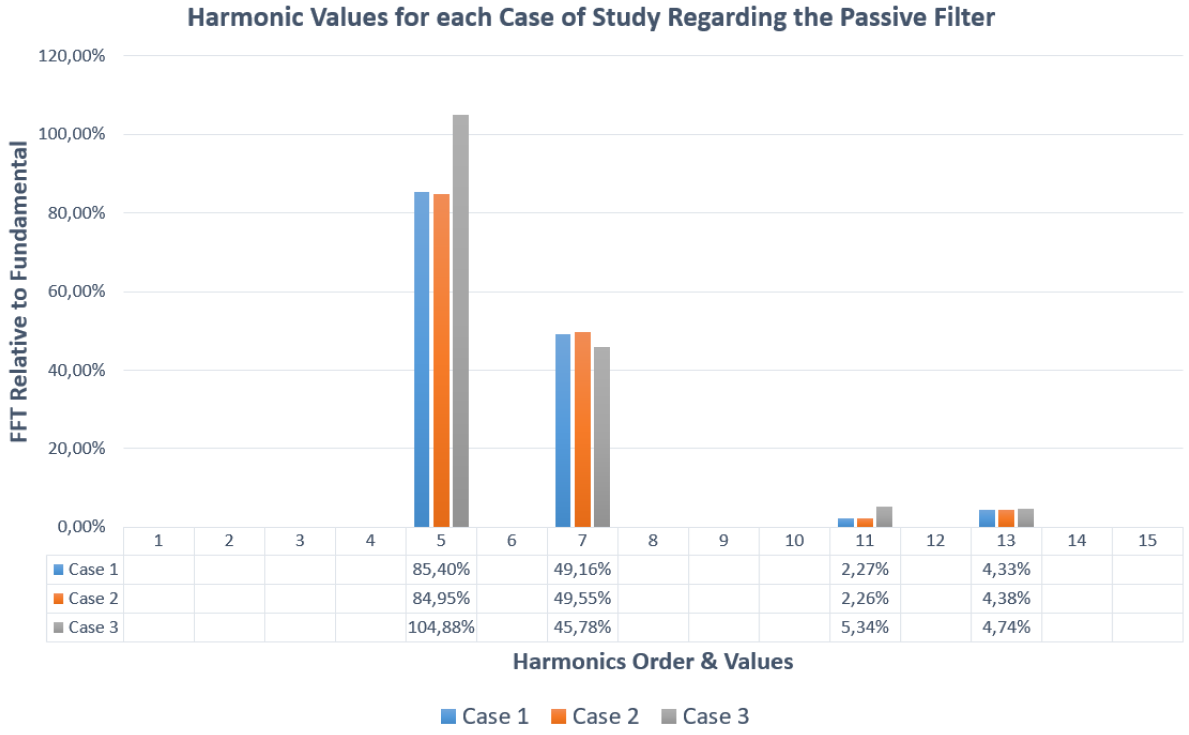

(b) FFT for three different cases regarding the current through the passive filter.

Figure 43 – FFT study on three different cases.

harmonic, each of which will be in quadrature with its harmonic respective current. First, it is shown that the voltage on the grid side and the load side are similar. Then, this difference is seen right below in the same figure, which shows the peak voltage of about 25 V.

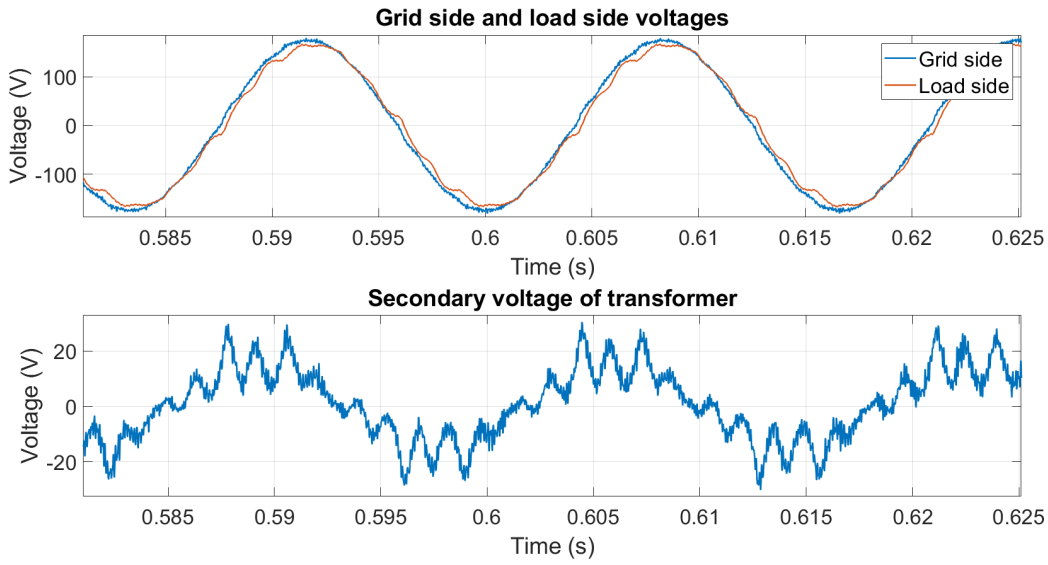

Figure 44 – Voltage through the coupling transformer on its secondary.

It is interesting to see qualitatively the results in the time domain in relation to the improvement in the waveform of the power grid current, in Figure 45, since the THD values were improved through the insertion of active impedances. Figure 45b brings an overview of the current behaviour in the power grid throughout the simulation. Then, Figures 45a, 45c and 45d bring the current waveform for each studied case.

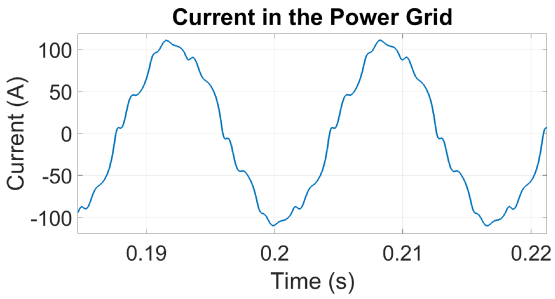

(a) Current waveform in Case 1.

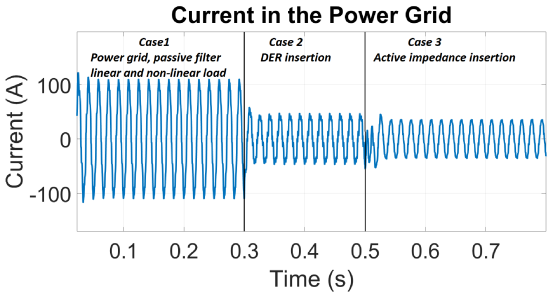

(b) Current waverform overview.

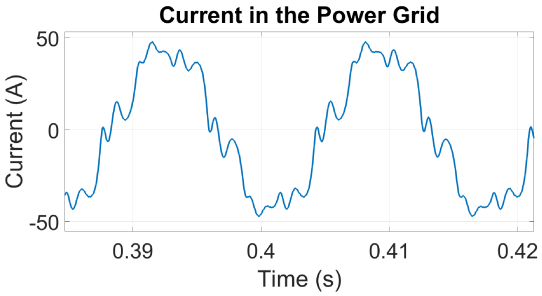

(c) Current waveform in Case 2.

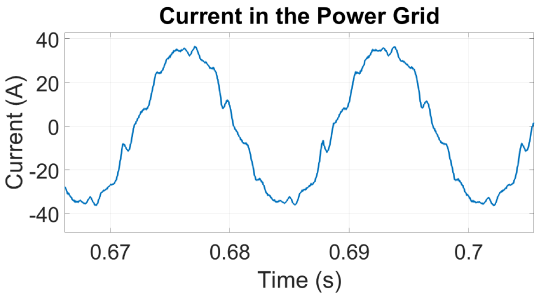

(d) Current waveform in Case 3.

Figure 45 – Qualitatively analyzed current waveform.

4.8.2 TDD Improvement

For the calculation of the TDD, it is important to define what will be the value of the maximum demand load, which will be the sum of the linear load currents and the sum of the non-linear load currents. Studying phase a separately:

$$I_L = I_{LL} + I_{NL} = \frac{S_{LL_{3\phi}}}{\sqrt{3} \cdot V_l} + \frac{S_{NL_{3\phi}}}{\sqrt{3} \cdot V_l} \approx 147\ A \tag{4.5}$$

Figure 46 brings the TDD value for the three different cases as seen before. The comparison of such results appears in the Table 7.

It is possible to see with this case study that TDD is the best index to validate the impact and improvement on harmonic distortions when using active impedance, since

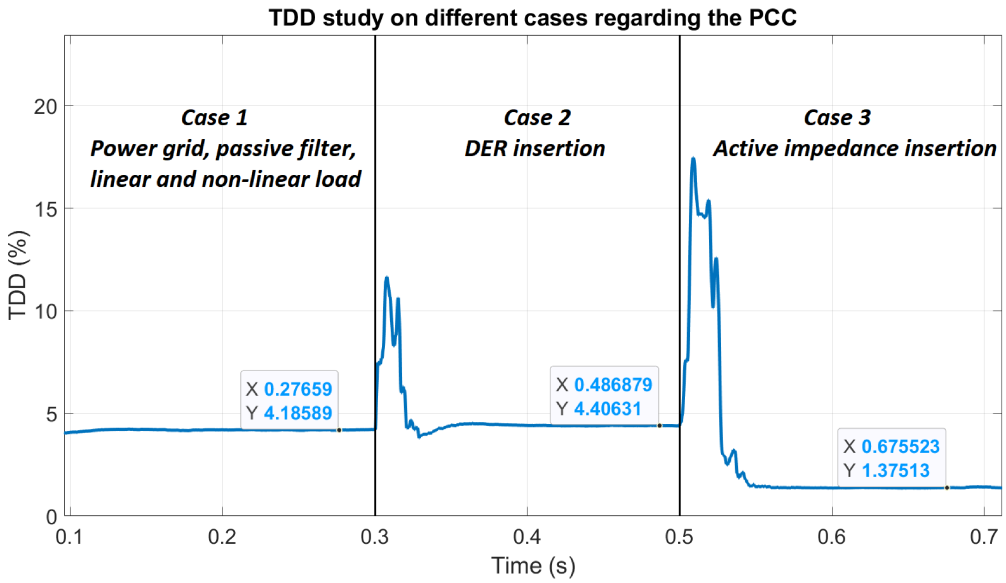

Figure 46 – Voltage through the coupling transformer on its secondary.

Table 9 – TDD values for three different cases regarding the PCC

Case	TDD
Case 1	4.19%
Case 2	4.41%
Case 3	1.38%

it is calculated with the same "base current" for the three cases.

4.9 Conclusion

In this chapter, a case study with a microgrid was developed. First, it started by calculating the total RMS voltage to be emulated by the coupling transformer on its secondary in order to emulate the desired active impedance. With this value, it was possible to determine the turns ratio of the transformer. Then, the values used for the converter and the LC filter were defined. Then, the gains for the converter control and the DC link were determined, both bringing dynamic stiffness study, in addition to a comparison between the use of the PI controller alone and combined with the repetitive controller. The first study was the start-up of the system, that is, the charging of the DC link from the power grid itself. Finally, a study of the improvement in the voltage and current THD was developed from the active impedances inserted with emphasis on the comparison with TDD.

5 Conclusion

In this chapter, the general conclusions of this thesis are presented, as well as proposals for future work. Although the scope was well defined, several issues were raised during its execution, its presentation being relevant.

5.1 Final Considerations

The concept and application of active impedances in a system are not new, but it is always worth taking a fresh look at other possibilities, as they can provide different and interesting solutions in other scenarios. This work aimed to contribute with a new option for this already known technology, which can be widely used in several applications, but was mainly thought and detailed here regarding the subject of microgrids and distributed generation.

The application studied here proved to be attractive when performing intelligent harmonic routing of the system, since this is done by combining active impedances with passive filters, thus making a hybrid filter. This application can become very important facing the challenges encountered for the implementation of microgrids in relation to the harmonic distortions.

Regarding the improvement of total harmonic distortion, it had pronounced and satisfactory results. While the insertion of DERs somehow alleviates the power required by the network to supply the full operation of the system loads, on the other hand, the total harmonic distortion values mainly in the current are deteriorated in this process, since the fundamental frequency decreases its magnitude on the power grid. In other ways, the TDD, which is immune to load variations, proved itself as the best tool for this study. When using the active impedance technique, the improvement in these values were considerable.

5.2 Future Works

For future works, the main point to be observed is precisely the application in microgrid stability. This application can be made from the perspective of negative impedance, which would be emulated by the active impedances.

There is an interest to develop theoretically into this application in addition to performing simulations validating such use, as done in the present study for harmonic distortions. Ultimately, the main continuity would be to do practical experiments. For this, it would be interesting to use Typhoon Hill applied to the microgrid of the Engineering building at UFMG, which is part of a project between the *Laboratório Tesla* and *Petrobras*, as previously mentioned, when this is up and running. The possibilities for this use are numerous depending on what will be most interesting from the characteristics of this microgrid.

5.3 Related Publications

The present work, before being concluded, generated a publication focusing on the application of active impedances improving harmonic routing and managing distortions in distribution networks:

FRAGA, C. C. S. M.; ANTUNES H. M. A.; SILVA, S. M. *"Aplicação de Dispositivos de Impedância Ativa para Roteamento Harmônico em Redes de Distribuição" – XXVI Seminário Nacional de Produção e Transmissão de Energia Elétrica*, 2022.

Bibliography

ADB. *Asian Development Bank: Handbook on Microgrids for Power Quality and Connectivity*. [s.n.], 2020. 1–113 p. ISBN 9789292622534. Disponível em: <http://dx.doi.org/10.22617/TIM200182-2>. Citado na página 37.

AHRENS, K. an Energy Policy for Europe. *Annals of Public and Cooperative Economics*, v. 45, n. 3-4, p. 447–457, 2007. ISSN 14678292. Citado na página 33.

AKAGI, H. Active harmonic filters. *Proceedings of the IEEE*, v. 93, n. 12, p. 2128–2141, 2005. ISSN 00189219. Citado na página 62.

AMARAL, F. V. *Estudo e Projeto de um Compensador para Inserção de Impedâncias Ativas em Sistemas Elétricos de Baixa Tensão*. 2016. 163 p. Citado 14 vezes nas páginas 13, 14, 47, 48, 49, 54, 58, 61, 69, 70, 71, 72, 81, and 82.

AMARAL, F. V. et al. Aplicação de Impedâncias Ativas na Mitigação do Fluxo de Harmônicos em Sistemas Radiais. *Anais da XI Conferência Brasileira Sobre Qualidade da Energia Elétrica*, 2015. Citado 3 vezes nas páginas 27, 51, and 54.

ANDREI, H. et al. Electrical power systems. *Power Systems*, p. 3–47, 2017. ISSN 18604676. Citado na página 50.

ANEEL. Nota técnica 0083/2012. p. 19, 2012. Disponível em: <http://www2.aneel.gov.br/aplicacoes/audiencia/arquivo/2012/065/documento/nota{_}tecnica{_}0083{_}danie>. Citado na página 50.

ANTUNES, H. M. A. Conversor Multifuncional Reconfigurável e Tolerante a Falhas para Microrredes de Energia Elétrica. 2018. Citado 2 vezes nas páginas 67 and 68.

ANTUNES, H. M. A. et al. Harmonic Compensation Using a Series Hybrid Filter in a Centralized AC Microgrid. *Journal of Control, Automation and Electrical Systems*, v. 29, n. 2, p. 219–229, 2018. ISSN 21953899. Citado 9 vezes nas páginas 14, 15, 75, 76, 105, 108, 110, 111, and 112.

BANTRAS, T. et al. Estimation and classification of power losses DUE to reduced Power Quality. *IEEE Power and Energy Society General Meeting*, IEEE, n. 1, p. 1–6, 2012. ISSN 19449925. Citado na página 50.

BARAN, M. E.; EL-MARKABY, I. Fault analysis on distribution feeders with distributed generators. *IEEE Transactions on Power Systems*, v. 20, n. 4, p. 1757–1764, 2005. ISSN 08858950. Citado na página 41.

BARNES, M. et al. Real-world MicroGrids - An overview. *2007 IEEE International Conference on System of Systems Engineering, SOSE*, 2007. Citado na página 35.

BELEIU, H. G. *Technical and Economical Consequences Of Evaluation*. Tese (Doutorado), 2011. Citado na página 51.

BELEIU, H. G. et al. Management of power quality issues from an economic point of view. *Sustainability (Switzerland)*, v. 10, n. 7, p. 1–16, 2018. ISSN 20711050. Citado 3 vezes nas páginas 13, 51, and 52.

BELLIDO, M. M. H. *Microrredes Elétricas: Uma Proposta de Implementação no Brasil*. 211 p. Tese (Doutorado) — UFRJ, 2018. Disponível em: <http://www.ppe.ufrj.br/images/publica{ç}{~{o}}es/doutorado/Marlon{_}Max{_}H>. Citado na página 36.

BERKELEY, L. et al. Overview of the CERTS Microgrid Laboratory Test Bed. *Electronics*, 2009. Citado na página 35.

BOLLEN, M.; HAGER, M. Power Quality: Interactions Between Distributed Energy Resources, the Grid, and Other Customers. *Electrical Power Quality and Utilization - Vol.1*, 2005. Citado na página 39.

BOWER, W. et al. The Advanced Microgrid Integration and Interoperability. *Sandia Report*, n. March, p. 1–56, 2014. Citado na página 35.

BOYCE. *EDO*. [S.l.: s.n.], 2006. 1040 p. ISBN 9780470458310. Citado na página 46.

BRITAIN, G. The Internal Model Principle of Control Theory The Internal Model Principle of Control Theory *. v. 1098, n. August, p. 457–465, 2015. Citado na página 65.

BRITO, M. et al. Estratégias De Anti-Ilhamento Aplicadas a Sistemas De Geração Distribuída Fotovoltaica. *Eletrônica de Potência*, v. 23, n. 2, p. 226–234, 2018. Citado na página 41.

CARNEIRO, A. V. Projeto, Desenvolvimento E Implementação De Microrrede. p. 177, 2017. Citado na página 36.

CELPE. www.celpe.com.br 1. 2019. Disponível em: <https://www.cinase.com.br/wp-content/uploads/2019/10/Caso-Fernando-de-Noronha{_}CELPE{_}compressed>. Citado na página 36.

CENTRE, J. R. Annual report. *Annual report.*, 2011. Disponível em: <https://ec.europa.eu/jrc/sites/jrcsh/files/jrc{_}ar{_}20>. Citado na página 33.

CHAKRABORTY, S.; WEISS, M. D.; SIMÕES, M. G. Distributed intelligent energy management system for a single-phase high-frequency AC microgrid. *IEEE Transactions on Industrial Electronics*, v. 54, n. 1, p. 97–109, 2007. ISSN 02780046. Citado na página 38.

CHANDAK, S.; ROUT, P. K. The implementation framework of a microgrid: A review. *International Journal of Energy Research*, v. 45, n. 3, p. 3523–3547, 2021. ISSN 1099114X. Citado na página 35.

CHEN, S. et al. Analysis and design of repetitive controller for harmonic elimination in PWM voltage source inverter systems. *IET Power Electronics*, v. 1, n. 4, p. 497–506, 2008. ISSN 17554543. Citado na página 66.

CHEN, S.; YU, H. A review on overvoltages in microgrid. *Asia-Pacific Power and Energy Engineering Conference, APPEEC*, IEEE, 2010. ISSN 21574839. Citado na página 42.

CHENG, P. T.; LEE, T. L. Distributed active filter systems (DAFSs): A new approach to power system harmonics. *IEEE Transactions on Industry Applications*, v. 42, n. 5, p. 1301–1309, 2015. ISSN 00939994. Citado na página 53.

CIONTEA, C. I.; IOV, F. A Study of Load Imbalance Influence on Power Quality Assessment for Distribution Networks. *Electricity*, v. 2, n. 1, p. 77–90, 2021. Citado na página 38.

CLUSTER, C. C. *Denmark: a European Smart Grid Hub*. [S.l.], 2011. Disponível em: <https://stateofgreen.com/files/download/5492>. Citado na página 34.

COTA, A. P. L. *Desenvolvimento de Ferramentas Computacionais para a Análise de Perdas em Conversores Estáticos: Aplicação ao Cálculo de Rendimento de UPSs Trifásicas de Dupla Conversão*. 2016. 195 p. Citado 3 vezes nas páginas 14, 68, and 69.

CURRIE, R. et al. Fundamental Research Challenges for Active Management of. *Power Quality*, p. 1024–1028, 2004. Citado na página 32.

DANLEY, D. Defining a Microgrid Using Using IEEE 2030.7. *America's Electric Cooperatives (NRECA)*, n. November, p. 2–10, 2019. Citado na página 37.

DAS, J. C. Power System Harmonics. *Power System Harmonics and Passive Filter Designs*, p. 1–29, 2015. Citado na página 46.

DIVYA, K. C.; ØSTERGAARD, J. Battery energy storage technology for power systems-An overview. *Electric Power Systems Research*, v. 79, n. 4, p. 511–520, 2009. ISSN 03787796. Citado na página 40.

EDRIS, A. et al. Paper prepared by the FACTS Terms & Definitions Task Force of the FACTS Working Group of the DC and FACTS Subcommittee. *Power*, v. 12, n. 4, p. 1848–1853, 1997. ISSN 08858977. Citado na página 37.

ERGE, T. Tests for Microgrids. *International Journal*, v. 22, p. 643–645, 2007. Citado na página 34.

FALCÃO, D. M. Smart Grids E Microredes : O Futuro Já É Presente. *VIII Simpase*, p. 1–11, 2009. Citado 2 vezes nas páginas 27 and 31.

FAU; UFU. Relatório Técnico 3/8 Definição de procedimentos de medição, distorções harmônicas, desequilíbrios de tensão, flutuações de tensão e variações de tensão de curta duração. 2014. Citado na página 50.

FRANÇA, G. J. *Desenvolvimento de Compensador Série para Mitigação Harmônica Distribuída e Correção Dinâmica de Fator de Potência*. Tese (Doutorado) — UFMG, 2013. Citado na página 56.

FRANÇA, G. J.; CARDOSO, B. J. Series-shunt compensation for harmonic mitigation and dynamic power factor correction. *Eletrônica de Potência*, v. 17, n. 3, p. 641–650, 2012. ISSN 14148862. Citado na página 28.

GUERRERO, J. Intelligent Microgrid Project Research in Spain and Denmark. p. 1–38, 2011. Citado na página 34.

HARRIS, W. R. *Sustainable Rural Microgrid: Engineering and Economics*. Tese (Doutorado) — Texas A&M University, 2017. Disponível em: <https://oaktrust.library.tamu.edu/handle/1969.1/165748>. Citado na página 35.

HATZIARGYRIOU, N. Microgrids, the key to unlock distributed energy resources? *IEEE power & energy magazine*, n. june, p. 2008–2010, 2008. Citado na página 33.

HATZIARGYRIOUA, N. et al. Smart metering and infrastructure. *Microgrids: an overview of ongoing research, development, and demonstration projects*, n. July 2007, p. 399–420, 2007. Citado na página 31.

HUGHES, T. P. *Network of Power - Electrification in Western Society*. [S.l.: s.n.], 1983. ISBN 0801828732. Citado na página 31.

HUSSAIN, B. et al. Integration of distributed generation into the grid: Protection challenges and solutions. *IET Conference Publications*, v. 2010, n. 558 CP, 2010. Citado 2 vezes nas páginas 38 and 42.

IEEE. 100-1996 - The IEEE Standard Dictionary of Electrical and Electronics Terms Sixth Edition. *Standard Dictionary*, v. 6th editio, 1996. Citado 2 vezes nas páginas 50 and 105.

IEEE. *IEEE 519-2014_Redline. Recommended Practice and Requirements for Harmonic Control in Electric Power Systems*. [s.n.], 2014. v. 2014. 1–101 p. ISBN 1559372397. Disponível em: <http://www.sinab.unal.edu.co:2365/xpl/mostRecentIssue.jsp?punumber=2227>. Citado na página 73.

JADEJA, R. et al. Control of Power Electronic Converters in AC Microgrid. *Power Systems*, v. 27, n. 11, p. 329–355, 2020. ISSN 18604676. Citado na página 45.

KATIRAEI, F. et al. Microgrid Management: controls and operation aspects of microgrids. n. june, p. 54–65, 2008. Citado na página 33.

KOYAMA, K. 2020 Energy Outlook in Japan and World. n. December 2019, p. 2019–2021, 2020. Citado na página 34.

KROPOSKI, B. et al. A look at microgrid technologies and testing projects from around the world. n. june, 2008. Citado na página 34.

KUO, S. Y. et al. Distributed active filters for harmonic resonance suppression in industrial facilities. *Fourth Power Conversion Conference-NAGOYA, PCC-NAGOYA 2007 - Conference Proceedings*, p. 391–397, 2007. Citado na página 53.

LAAKSONEN, H. J. Protection principles for future microgrids. *IEEE Transactions on Power Electronics*, v. 25, n. 12, p. 2910–2918, 2010. ISSN 08858993. Citado na página 42.

LEGRAND. Sizing conductors and selecting protection devices. *Power Guide*, 2009. Citado na página 38.

LEI, Z.; AI, X.; CUI, M. Coordinated control strategy based on network parameters for voltage sags compensating in microgrid. *2010 5th International Conference on Critical Infrastructure, CRIS 2010 - Proceedings*, IEEE, p. 1–5, 2010. Citado na página 42.

LISERRE, M.; BLAABJERG, F.; HANSEN, S. Design and control of an LCL-filter based three-phase active rectifier. *Conference Record - IAS Annual Meeting (IEEE Industry Applications Society)*, v. 1, p. 299–307, 2001. ISSN 01972618. Citado na página 106.

LISERRE, M.; BLAABJERG, F.; HANSEN, S. Design and control of an LCL-filter-based three-phase active rectifier. *IEEE Transactions on Industry Applications*, v. 41, n. 5, p. 1281–1291, 2005. ISSN 00939994. Citado na página 107.

LOPES, L. A.; ZHANG, Y. Islanding detection assessment of multi-inverter systems with active frequency drifting methods. *IEEE Transactions on Power Delivery*, v. 23, n. 1, p. 480–486, 2008. ISSN 08858977. Citado na página 41.

MARIAM, L.; BASU, M.; CONLON, M. F. Microgrid: Architecture, policy and future trends. *Renewable and Sustainable Energy Reviews*, v. 64, p. 477–489, 2016. ISSN 18790690. Citado 3 vezes nas páginas 17, 43, and 44.

MARIANO, P. henricky. Procedimentos de Distribuição MÓDULO 8 -QUALIDADE DA ENERGIA ELÉTRICA. 2020. Citado na página 50.

MARNAY, C.; RUBIO, F. J.; SIDDIQUI, A. S. Shape of the microgrid. *Proceedings of the IEEE Power Engineering Society Transmission and Distribution Conference*, v. 1, n. WINTER MEETING, p. 150–153, 2001. ISSN 21608563. Citado na página 42.

MILANO, F. et al. Foundations and challenges of low-inertia systems (Invited Paper). *20th Power Systems Computation Conference, PSCC 2018*, 2018. Citado na página 38.

MOHAN; UNDELAND; ROBBINS. *Power electronics*. [S.l.: s.n.], 2003. Third Edit. 811 p. ISSN 02562499. ISBN 9780471226932. Citado 2 vezes nas páginas 13 and 46.

MOROZUMI, S. Microgrid demonstration projects in Japan. *Australian Journal of Primary Health*, v. 9, n. 2-3, p. 149, 2003. ISSN 13242296. Citado na página 34.

OLIVEIRA, A. F. B. et al. Aplicação de Controle Repetitivo a Inversor PWM Monofásico com Filtro LC de Saída Utilizado em Fonte programável C.A. *Eletrônica de Potência*, v. 18, n. 4, p. 1161–1169, 2013. Citado 4 vezes nas páginas 14, 65, 66, and 67.

OUDALOV, A.; FIDIGATTI, A. Adaptive Network Protection in MIcrogrids. *ABB International Journal of Distributed Energy Resources*, v. 5, p. 201–227, 2009. Citado 2 vezes nas páginas 41 and 42.

PATEL, Y. P.; WEI, L.; NASIRI, A. LCL filter resonance mitigation technique for voltage source converters. In: *3rd International Conference on Renewable Energy Research and Applications, ICRERA 2014*. [S.l.: s.n.], 2014. v. 1, p. 854–858. ISBN 9781479937950. Citado na página 106.

PENG, F. Z.; LI, Y. W.; TOLBERT, L. M. Control and protection of power electronics interfaced distributed generation systems in a customer-driven microgrid. *2009 IEEE Power and Energy Society General Meeting, PES '09*, 2009. Citado na página 37.

PICCINI, A. R. et al. Implementation of a photovoltaic inverter with modified automatic voltage regulator control designed to mitigate momentary voltage dip. *Energies*, v. 14, n. 19, 2021. ISSN 19961073. Citado na página 38.

PIRES, I. A.; FRANÇA, G. J.; CARDOSO, B. J. Distributed Series/Hybryd-Shunt Compensation for Harmonic Mitigation in Commercial Facilities. *The 2014 International Power Electronics Conference*, p. 3270–3277, 2014. Citado 2 vezes nas páginas 28 and 61.

POGAKU, N.; PRODANOVIĆ, M.; GREEN, T. C. Modeling, analysis and testing of autonomous operation of an inverter-based microgrid. *IEEE Transactions on Power Electronics*, v. 22, n. 2, p. 613–625, 2007. ISSN 08858993. Citado na página 42.

REIS, M. V. et al. Evaluation of active anti-islanding methods based on the ABNT NBR IEC 62116 and IEEE STD 929-2000 standards. *2015 IEEE 13th Brazilian Power Electronics Conference and 1st Southern Power Electronics Conference, COBEP/SPEC 2016*, IEEE, 2015. Citado na página 38.

REZNIK, A. et al. LCL filter design and performance analysis for small wind turbine systems. *PEMWA 2012 - 2012 IEEE Power Electronics and Machines in Wind Applications*, p. 1–7, 2012. Citado na página 105.

RIBEIRO, L. A. S. et al. Isolated micro-grids with renewable hybrid generation: The case of Lençóis island. *IEEE Transactions on Sustainable Energy*, v. 2, n. 1, p. 1–11, 2011. ISSN 19493029. Citado na página 36.

RODRIGUES, I. R. A. *Estudo de proteção elétrica de uma microrrede baseada na rede de 34 barras do IEEE*. 145 p. Tese (Doutorado) — UFMG, 2017. Disponível em: <https://www.ppgee.ufmg.br/defesas/1366M.PDF>. Citado na página 36.

ROGERS, K. M.; OVERBYE, T. J. Power flow control with Distributed Flexible AC Transmission System (D-FACTS) devices. *41st North American Power Symposium, NAPS 2009*, IEEE, v. 61801, 2009. Citado na página 28.

SANCHEZ, F. K. . B. M. . A. M. . L. Y. . G. IEEE may/june 2008. n. june, p. 54–65, 2008. Citado na página 43.

SEP, U. O. N. AC Overloading. p. 1–4, 2020. Citado na página 38.

SHREYAS, S. et al. Stability analysis of microgrids. *International Journal of Recent Technology and Engineering*, v. 8, n. 1 Special Issue 4, p. 501–508, 2019. ISSN 22773878. Citado na página 38.

SILVA, A. F. et al. Observer-based state feedback controller for LCL filter used in PV applications with grid current measurement only. *2015 IEEE Energy Conversion Congress and Exposition, ECCE 2015*, p. 3303–3307, 2015. Citado na página 105.

SILVA, S. M. *Estudo e projeto de um restaurador dinâmico de tensão*. 1999. 215 p. Citado 2 vezes nas páginas 64 and 65.

SILVA, S. M.; FILHO, B. J. C. Component-minimized voltage sag compensators. *Conference Record - IAS Annual Meeting (IEEE Industry Applications Society)*, v. 2, p. 883–889, 2002. ISSN 01972618. Citado na página 64.

SOSHINSKAYA, M. et al. Microgrids: Experiences, barriers and success factors. *Renewable and Sustainable Energy Reviews*, v. 40, p. 659–672, 2014. ISSN 13640321. Citado na página 39.

TON, D.; SMITH, M. The U.S. Department of Energy's Microgrid Initiative. 2012. Disponível em: <http://dx.doi.org/10.1016/j.tej.2012.09.013>. Citado na página 35.

UNESCO. *View of UNESCO Science Report_ Towards 2030.pdf*. Paris, 2015. 125–127 p. Citado na página 32.

USTUN, T. S.; OZANSOY, C.; ZAYEGH, A. Recent developments in microgrids and example cases around the world - A review. *Renewable and Sustainable Energy Reviews*, Elsevier Ltd, v. 15, n. 8, p. 4030–4041, 2011. ISSN 13640321. Disponível em: <http://dx.doi.org/10.1016/j.rser.2011.07.033>. Citado 2 vezes nas páginas 32 and 41.

WANG, B.; SUN, M.; DONG, B. The existed problems and possible solutions of distributed generation microgrid operation. *Asia-Pacific Power and Energy Engineering Conference, APPEEC*, n. April, p. 2763–2768, 2011. ISSN 21574839. Citado na página 41.

WANG, C. et al. A seamless operation mode transition control strategy for a microgrid based on master-slave control. *Science China Technological Sciences*, v. 55, n. 6, p. 1644–1654, 2012. ISSN 16747321. Citado na página 108.

WWF-BRASIL. Geração de energia em fernando de noronha: Alternativas para a diminuição de emissões de co2 no transporte e eletricidade brasil 2021. 2020. Citado na página 36.

XIALING, X.; XIAOMING, Z. Overview of the researches on distributed generation and microgrid. *Engineering Conference*, p. 966–971, 2007. Citado na página 38.

YAZDANI, A.; IRAVANI, R. *Converters in Power Systems Preface*. [S.l.: s.n.], 2018. ISBN 9780470521564. Citado na página 110.

Appendix

APPENDIX A – Derivative from Rotation Vectors

The mathematical operation of deriving an equation is commonly seen as a problem in practice, due to disturbances and noise present in measurement systems, it is practically impracticable to use this device, for example, in algorithms and control systems. Proof of this is that PID controllers have its use almost resctricted to PI actions.

Electrical systems are basically made up of sine or cosine waves. This brings a range of very important benefits for us mathematically speaking. One of these points is precisely the derivative of these functions. The derivative of a sine function is basically its displacement in time of 90^o in addition to having its magnitude multiplied by its angular velocity.

Usually, we have the derivative table of these functions as seen in Table 10.

Table 10 – Derived Functions on Time Domain.

f(t)	f'(t)
sin(ωt)	cos(ωt)
cos(ωt)	-sin(ωt)

If we take a generic phasor written in algebraic form we have the Equation A.1. If we want to derive this vector by getting its form v' we have the Equation A.2 and the Figure 47 as a result:

$$v = v_\alpha + jv_\beta \tag{A.1}$$

$$v' = jv \tag{A.2}$$

Developing algebraically the equations A.1 and A.2, we have the Equation A.3 resulting on the desired derivative value on frequency domain.

$$v' = -v_\beta + jv_\alpha \tag{A.3}$$

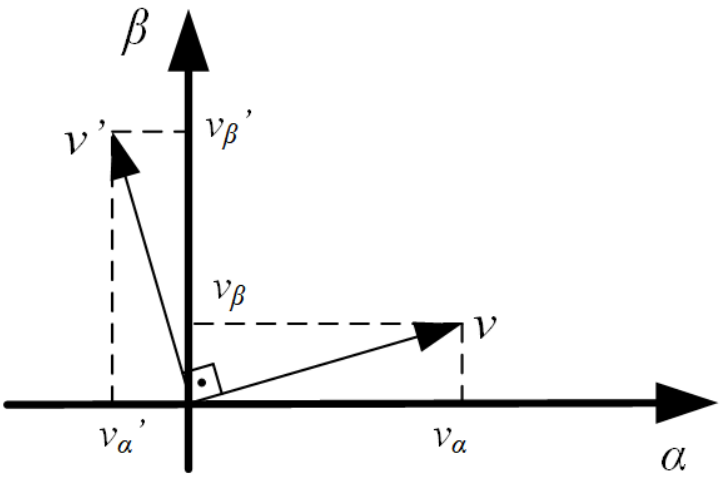

Figure 47 – Study of the derivative of a sinusoidal function.

APPENDIX B – Distributed Energy Resource Modelling

This appendix aims to deal with the modeling of the LCL filter of the DER in addition to its current loop being able to inject active and/or reactive power and at last the DC link loop.

B.1 LCL Filter Design

To provide the connection of the converter supplying the electrical network, it is common to use the LCL filter instead of the pure inductive filter. In this way, it is possible to attenuate the multiple harmonics of the switching frequency of the output current regarding the current harmonic distortion rate limits (IEEE, 1996). With this configuration, it is possible to obtain an attenuation in the output current equal to 60dB/decade, allowing a reduction in the weight and size of the filter, with a consequent reduction in costs (REZNIK et al., 2012) and (SILVA et al., 2015). Figure 48 shows the per phase electrical circuit of an LCL filter.

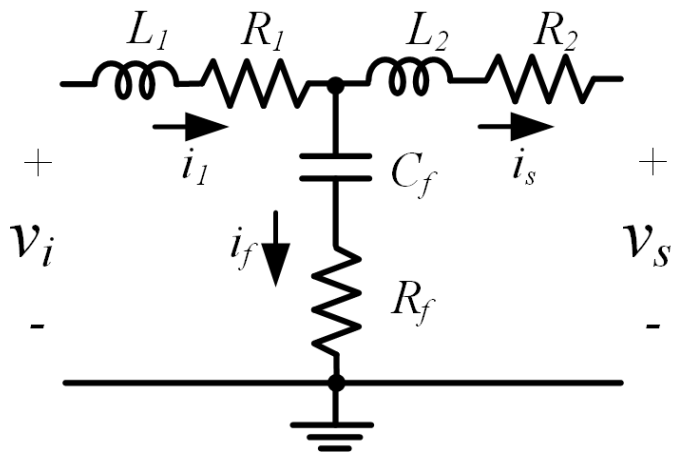

Figure 48 – LCL filter scheme per phase, adapted from (ANTUNES et al., 2018).

(REZNIK et al., 2012) present in their work a methodology for calculating the parameters of the LCL filter. The inductor at the output of the VSI is responsible for making it behave as a current source. To calculate the L_1 inductance, a current ripple criterion of 30% is adopted, calculated using Equation B.1.

$$L_1 = \frac{V_{dc}}{6 f_{sw} \Delta i_{Lmax}} \tag{B.1}$$

Where:

- V_{dc} – DC link Voltage (V);
- f_{sw} – Converter switching frequency (Hz);
- Δi_{Lmax} – Maximum current ripple in the inductor (A).

The filter capacitor is responsible for absorbing the converter switching ripple. For its modelling, it is considered that with the connection of the capacitor there is a variation of the power factor seen by the electrical network around 5%. The capacitance per phase is calculated using Equation B.2 (LISERRE; BLAABJERG; HANSEN, 2001).

$$C_f = 0.05\frac{S_n}{2\pi f_g E_n^2} \tag{B.2}$$

Where:

- S_n – Apparent three-phase power of the inverter (VA);
- f_g – Electric network frequency (Hz);
- E_n – Line voltage (V).

The output inductor L_2 re-converts the structure to impose current source characteristic in addition to filtering the output current. Equation B.3 presents the calculation of the output inductor L_2 as a function of the attenuation factor K_a, which is commonly adopted as being equal to 20%.

$$L_2 = \frac{\sqrt{\frac{1}{K_a^2}} + 1}{(2\pi f_g E_n)^2 C_f} \tag{B.3}$$

The LCL filter with pure capacitor has the problem of harmonic resonance associated with its operation, which can cause an increase in the THD_i at its output. To solve this problem, it is possible to use an active or passive damping technique (PATEL; WEI; NASIRI, 2014). A widely used passive technique is obtained from the dimensioning of a resistance in series with the filter capacitor. The equation that presents the transfer function of the LCL filter with passive damping is:

$$\frac{i_s(s)}{v_i(s)} = \frac{C_f R_f s + 1}{L_1 C_f L_2 s^3 + C_f R_f (L_1 + L_2)^2 + (L_1 + L_2)s} \tag{B.4}$$

Figure 49 presents the Bode diagram of the filter transfer function defined in Equation B.4. It is possible to observe that without damping resistance there is a large

harmonic amplification peak, but that is eliminated with the insertion of resistance with loss of performance above the cutoff frequency. However, it should be noted that the addition of the damping resistance reduces the filter attenuation to 40dB/decade.

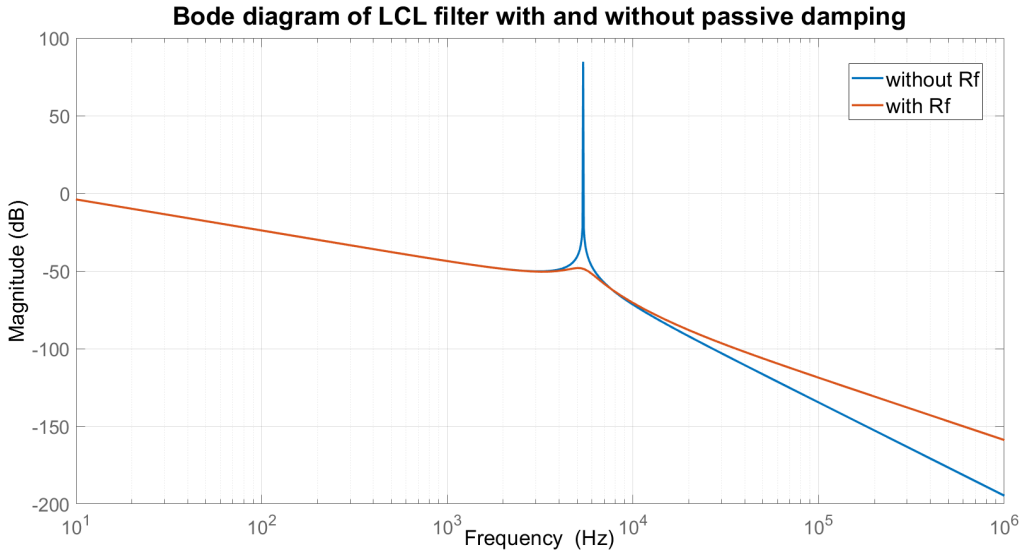

Figure 49 – Bode diagram of LCL filter with and without passive damping.

The damping resistor is calculated by Equation B.5 as being equal to one third of the impedance of the capacitor at the angular resonant frequency (ω_{res}).

$$R_f = \frac{1}{3\omega_{res}C_f} \tag{B.5}$$

The electrical resonance frequency of the LCL filter is calculated by Equation B.6. It should be noted that depending on the resonant frequency required for the converter control design, the capacitance of the LCL filter can be adjusted.

$$f_{res} = \frac{1}{2\pi}\sqrt{\frac{L_1 + L_2}{L_1 L_2 C_f}} \tag{B.6}$$

For the LCL filter to have a good performance, the following must be respected (LISERRE; BLAABJERG; HANSEN, 2005):

$$10f_g \leq f_{res} \leq f_{sw} \tag{B.7}$$

B.2 Current Loop Control

In this section, the modelling of the DER controllers with the configuration shown in Figure 50 is discussed. All control is done in *dq0* coordinates in the synchronous frame.

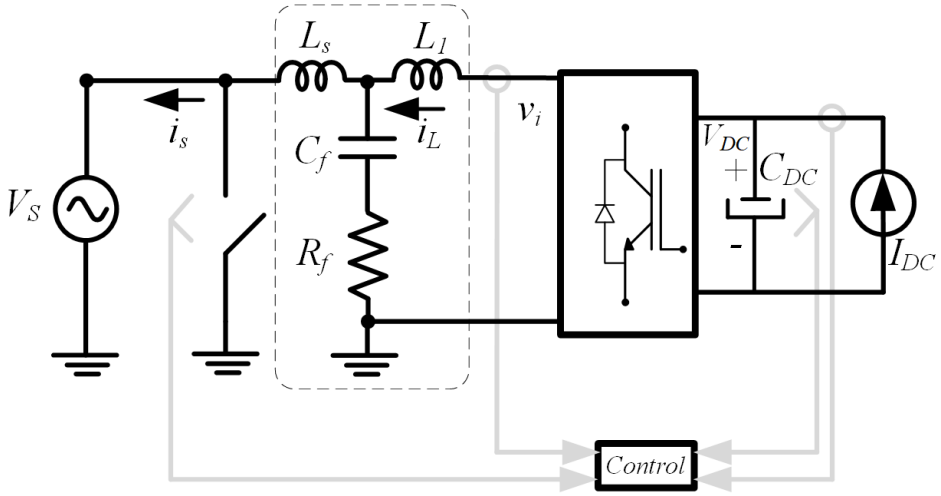

Figure 50 – DER configuration and measurements, adapted from (ANTUNES et al., 2018).

The reactive injection is done with a command to the *iq* loop, with open loop operation of the converter. A methodology for the design of each control loop of the network supplier is presented below.

Initially, the VSI equations in the time domain will be obtained, considering that the impedance of the capacitor in the LCL filter is very high at the fundamental frequency, which characterizes it as an open circuit (WANG et al., 2012). From the equivalent circuit per phase shown in Figure 51, we have Equation B.8.

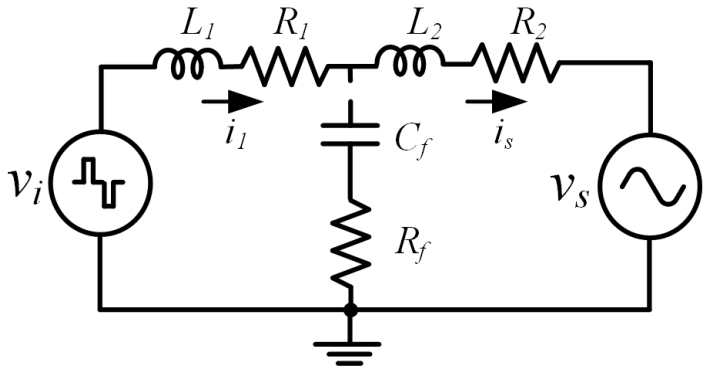

Figure 51 – Equivalent circuit per phase of inverter and mains at fundamental frequency, adapted from (ANTUNES et al., 2018).

$$v_i(t) = Ri_s(t) + L\frac{di_s(t)}{dt} + v_s(t) \tag{B.8}$$

Where: $R = R_1 + R_2$ and $L = L_1 + L_2$.

Transforming Equation B.8 to referential $\alpha\beta 0$ using the Clark transformation we

have:

$$v_{\alpha\beta0}(t) = [C]v_{abc}(t) \rightarrow v_{abc}(t) = [C]^{-1}v_{\alpha\beta0}(t) \tag{B.9}$$

$$v_{i(\alpha\beta0)}(t) = Ri_{s(\alpha\beta0)}(t) + L\frac{di_{s(\alpha\beta0)}(t)}{dt} + v_{s(\alpha\beta0)}(t) \tag{B.10}$$

Converting Equation B.10 from frame $\alpha\beta0$ to $dq0$ using the Park transformation, it is possible to obtain the following equations:

$$v_{dq0}(t) = [C]v_{\alpha\beta0}(t) \rightarrow v_{\alpha\beta0}(t) = [C]^{-1}v_{dq0}(t) \tag{B.11}$$

$$v_{i(dq0)}(t) = Ri_{s(dq0)}(t) + L\frac{di_{s(dq0)}(t)}{dt} + Li_{s(dq0)}\frac{d([P]^{-1})}{dt}[P] + v_{s(dq0)}(t) \tag{B.12}$$

Developing and separating the previous equation in axes:

$$v_{id}(t) = Ri_{sd}(t) + L\frac{di_{sd}(t)}{dt} + v_{sd}(t) - \omega Li_{sq} \tag{B.13}$$

$$v_{iq}(t) = Ri_{sq}(t) + L\frac{di_{sq}(t)}{dt} + v_{sq}(t) + \omega Li_{sd} \tag{B.14}$$

$$v_{i0}(t) = Ri_{s0}(t) + L\frac{di_{s0}(t)}{dt} + v_{s0}(t) \tag{B.15}$$

In Equations B.14 and B.15 it is possible to verify the existence of a cross coupling with the terms ωLi_{sq} and ωLi_{sd}, in addition to the dependence with v_{sd} and v_{sq}. In Equation B.15, there is only the dependence with the term v_{s0}. By feeding the loops with the opposite sign of the crossed terms of current and voltage with a *feedforward* action, it is possible to obtain the block diagram seen in Figure 52.

Thus, open-loop transfer functions in the Laplace domain are obtained.

$$\frac{i_{sd}(t)}{v_{id}(t)} = \frac{i_{sq}(t)}{v_{iq}(t)} = \frac{1}{sL + R} \tag{B.16}$$

The transfer function is of first order. To increase the operating speed of the loop, a PI controller will be used, according to the block diagram in Figure 53. As the VSI has no neutral, it is not necessary to control the zero sequence component of the current.

Developing the closed loop transfer function Figure 53 it is possible to obtain:

$$\frac{i^*_{sd}(t)}{i_{sd}(t)} = \frac{i^*_{sq}(t)}{i_{sq}(t)} = \frac{1}{s\tau_i + 1} \tag{B.17}$$

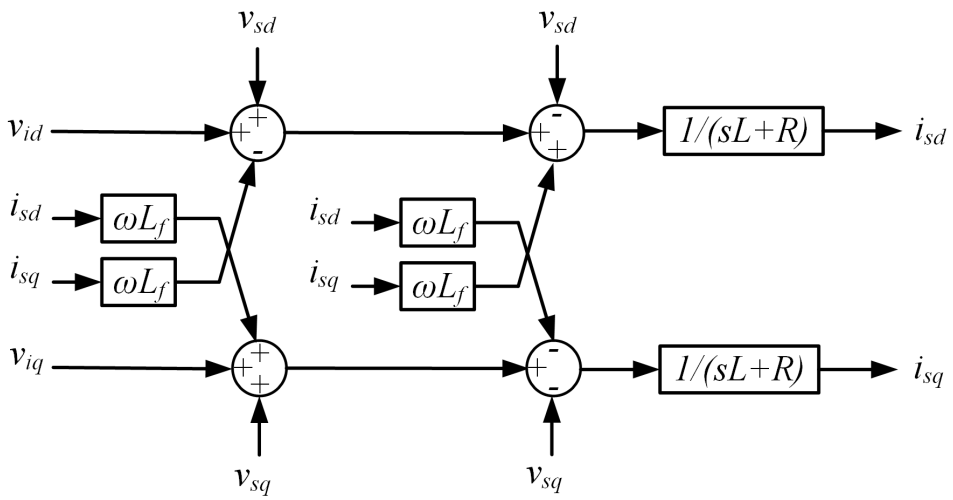

Figure 52 – Decoupling with feedforward action, adapted from (ANTUNES et al., 2018).

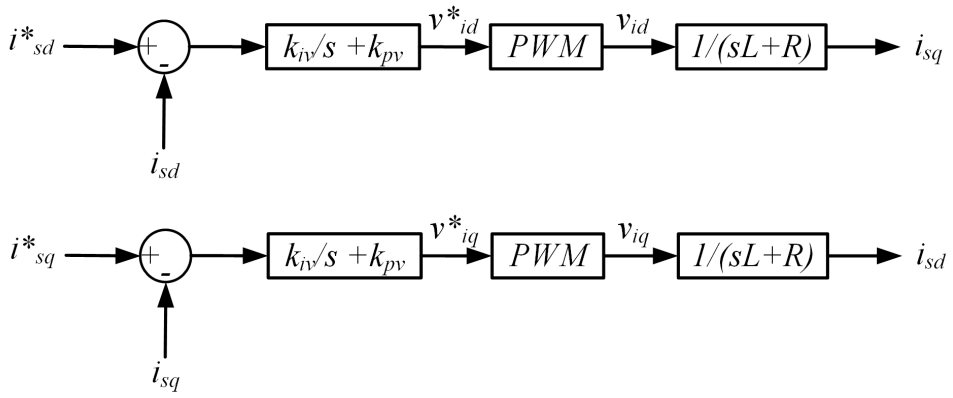

Figure 53 – Closed loop current control, adapted from (ANTUNES et al., 2018).

Where: $\tau_i = L/R$

To define the k_{pi} and k_{ii} gains of the current loop, the pole allocation technique is used. The cutoff frequency (ω_c) of the closed-loop transfer function presented in Equation B.17 is given by:

$$\omega_c = \frac{1}{\tau_i} \tag{B.18}$$

To eliminate the effect of switching harmonics in the control loop, a cutoff frequency equal to (1/10) of the inverter switching frequency is adopted (YAZDANI; IRAVANI, 2018). In this way, the gain k_{pi} and k_{ii} of the PI controller is obtained through the equations:

$$k_{pi} = \omega_c L \tag{B.19}$$

$$k_{ii} = \omega_c R \tag{B.20}$$

B.3 DC Link Loop Control

When the primary source connected to the DC link of the covnerter is of the current source type, it is necessary to ensure that the voltage is stabilized, which is done by means of a direct axis current command. In this way it is ensured that energy is transferred from the capacitor to the mains, or vice versa, maintaining converter operation. Neglecting the losses in the inverter of the grid supplier, we have the following modeling of the dc bus. of the VSI, as shown in Figure 54 (ANTUNES et al., 2018).

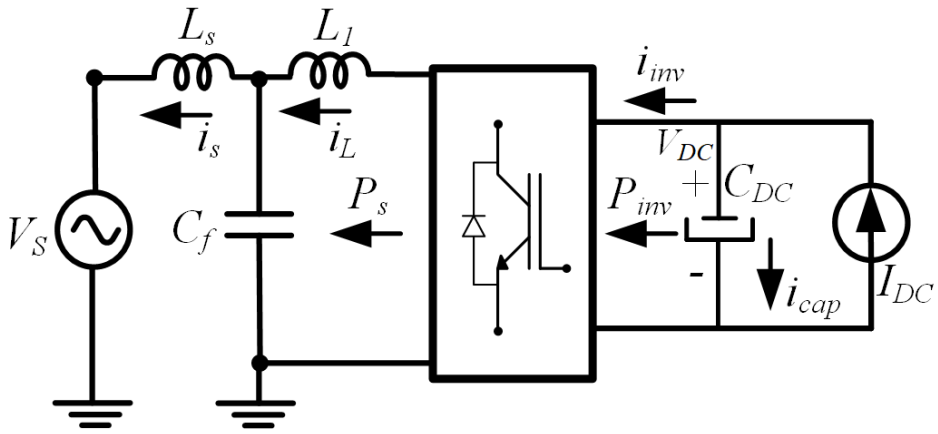

Figure 54 – DC link modelling, adapted from (ANTUNES et al., 2018).

The time domain equation that describes it is:

$$i_{DC} - i_{inv} = C_{DC}\frac{dV_{DC}}{dt} \tag{B.21}$$

Converting it to the Laplace domain:

$$i_{DC}(s) - i_{inv}(s) = sC_{DC}V_{DC} \tag{B.22}$$

Neglecting the inverter losses and considering the steady state operation (DC link voltage constant) we have:

$$P_{inv} = P_s \tag{B.23}$$

$$V_{DC}i_{inv} = \frac{3v_d i_d}{2} \tag{B.24}$$

$$i_{inv} = \frac{3v_d i_d}{2V_{DC}} \tag{B.25}$$

The block diagram of the dc bus. is shown in Figure 55. The DC link control is done through a voltage control loop with PI controller, in cascade with the current loop. It will be considered that the current loop is much faster than the voltage loop, and thus its dynamics can be neglected. The effect of the disturbance of the current i_{inv} will be canceled with its feedback, as illustrated in Figure 56, which guarantees a good dynamic response to the system.

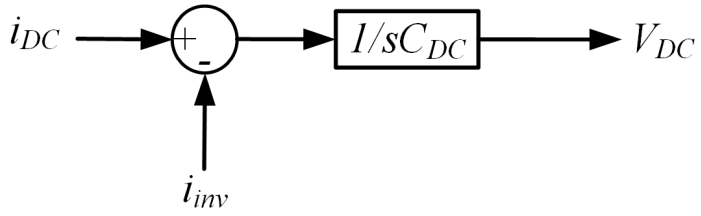

Figure 55 – Block diagram of the DC link, adapted from (ANTUNES et al., 2018).

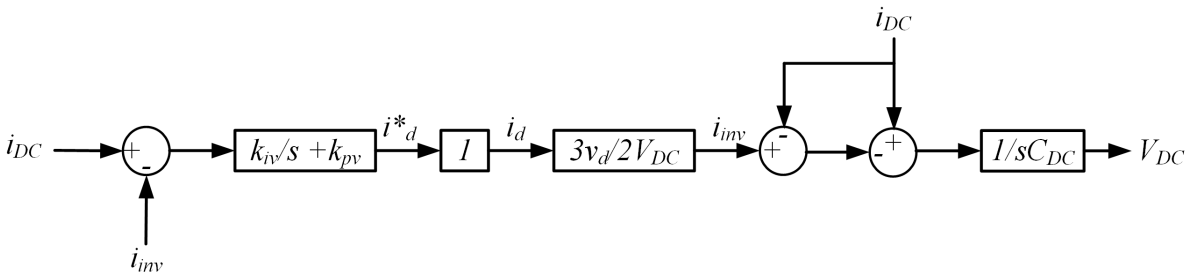

Figure 56 – Closed loop block diagram of DC link voltage control, adapted from (ANTUNES et al., 2018).

The closed loop transfer function is as follow, where: $G = -3v_d/2V_{DC}$:

$$\frac{V^*_{DC}(s)}{V_{DC}(s)} = \frac{sGk_p + k_i G}{s^2 C_{DC} + sGk_p + k_i G} \tag{B.26}$$

For the voltage loop controller design, the pole allocation technique will be used. The voltage loop poles ω_{c1} and ω_{c2} are allocated one decade apart, with the fastest pole having a frequency equal to one decade of the current loop cutoff frequency. The DC link voltage loop PI controller gains are then defined as:

$$k_p = \frac{(\omega_{c1} + \omega_{c2})C_{DC}}{G} \tag{B.27}$$

$$k_i = \frac{\omega_{c1}\omega_{c2}C_{DC}}{G} \tag{B.28}$$